GRADUATE PROGRAM IN CHEMICAL ENGINEERING

Daniel Dornellas Athayde

Synthesis and characterization of perovskite materials for production of mixed ionic and electronic conduction membranes

Supervisor: Prof. Dr. Wander Luiz Vasconcelos

Belo Horizonte, January 2016

GRADUATE PROGRAM IN CHEMICAL ENGINEERING

Daniel Dornellas Athayde

Synthesis and characterization of perovskite materials for production of mixed ionic and electronic conduction membranes

Dissertation presented in the Graduate Program in Chemical Engineering of Universidade Federal de Minas Gerais as a requirement for obtaining the Master's Degree in Chemical Engineering.

Research Field: Energy and Materials

Supervisor: Prof. Dr. Wander Luiz Vasconcelos

Belo Horizonte, January 2015

Athayde, Daniel Dornellas.
A865s Synthesis and characterization of perovskite materials for production of mixed ionic and electronic conduction membranes [manuscrito] / Daniel Dornellas Athayde. - 2015.
xvi, 124 f., enc.: il.

Orientador: Wander Luiz Vasconcelos.

Dissertação (mestrado) - Universidade Federal de Minas Gerais, Escola de Engenharia.

Bibliografia: f. 109-124.

1. Engenharia química - Teses. I. Vasconcelos, Wander Luiz. II. Universidade Federal de Minas Gerais. Escola de Engenharia. III. Título.

CDU: 66.0(043)

UNIVERSIDADE FEDERAL DE MINAS GERAIS
ESCOLA DE ENGENHARIA
PROGRAMA DE PÓS-GRADUAÇÃO EM ENGENHARIA QUÍMICA

"Synthesis and characterization of perovskite materials for production of mixed ionic and electronic conduction membranes"

Daniel Dornellas Athayde

Dissertação submetida à Banca Examinadora designada pelo Colegiado do Programa de Pós-graduação em Engenharia Química da Escola de Engenharia da Universidade Federal de Minas Gerais, como parte dos requisitos à obtenção do título de **MESTRE EM ENGENHARIA QUÍMICA**.

200ª DISSERTAÇÃO APROVADA EM 27 DE JANEIRO DE 2016 POR:

Pesquisador Dr. Eduardo Henrique Martins Nunes
Fundep

Profa. Dra. Vanessa de Freitas Cunha Lins
DEQ/UFMG

Dr. Alysson Martins Almeida Silva
UFMG

Prof. Dr. Wander Luiz Vasconcelos
Orientador - DEMET/UFMG

Dedication

To my parents, Ricardo and Stella,

To my lovely wife, Natália

And everyone who have helped me these years.

Acknowledgements

Special thanks to my family, who have always supported me. My father for being my inspiration for becoming a constant questioner of the facts around me, and my mother, a passionate person who showed me how important it is to pursue my dreams.

Also, special thanks to my wife for creating in me the intention to pursue the Master's degree and for remaining by my side at every moment, always offering support and love.

Many thanks to my supervisor, Prof. Dr. Wander Vasconcelos who guided me on the challenges involved on creating and developing a research project.

This project would not have been possible without the support of the staff from LMC, specially Daniela, Eduardo, Alysson and Douglas for the countless discussions we have had since the beginning of this project, and Daiana and Marcus for helping me with the experimental part. In addition, I owe particular thanks to Prof. Joe Diniz da Costa for the support and advices.

Thanks to CAPES for the scholarship, providing me the financial support for completion of this research project.

Thanks for the technical professionals from Magnesita whose support was essential for production and treatment of some samples. In addition, I would like to acknowledge the Center of Microscopy at the Universidade Federal de Minas Gerais for providing the equipment and technical support for experiments involving electron microscopy. Moreover, thanks for the XRD laboratory of the Metallurgical Engineering Department at Universidade Federal de Minas Gerais.

Finally, many thanks for all my friends and people that somehow were involved in my life during these two years.

Abstract

The need of a clean energy delivery is increasing daily with the changes taking place around the planet. Oxygen separation methods for coal power plants are a good option to reach the demands and goals, since some idealized systems show great potential for controlling carbonic gas emissions. Recent studies with dense membranes are optimistic about the application of this technology in the oxygen separation process. Perovskites have been used as a strategic material to produce dense membranes, since it has the ability to transport ions and electrons simultaneously. Best results reported so far are for the $Ba_{0.5}Sr_{0.5}Co_{0.8}Fe_{0.2}O_{3-\delta}$ (BSCF) perovskite. In this work, the BSCF perovskites were synthesized by two variations of the sol-gel method in order to reach the optimum properties for the preparation of dense membranes. A correlation between the material properties and synthesis parameters were studied and a route was suggested for future studies. Also, partial substitution of cesium, yttrium and scandium on the perovskite structure was performed in order to assess the ability of the structure to accommodate foreign cations and change the properties of the final material. Partial substitution with cesium on the A-site was not possible, however yttrium and scandium were successfully incorporated. Oxygen vacancy concentration allowed estimation of improvements on the oxygen permeation of the membranes. Moreover, the stability of the perovskite with scandium was measured under CO_2 atmosphere, confirming promising improvements on the membrane's stability.

Keywords: Oxygen separation, perovskites, membranes, sol-gel.

Contents

Figures summary

Table content

Abbreviations list

BSCF	$Ba_{0.5}Sr_{0.5}Co_{0.8}Fe_{0.2}O_{3-\delta}$
LSCF	$La_{1-X}Sr_{X}Co_{1-Y}Fe_{Y}O_{3-\delta}$
TG	Thermogravimetry
XRD	X-ray Diffraction
SEM	Scattered Electron Microscope
FTIR	Fourier Transform Infrared Spectroscopy
PSA	Pressure Swing Adsorption
MIEC	Mixed Ionic-Electronic Conducting membranes
EDTA	Ethylenediaminetetraacetic acid
DTG	Derivative Thermogravimetry
DSC	Differential Scanning Calorimetry
TPD O2	Temperature Programmed Desorption of Oxygen
EDS	Energy-Dispersive X-ray Spectroscopy
BSCF-Cs	$Cs_x(Ba_{0.5}Sr_{0.5})_{1-x}Co_{0.8}Fe_{0.2}O_{3-\delta}$
BSCF-Y	$Ba_{0.5}Sr_{0.5}(Co_{0.8}Fe_{0.2})_{1-x}Y_xO_{3-\delta}$
BSCF-Sc	$Ba_{0.5}Sr_{0.5}(Co_{0.8}Fe_{0.}2)_{1-x}Sc_xO_{3-\delta}$

1. Introduction

Oxygen plays a key role in the industrial sector, with an estimated industrial production of 100 million tons every year [1]. O_2 is used in the production of glass, metals, cement, chemicals and petrochemicals. The O_2 market has experienced continuous growth, making the separation of oxygen from air an important technology [2,3]. O_2 is becoming the reactant of choice in clean coal energy delivery, a process known as oxy-fuel coal combustion [4]. In this process, coal is burnt with a stream containing O_2 and recycled CO_2, thus generating a high concentration CO_2 flux gas, which can be easily transported and stored to avert the emission of greenhouse gases.

O_2 can be separated from atmospheric air using an air separation unit. Among the commercial technologies commonly applied for oxygen separation, cryogenic distillation is the most used to produce high purity ~99 % O_2. However, it is an energy intensive process as it operates at temperatures as low as -185 °C and under high pressure, which leads to both large capital investments and high operating costs. Another process commonly used is pressure swing adsorption (PSA). In this process gas is adsorbed at room temperature delivering ~95 % O_2 purity, at small to medium scale plants [2,4]. In addition to these mature technologies, a more recent technology based on ionic transport membranes (ITM) has been gathering pace which is evidenced by the large number of scientific publications and patents published since 2000, and by the potential of this new technology to reduce the energy costs of O_2 production by at least 35 % [4].

In the forefront of oxygen transport membranes are perovskite materials. These are known as mixed ionic electronic conductors (MIEC), as perovskites can transport both oxygen ions and electrons concomitantly. Perovskites exhibit a crystal cubic structure as displayed in Fig. 1, described by the general formula ABO_3 where the cation A is surrounded by twelve equidistant oxygen atoms and the cation B is surrounded by six oxygen atoms [5]. In perovskite oxides used for oxygen separation the A-site is commonly occupied by elements from the rare earth, alkali or alkaline families such as La, Na, Ca, Sr or Ba [3]. While the ideal ABO_3 structure does not show ionic conducting properties, the partial substitution of cations present at the A and B-sites creates point defects, or oxygen vacancies, which allows for oxygen ion conduction. As the oxygen

flux is highly dependent on the number of vacancies, the partial substitution of A or B-site cations is a common strategy for improving the performance of perovskite membranes [5]. When doped with different cations, a general formula for perovskites is $A_XA'_{1-X}B_YB'_{1-Y}O_{3-\delta}$, where δ is the concentration of oxygen vacancies in the structure, and x and y vary from zero to one. Several strategies for partial substitution of A and B-site cations have been used to reach oxygen fluxes that are economically attractive [5]. $Ba_{1-X}Sr_XCo_{1-Y}Fe_YO_{3-\delta}$ (BSCF) and $La_{1-X}Sr_XCo_{1-Y}Fe_YO_{3-\delta}$ (LSCF) are the most studied perovskites.

MIEC membranes are dense, so the direct passage of the oxygen molecules is blocked. Therefore, the transport of oxygen ions (O2-) occurs via the vacancies in the perovskite structure. As only O2- can diffuse through the MIEC membrane, the purity of O2 in the permeate stream can be as high as 100 %, provided that the membrane does not have any defects. The transport of O2- takes place due to a driving force associated with the partial oxygen pressure in feed side being higher than in the permeate side [5].

Many routes can be used to synthesize perovskite materials, including solid state reaction, co-precipitation, hydrothermal, spray and freeze drying, and sol-gel process. The selection of the synthesis method is extremely important for the performance of the membrane. It has been established that for similar operating conditions with a particular compound, membranes synthesized by different methods result in different values for oxygen permeation flux. Clearly, the unique microstructure obtained by each method has a great impact on the ionic and electronic conduction of the material [5]. Further, there are a number of methods used to prepare perovskite membranes where the combination of synthesis methods and membrane preparation methods becomes very important to deliver membranes with high oxygen fluxes.

A large array of perovskite compounds have been investigated over the last two decades, where cations in both A and B-sites of the crystal structure were systematically studied. The most established and optimized compound giving best oxygen fluxes is BSCF followed by a more stable but lower oxygen flux LSCF. The effect of doping of these compounds also proved to improve oxygen fluxes together with surface modification to increase the kinetic effect of breaking down the oxygen molecule into oxygen ions. The synthesis method for the preparation of perovskite compounds is very important as all

cations should be fully incorporated in the A and B-sites of the crystal structure. Lack of cation incorporation results in the formation of undesirable metal oxides which are generally non-ionic domains or domains with extremely low ionic conduction [5].

This study provides the background for the potential of the perovskite technology, synthesis methods and further strategies for production of new perovskite compounds. In addition, it includes a detailed description and discussion of the experimental work, in which perovskite compounds were synthesized by two variations of the Pechini method, along with production of new perovskite compounds by partial substitution with different cations.

2. Bibliographic Review

2.1. Oxygen separation

Oxygen plays a key role in the industrial sector, since about 100 million tons of O_2 are produced every year [1]. It has been used in a wide range of applications and the market is continuously increasing, making the separation of oxygen from air an important technology for this sector [1-3]. A remarkable application for O_2 is in coal power plants, in which a new concept of clean coal energy delivery is important in the current scenario of pollutant emissions. It consists in the concept of energy produced from coal power plants with a low emission of pollutants, specifically focusing on CO_2 emissions [2]. In the pursuit of a clean coal energy delivery, two main examples of processes were idealized for coal power plants, which require the use of an oxygen separation step, namely oxy-fuel combustion and coal gasification [4].

An oxy-fuel power plant relies on the ideal of coal combustion in the presence of a stream of pure oxygen. As a result, the flue gas will contain mainly CO_2 and water vapor with small amounts of ashes and impurities. Water is easily removed from flue gas and the almost pure CO_2 can be captured by many techniques as reported elsewhere [6-8]. Another advantage associated with oxy-fuel systems is that the flue gas can be used to dilute the oxygen before its combustion and, consequently, as a mechanism for an enhanced control of the boiler temperature [2]. Figure 1 illustrates a simplified scheme of an oxy-fuel system integrated to a coal power plant.

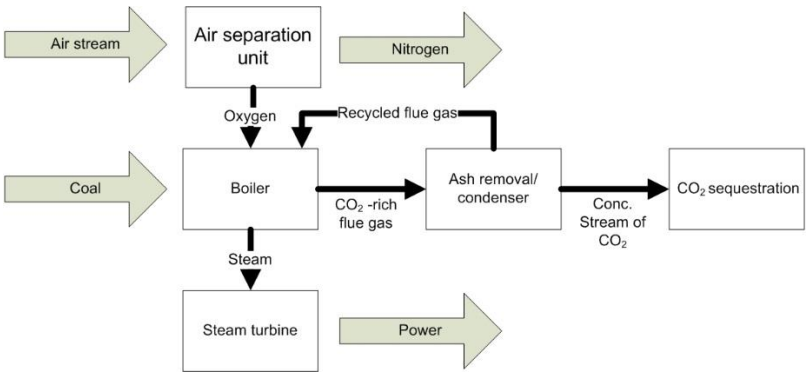

Figure 1 – Oxy-fuel coal power system (adapted from [2])

The other idealized system is the coal gasification process, which consists on the production of syngas obtained from a mixture of H_2 and CO using coal, steam, and oxygen. Its high efficiency reduces the emissions of SO_X, NO_X and particulate matter, making it an attractive technique for the power generation sector. The early coal gasifiers showed limited success, but with the use of pure oxygen, they were enabled to reach the optimum parameters for the syngas synthesis. Emissions of CO_2 in modern power plants using the coal gasification process is nowadays about 20 % lower when compared to a similar older power plants, which indicates an expressive potential for future improvements in this technology [2]. A basic scheme of a coal gasification system is shown in Figure 2.

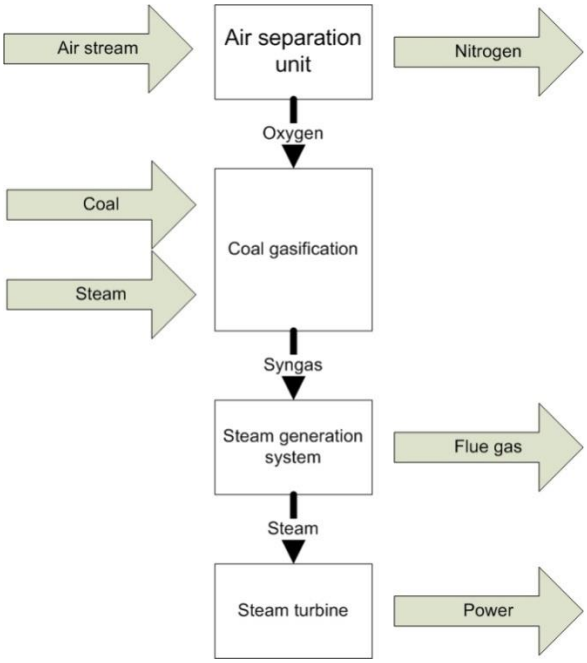

Figure 2 – Scheme of a coal gasification system (adapted from [2])

Regarding the air separation unit, there are two technologies being currently used in large commercial installations. Among the technologies commonly applied for oxygen separation, cryogenic distillation has been the most used technology so far. It operates at temperatures as low as -185 °C and under high pressures, which leads to both large capital investments and high operating costs [2,4,9]. A large-scale O_2 separation based on cryogenic distillation is available. However, when coupled to a coal gasifier or oxy-fuel

power plant the energy efficiency is reduced by 30-40 % because cryogenic distillation is an energy intensive process [2].

The other method commonly used is a non-cryogenic distillation process also known as pressure swing adsorption (PSA), in which the gas is adsorbed at room temperature and under high pressures [4]. The final stream has both a high purity (up to 99.99 %) and large recovery rates (up to 94 %). Recent studies are increasing the PSA efficiency by the development of novel adsorbents. For oxygen separation, the adsorbent generally used are zeolites, but their application is restrict to small and medium scale ranges [2]. The adsorbents used in the PSA process may show a microporous structure. Nonetheless, the accurate characterization of these adsorbents is still a challenge. As a result, accurate prediction of the gas-solid interaction that takes place inside the adsorbent pores is a difficult task. Moreover, the prediction of multicomponent gas adsorption characteristics, such as equilibria, kinetics and heats, is difficult due to the lack of experimental data available in the literature [10].

In addition to these mature technologies, a new trend to use dense membranes has been reported in research studies, due to their great potential for application in oxygen separation units. Some of these membranes are both ionic and electronic conductors, and are known as MIEC (mixed ionic-electronic conducting) membranes. When integrated to a coal power generation plant, this technology reduces the energy cost of O_2 separation by at least 35 % [2,11]. Furthermore, MIEC membranes can be used at high temperatures because of their expressive thermal stability, and exhibit high oxygen flux, which makes these membrane promising materials for using in a wide variety of industrial applications, including energy production [2]. Increased attention has been focused on these materials, as it can be observed by the large number of scientific publications and patents related to this subject published since 2000 [4].

Comparison between these three technologies used for oxygen separation is reported in many works [12-14]. Aspects of each technology are listed in Table 1 with the status of the technologies ranging from the mature cryogenic distillation to the developing dense membranes. Since dense membranes represent the most promising alternative to current mature technology due to their ability of large scale and high purity oxygen production, this work is most focused on dense membranes from now on.

Table 1 – Comparison of main alternatives for oxygen production from air separation

Methods	Status	Oxygen production	Oxygen purity
Cryogenic distillation	Mature	Large-scale	99 %
Pressure Swing Adsorption	Mature	Small and Medium-scale	95 %
Dense membranes	Developing	Large-scale	100 %

There are two main alternatives of dense membranes for oxygen separation applications, namely the traditional oxygen pumps and MIEC membranes. The main difference between these two technologies is associated with the driving force ascribed to the oxygen separation. Traditional oxygen pumps are produced from a class of compounds called fluorites and exhibit significant permeation of oxygen ions. However, they cannot transport electrons through the membrane. Due to the charge nature of the oxygen ion diffusing within the membrane, it is necessary to maintain the overall charge gradient between both sides. Thus, it is necessary to couple an external electrical circuit to the membrane surface in order to transport electrons and maintain the overall charge balance throughout the bulk (Figure 3a). In this case, the driving force is the electrical potential gradient, which allows a fine control of the amount of oxygen generated via a controlled variation of the electrical current applied to the system. On the other hand, MIEC membranes are capable of conducting ions and electrons simultaneously, which is a convenient property when compared to traditional oxygen pumps. The dense MIEC membrane inhibits the direct diffusion of oxygen molecules and oxygen ions migrate selectively through the material, while electrons are transported in the opposite direction. Hence, it can operate without the need of an external electrical circuit, representing an inherent improvement to the process. Consequently, the driving force here is associated with a chemical potential gradient, which is attributed to a difference of the oxygen partial pressure between the feed and permeate sides of the MIEC membrane for oxygen separation purpose. The material used in this case belongs to a structural family of

compounds called perovskite and a scheme of this membrane is exhibited in Figure 3b [3,5].

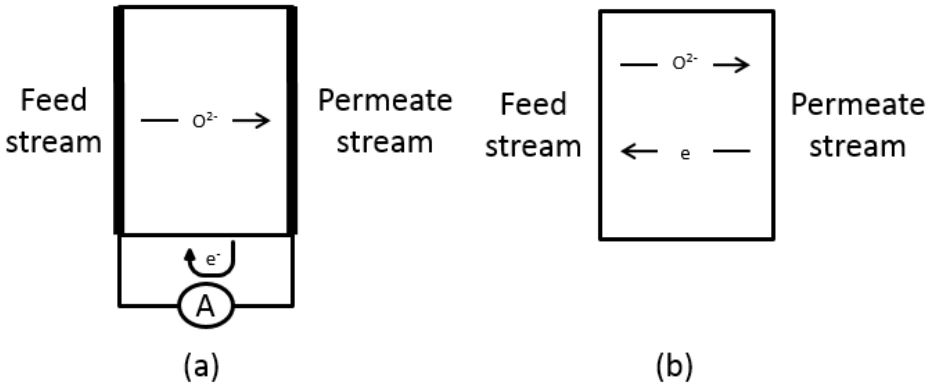

Figure 3 - Membrane processes for oxygen separation: (a) solid electrolyte cell (oxygen pump) and (b) mixed ion-electronic conducting membranes [3,5]

High temperatures are required for activating the oxygen transport through a MIEC membrane. The best results reported so far for these materials were obtained using temperatures ranging from 800 to 1100 °C. Since the oxygen transport is carried out through the material structure and not through its pores, the selectivity of MIEC membranes is theoretically infinite. Therefore, only oxygen can diffuse through the material, which reveals a great potential application for production of high purity oxygen streams by using perovskites [5].

In addition to the two membranes exhibited in Figure 3, there are two other classes of membranes that are under intensive development over the past years. They are called dual phase membranes. The dual phase membranes consist of a membrane with two separated phases distributed throughout the material (Figure 4). One phase is responsible for the ionic oxygen transport, whereas the other one is associated with the electronic transport. Therefore, the phase related to the electronic transport must show a significant electronic conduction and may consist of a dispersion of metallic or ceramic materials [5].

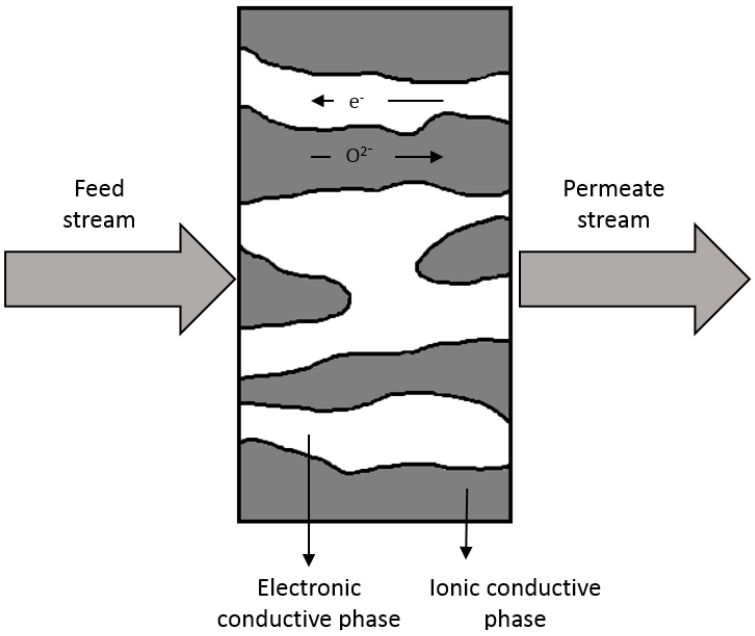

Figure 4 - Dual phase membrane for oxygen separation (adapted from [3])

Because of the drawbacks ascribed to the poor mechanical stability usually exhibited by ultrathin membranes based on perovskite compounds, the application of asymmetric membranes also has been widely investigated. Figure 5 depicts a schematic representation of an asymmetric ceramic membrane. These membranes are based on the use of a macroporous support to provide mechanical stability for the top layer, which prevents the membrane unit failure under the operating conditions [15]. It is important mentioning that only the top layer exhibits separating capacities. Thus, the macroporous support must show a low resistance to the permeate flow. Intermediate layers bridge the gap between the large pores of the support and the dense structure of the top layer [3]. Differences between the thermal expansion coefficient of the support and top layer may be a point of concern for applications at high temperatures, which is the case for oxygen transport through perovskites. This behavior could result in the propagation of cracks in the material, leading to the decrease of its separation efficiency. However, membranes fabricated using supports and top layers of a same material have been successfully prepared and the results obtained are encouraging [15,16].

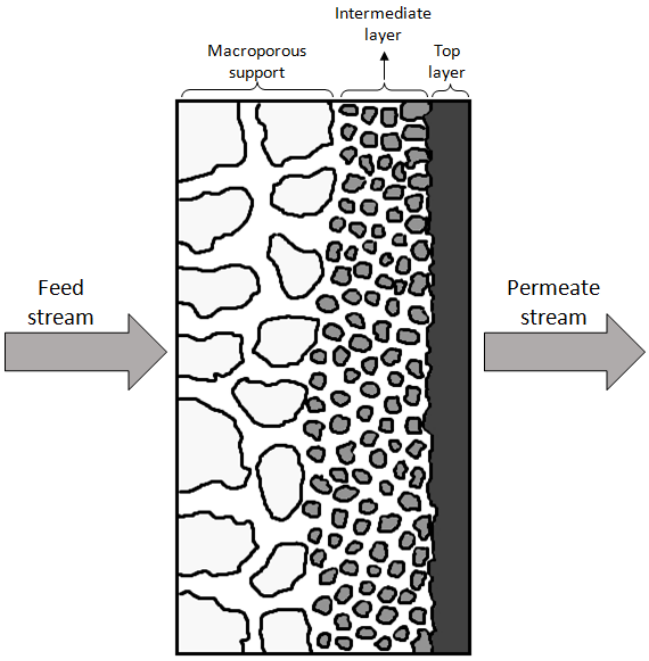

Figure 5 – Typical morphology of an asymmetric membrane

With respect to the materials used for preparing these membranes, those exhibiting a perovskite-type structure are an interesting alternative. It is well known that these materials usually exhibit outstanding catalytic, electronic and magnetic properties. Furthermore, the ability of electronic conduction, which allows the oxygen separation process without the need of associating the membrane with an external electrode system, coupled to high oxygen permeation rates, make perovskites promising candidates for performing O_2-separation [13]. Therefore, this work is most focused on MIEC membranes obtained from perovskite materials. Further information about other materials and membranes for oxygen separation from air may be found elsewhere [5].

2.2. Perovskite materials

Perovskites exhibit a structure similar to that exhibited in Figure 6, in which large metal ions give rise to a simple cubic structure with oxygen atoms present at the faces of the cube, and a small metal ion located at the center. The general formula ABO_3 is used to describe this structure where the cation A is surrounded by twelve equidistant oxygen atoms and the cation B is surrounded by six oxygen atoms. $CaTiO_3$ is a classic perovskite crystal, where Ca is a cation of large ionic radius and Ti is a small and highly charged cation [5,17]. In perovskite oxides used for oxygen separation the A-site is commonly

occupied by elements from the rare earth, alkali or alkaline families. La, Na, Ca, Sr or Ba are the atoms usually observed at these sites. The B-site is occupied by transition metal cations, including Fe, Co, Ni or Cu [3]. The overall charge of the perovskite crystal must maintain the charge balance and the charges of each cation is usually represented by the compositional formula of $A^{2+}B^{4+}O_3$. However, other formulas such as $A^{1+}B^{5+}O_3$ and $A^{3+}B^{3+}O_3$ are also observed [5].

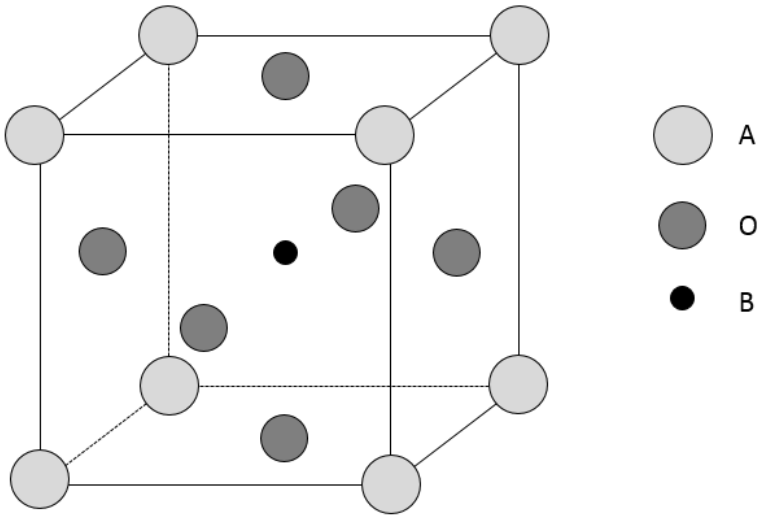

Figure 6 - Crystal structure of ABO_3 perovskite [2]

The shape of the crystal formed is strongly related to the cation size. Goldschmidt suggested a factor known as "Goldschmidt factor" (t) given by Equation (1):

$$t = \frac{(r_A + r_O)}{\sqrt{2}(r_B + r_O)} \quad (1)$$

where r_A and r_B represent the radii of the cations located at the A and B sites, and r_O is the ionic radius of oxygen [18]. The typical structure of a perovskite is preserved if the t factor is within the range of 0.75-1. For crystals showing Goldschmidt factors above 1, the distortion becomes significant and other crystal structures may be observed [2].

While the ideal ABO_3 structure does not show ionic conducting properties, the partial substitution of cations present at the A and B-sites creates point defects, or oxygen vacancies, which allows the ionic conduction. This is possible only because of the high stability of the perovskite structure and, as long as the crystal maintain the ideal cubic

symmetry, these oxygen vacancies can be occupied by the diffusing ions while they are free to diffuse along energetically equivalent crystallographic sites [2,3]. Since it has been shown that the oxygen flux is highly dependent on the number of vacancies, the partial substitution of A or B-site cations is a common strategy for improving the performance of the material [19,20]. Also, the electronic conductivity of the compound is influenced by the B-site cations, depending on its nature and generally is more evident than the ionic conductivity. For instance, Teraoka et al. (1988) [21] tested the electronic and ionic conductivities for perovskite materials at 800 °C in air and reported values of 10^2-10^3 S cm^{-1} and 10^{-2}-1 S cm^{-1}, respectively [21]. Therefore, the electronic conduction usually does not represent a limiting step for the overall oxygen transport in perovskites [3].

When doped with different cations, a general formula for perovskites is $A_XA'_{1-X}B_YB'_{1-Y}O_{3-\delta}$, where δ is the concentration of oxygen vacancies in the structure, and x and y vary from zero to one. Several strategies for partial substitution of A and B-site cations have been used to reach oxygen fluxes economically attractive, creating a large number of perovskite materials [5,22,23]. Teraoka et al. [21,24,25] first published studies devoted on the development of oxygen and electrical conductive properties of perovskite membranes using compounds based on $SrCo_{0.8}Fe_{0.2}O_{3-\delta}$. They reported that these materials exhibited high oxygen permeation when exposed at high temperatures to a helium flow in one side while the other side is kept in air. This material did not exhibit sufficient chemical and mechanical stability. However, the initial experimental data led the research community to test new chemical formulas to obtain novel perovskite materials with improved chemical stability and oxygen permeability [5].

$Ba_{1-X}Sr_XCo_{1-Y}Fe_YO_{3-\delta}$ (BSCF) and $La_{1-X}Sr_XCo_{1-Y}Fe_YO_{3-\delta}$ (LSCF) have been the most studied perovskites for producing O_2-enriched gas streams. BSCF usually shows higher oxygen fluxes (10-15 $mL.min^{-1}.cm^{-2}$) than LSCF. Nonetheless, BSCF is unstable at temperatures below about 825 °C, which could lead to both the crystal phase change and membrane unit failure. On the other hand, LSCF displays superior chemical and mechanical properties, giving rise to a more stable membrane when exposed to CO_2 and water, but with lower oxygen fluxes (about 1 $mL.min^{-1}.cm^{-2}$). Its higher stability allows the LSCF membrane to operate for long periods; some researchers reported their successful operation for times over 1000 hours [13]. This trade-off between chemical

stability and oxygen permeation is a constant challenge for researches and considerable efforts have been made in order to improve both properties in one single compound.

2.3. Non-stoichiometric solids

Chemical compounds with fixed proportions of constituents, namely fixed ratio between cations and anions, are special cases and deviations from this pattern, known as non-stoichiometric solids, are not difficult to observe in nature. Defects or imperfections lead to the reduction of Gibbs free energy for a particular compound up to a certain defect concentration in which the compound reaches its minimum Gibbs free energy [5,26]. The presence of defects in the material also causes an increase in entropy, since there are many possible positions that can be occupied by defects. According to the principles of the defect theory, a high amount of energy is required for an ion to move among lattice positions, thus the concentration of defects increases at higher temperatures. However, when defects are present, such as unoccupied lattice positions in the structure (vacancies), ions have lower activation energy for diffusion [26]. Therefore, the defect concentration strongly affects the mobility of ions within the material structure [5,27].

The imperfections present in crystalline solids can be categorized as point defects, linear defects or two-dimensional defects. Defects such as vacancies (vacant lattice sites), interstitial ions (ions at the interstices between lattice sites) and impurity atoms are examples of point defects. It is well established that point defects show a great influence on the ionic conductivity of dense membranes [5,26,27].

The presence of oxygen vacancies plays a key role in the transport of ions through dense membranes. When a foreign atom is incorporated into the host crystal, forming a solid solution, it may give rise to a new phase when this scenario leads to the lowering of the system energy. If the foreign atom shows an electrical charge quite different from the host atoms, a charge compensation process must take place in order to maintain the charge balance of the system. For example, when CaO forms a solid solution with ZrO_2 and a Ca^{2+} ion substitutes for Zr^{4+} in the host crystal, the amount of oxygen anions decreases, leading to the creation of an oxygen vacancy in order to maintain the charge balance. In this case, the formula used might be $Zr_{1-x}Ca_xO_{2-\delta}$. At high temperatures, the reduced

energy barrier caused by the concentration of vacancies is low enough to allow the diffusion of ions through the structure from a vacancy to another [26].

As aforementioned, the concentration of defects is dependent on the temperature, though for oxides it is also dependent on the oxygen partial pressure. Therefore, inorganic compounds may act as a prevalent ionic conductor or as a prevalent electronic conductor in different process parameters [5]. Regarding the electronic conductivity, nonstoichiometric oxides may act as either p-type or n-type semiconductors. In the case of nonstoichiometry caused by either a deficiency of oxygen or excess of cations, the formation of oxygen vacancies takes place with the formation of two electrons (Equation 2), leading to the creation of an excessive concentration of electrons. This kind of material is called n-type semiconductor. If the nonstoichiometry is caused by either the excess of oxygen or deficiency of cations, the formation of cation vacancies occurs simultaneously with the formation of electron holes. Considering the positive electron-hole concentration, this material is known as a p-type semiconductor [5,26]. Thus, when the defects present in a material cause the formation of either electrons or electron holes, they are easily transported through the structure, making the material an electronic conductor. In addition, the presence of multivalent cations in mixed oxides leads to hopping of electrons between cations with different valence states [5].A review of concepts such as semiconductors, electrons, and electron holes may be found in specific literature [28].

In order to predict the formation of defects, electrons and electron holes, an approach similar to the mass balance used for chemical reactions has been applied, as it can be observed in Equations 2 to 5. In these equations O_O^X represents a neutral oxygen atom at the anion site of the crystal, $V_O^{\cdot\cdot}$ an oxygen vacancy, $O_i^{''}$ an interstitial oxygen (it will be transported between oxygen vacancies), e an electron, and h an electron hole. Equations 2 to 5 were expressed according to the Kröger-Vink notation [5,26].

$$O_O^X \leftrightarrow V_O^{\cdot\cdot} + \frac{1}{2}O_2 + 2e \quad (2)$$

$$\frac{1}{2}O_2 \leftrightarrow O_i^{''} + 2h \quad (3)$$

$$\text{null} \leftrightarrow e + h \tag{4}$$

$$O_O^X \leftrightarrow O_i'' + V_O^{\cdot\cdot} \tag{5}$$

Each of these equations involves an equilibrium constant K. It is well know that K depends on the temperature and, as it can be noticed, one of the parameters to calculate K is P_{O_2}, which provides the relation between the oxygen vacancy concentration with temperature and oxygen partial pressure.

2.4. Transport mechanism

Since a MIEC membrane is dense, direct passage of the oxygen molecules is blocked and it is necessary to form the interstitial oxygen ion, which is represented by O^{2-}. Surface reactions take place on the membrane surface to dissociate the oxygen molecules at the feed side (high oxygen partial pressure) in which the O_2 molecule reacts with electrons and then form the oxygen ion. The formed oxygen ion permeates through the MIEC membrane from the high oxygen partial pressure side to the low oxygen partial pressure side, while an opposite and simultaneous transport of electrons compensates the overall charge balance of the membrane. At the permeate side (low oxygen partial pressure) the oxygen ions react to form oxygen molecules and release electrons that now are free to be transported through the membrane. The gas flow at the permeate side is responsible to drag the formed oxygen molecule and giving rise to a stream with low oxygen partial pressure [3,29]. An overall scheme of the transport process is detailed in Figure 7.

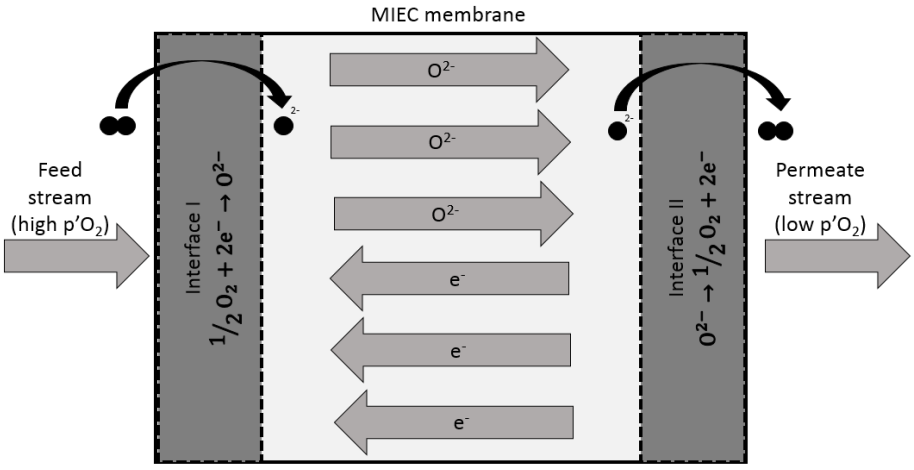

Figure 7 - Conduction mechanism in MIEC membranes [30]

The kinetic mechanism of oxygen transport through a dense membrane can be described in five stages [30]:

- Mass transfer of oxygen molecule from the feed side (high oxygen partial pressure) to the interface of the membrane;
- Adsorption of an oxygen molecule and subsequent reaction at the interface I with the dissociation into oxygen ions;
- Bulk diffusion of the oxygen ions through the membrane;
- Reaction in the surface of the membrane (interface II) with association of oxygen ions and subsequent desorption of the oxygen molecule;
- Mass transfer of oxygen molecule from the membrane interface to the gas permeate stream (low oxygen partial pressure).

Figure 8 represents the concentration profile of the oxygen through the membrane showing the influence of the five stages listed above.

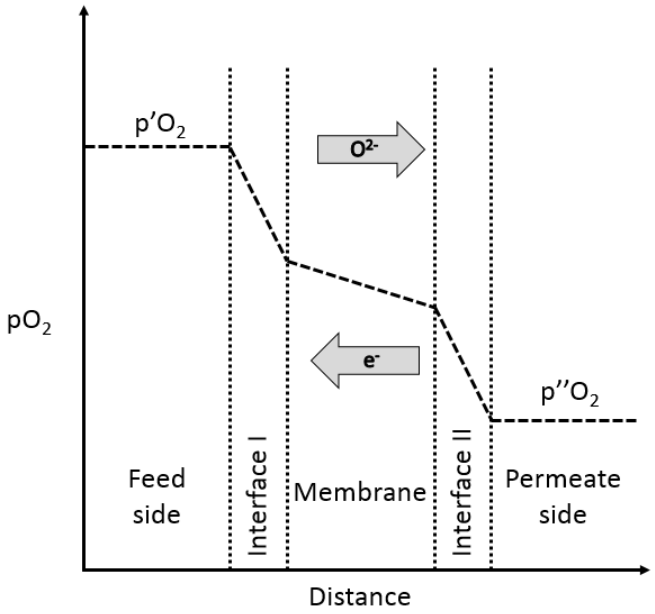

Figure 8 – Concentration profile of oxygen during its transport through a perovskite membrane [5]

Each stage represents different degrees of resistance for the total oxygen transport and the one with highest resistance will be the rate limiting step for the overall kinetic. When the bulk diffusion is the determining step, the overall oxygen permeation flux can be expressed by a simplification of the Wagner equation:

$$J_{O_2} = \frac{1}{4^2F^2L}\int_{\mu_{O_2}(II)}^{\mu_{O_2}(I)} t_i t_e \sigma_t d\mu_{O_2} \quad (6)$$

J_{O2} is the oxygen permeation flux in mol m^{-2} s^{-1}, F is the Faraday constant, L is the membrane thickness, t_i and t_e are the ionic and electronic transfer numbers, σ_t the overall conductivity and μ_{O_2} the chemical potential of the oxygen molecule at the interfaces. The oxygen permeation flux will increase by reducing the membrane thickness when the bulk diffusion is the limiting step, both influences easily understood from Equation 6 [4,5].

The strong correlation between membrane thickness and oxygen permeation flux represents a great potential for improving the oxygen permeation in membranes [8]. Nevertheless, the dependence of the oxygen permeation with the membrane thickness is observed only until a certain value (Lc) called critical thickness. Below this value, the surface reactions in both sides become more relevant to the overall kinetic of the process than the bulk diffusion. As a consequence, there are two regions in the graph detailing the oxygen flux as function of membrane thickness, as shown in Figure 9. The region with membrane thicknesses below Lc is the kinetic-controlled region and for values above Lc it is called Diffusion-controlled region [15].

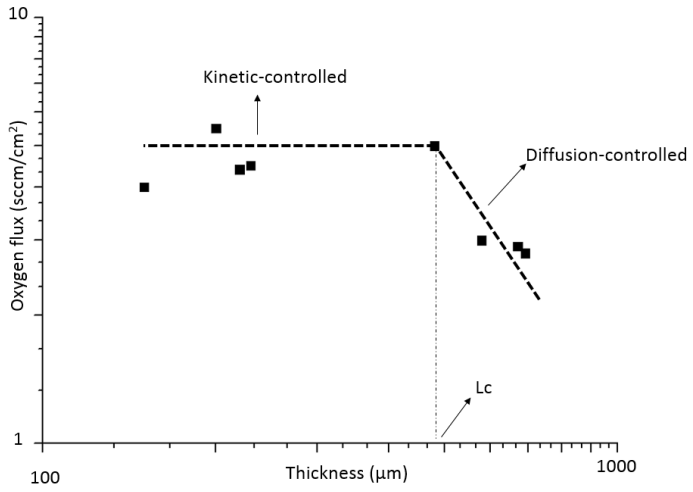

Figure 9- Limiting factor for oxygen diffusion in MIEC membranes [5]

The transport mechanism for membranes with thicknesses above Lc is greatly influenced by the membrane thickness, but for membranes thinner than Lc the oxygen flux can be considered constant when ploted as a function of the membrane thickness [30]. Further

improvements of the oxygen permeation flux can be achieved by forcing different surface reaction paths, such as the use of certain catalysts, or by changing the morphology of the surface [9,31].

Typical values of Lc usually ranges from 20 to 3000 μm [30]. It depends on both the oxygen partial pressure in membrane interfaces and temperature used as expressed by Equation 7, where D_V is the oxygen vacancy diffusion coefficient, k_f is a kinetic constant and p'_{O_2} and p''_{O_2} are the oxygen partial pressure at the feed and permeate sides, respectively:

$$L_c = \frac{D_V}{2\,k_f}\left(\frac{1}{p'^{0.5}_{O_2}} + \frac{1}{p''^{0.5}_{O_2}}\right) \qquad \text{Equation 7}$$

Lower temperatures or oxygen partial pressures lead to a high Lc, making the improvement of oxygen permeation rate by reducing membrane thickness significantly limited [4]. Lc is not considered an intrinsic property of the material, since it depends on the process parameters. Nonetheless, the presence of certain cations may influence Lc, as shown by the influence of x value in the compound $A_XA'_{1-X}B_YB'_{1-Y}O_{3-\delta}$ [5,32].

For the case where surface reactions are the rate limiting step, the Wagner equation (Equation 6) cannot be used. The pursue for different models for this case motivated some groups to suggest mechanisms for the surface-exchange reaction with sequential steps, such as adsorption from the gas phase or charge transfer reaction between the adsorbed species and the bulk, which can be found elsewhere [5]. Additionally, some authors have incorporated all limiting cases of transport into a single model for the oxygen permeation flux through perovskite membranes [33-35]. After several assumptions, models were proposed for LSCF disk-shaped and tubular membranes and they are a good basis for scaled-up engineering calculations, however each model still has its limitations and they need to be well understood. Specific details of each case, such as assumptions, parameters and limitations, and its respective equation are listed in other works [4,5].

Although improvements in the membrane performance can be achieved by lowering the membrane thickness, when the overall process is diffusion-controlled, the mechanical stability of the membrane behaves inversely. In other words, the mechanical stability of

flat membranes is lowered with decreasing their thickness. On the basis of this behavior many research groups are focusing on the preparation of asymmetric membranes since ultrathin membranes exhibit high gas fluxes [15]. However, since they do not have enough mechanical resistance to withstand high pressure gradients, a support is required to ensure the viability of industrial applications. This support represents a resistance for the oxygen transport through the membrane. However, recent studies have shown a great potential for the utilization of asymmetric membranes [15].

2.5. Synthesis methods

Many routes can be used to synthesize perovskite materials, including solid state reaction, co-precipitation, hydrothermal, spray and freeze drying, and sol-gel process [36]. The selection of the synthesis method is extremely important for the performance of the membrane, as it is established that for similar operating conditions with a particular compound, membranes synthesized by different methods result in different values for oxygen permeation flux. Clearly, the unique microstructure obtained by each method has a great impact on the ionic and electronic conduction of the material [5].

2.5.1. Solid state reaction

Also known as conventional powder method, it is the simplest and most traditional method for synthesis of ceramic compounds [37]. It consists in the mechanical mixing of powders of oxides, carbonates or salts, and in the heat treatment of the obtained mixtures at high temperatures (typically around 120 0°C) for long times (about 8-24 hours) in order to allow the mobility of cations through the crystalline grains [36,38]. For a reasonable reaction rate, the recommended temperature for this method is at least two thirds of the melting point, thus the reaction occurs in the solid state. High temperatures are used because ceramic crystals usually show high coordination numbers, varying from 4 to 12, creating an expressive resistance for the cation to overcome the energy required for the cation to leave its position and diffuse towards a different site and form the new structure. Some systems might decompose at the high temperatures, which has been a point of concern for scientists [37].

Reaction rates usually are considerably small and strongly affected by the used temperature. In other words, if the intention is to obtain the material in a short time, one must increase the reaction temperature. Initially the reaction only occurs at the interface of the mixed solids and only after the substance in the interface has completely reacted, the reaction continues as ions diffuse from the bulk to the interface between particles. At higher temperatures both the reaction rate at the interface and diffusion of ions are accelerated, which shortens the reaction time. Since diffusion is often the limiting step for the overall reaction rate, it is required that the precursors show a small particle size and are well mixed in order to both increase the interfacial area between particles and shorten the diffusional path length for ions [37].

In addition, the particle size of the final material, usually with broad size distribution, is highly dependent on both the mechanical mixture and grinding processes of the starting powder. The preparation of particles with sizes below 1μm is technically difficult and energy expensive. Other drawback is the homogeneity and purity of the final powder, which are relatively poor [36]. The method requires a high amount of energy because of the high temperatures usually employed. In addition, it may occur the volatilization of toxic components during the long reaction times [5]. Conveniently, the precursors for this method are readily available [38].

Since the solid state reaction process is the most traditional method for preparing ceramic materials, there is a significant amount of experimental data available in the literature that are related to this synthesis route. An analysis of the relationship between structure stability and cation substitution was carried out by Nagai et al. (2007). Perovskites compounds synthesized were $La_{0.1}Sr_{0.9}CoO_{3-\delta}$ and $SrCo_{0.9}X_{0.1}O_{3-\delta}$ in which X was Ni, Cu, Zn, Cr, Fe, Al, Ga, In, Ce, Ti, Zr, Sn, V or Nb. The precursors were ball milled for 3 hours and subsequently calcined at 900 °C for 12 hours. Final milling of the powders was performed before sintering at 1150-1200 °C. Some of the compounds prepared displayed second phases, probably because of the low solubility of some cations in the solid solution. No correlation was found between the results of oxygen permeability and the structure stability, suggesting that there is no trade-off relation between these factors. A complete analysis of the XRD patterns of each compound can be found in the original article [39]. Other approach to the stabilization of perovskites was studied by Cheng et

al. (2008). They obtained $BaCo_{0.7}Fe_{0.3-x}Nb_xO_{3-\delta}$ perovskites synthesized by the solid state method and calcined at 1000 °C. The authors reported that hexagonal structures were observed when x was below 0.08 while Perovskite structures were obtained only when x was above 0.08. Moreover, DTA analysis pointed out that increasing the Nb doping (x varied between 0.0 and 0.2) can restrain phase transformation and stabilize the cubic perovskite structure [40]. Juste et al. (2008) synthesized $La_{1-x}Sr_xFe_{1-y}Ga_yO_{3-\delta}$ with a calcination step at 1000 °C for 8 hours and obtained a material with the presence of minor secondary phases, identified as La_2O_3, precursor not reacted, and $SrFeLaO_4$. According to the author, the synthesis method used is the main cause of the presence of these impurities [41].

Samples of $Ba_{1-x}Sr_xCo_{1-y}Fe_yO_{3-\delta}$ and $La_{0.3}Ba_{0.7}Co_{0.2}Fe_{0.8}O_{3-\delta}$ were synthesized for performance studies by Waindich et al. (2009). The precursors were calcined at 1200 and 1250 °C for 24 hours and 15 hours, respectively. After sintering both materials, they were compared with a commercial perovskite ($Ba_{0.5}Sr_{0.5}Co_{0.8}Fe_{0.2}O_{3-\delta}$) by SEM and a higher porosity was observed in the two samples prepared by solid state reaction, even though all samples were expected to be dense. This unwanted property may be related to either the preparation or sintering conditions [42]. Recently, Geffroy et al. (2010), have synthesized $La_{(1-x)}Sr_xFe_{(1-y)}Ga_yO_{3-\delta}$ to analyze the influence of Ga on the oxygen permeation and the surface exchange coefficients for some compositions. The mean particle size obtained was 0.3 μm and a XRD analysis revealed that perovskite powders with high Sr and Ga amounts exhibit traces of the La precursor, La_2O_3 and $SrFeLaO_4$ [43]. Different calcination temperatures were used by Luo et al. (2010) to determine in which temperature the pure perovskite is obtained by the solid state method. The synthesis of $BaCo_{0.7}Fe_{0.2}Ta_{0.1}O_{3-\delta}$ for use in reactors for the partial oxidation of methane to syngas was performed with calcination temperatures of 200 – 950 °C for 10 hours. Only at temperatures above 900 °C pure perovskites were obtained. Below this temperature, some unreacted precursors or intermediary products could be observed in the samples [44].

Another performance analysis was executed by Fan et al. (2011), which used the solid state method for the synthesis of perovskites with partial substitution of niobium as B-site cation. The general formula of the obtained compound was $Ba_{0.5}Sr_{0.5}(Co_{0.8}Fe_{0.2})_{1-x}Nb_xO_{3-\delta}$. The samples were calcined at 950-1000 °C for 10 hours with an intermediate

milling for 2 hours. XRD analysis pointed out the absence of second phase formation in all the compositions. Except for the composition of x = 0.5, all samples were gastight, enabling oxygen permeation measurements [45]. Reichmann et al. (2014) produced $La_{0.5}A_{0.5}Fe_{0.7}Ga_{0.3}O_{3-\delta}$and $La_{0.5}A_{0.5}Fe_{0.7}Co_{0.3}O_{3-\delta}$, where A is Ba, Ca or Sr. The mixture was heat treated at 1000 °C for 8 hours. The grain sizes obtained after milling were approximately 1 to 2 μm. XRD analysis of the sintered membranes showed that the materials exhibit a well-defined perovskite structure with few secondary phases, except by the $La_{0.5}A_{0.5}Fe_{0.7}Ga_{0.3}O_{3-\delta}$ membrane, in which the perovskite phase corresponds to a minor phase with the membrane showing a partially crystallized structure [27].

Other examples of perovskite compounds synthesized by this method, for many different applications, can be extensively found in literature [31,44,46-62]. This method can be associated with continuous milling of the powders without the need of external heating. Also known as mechanochemical route, it gives rise to finer particles [63].

It is clear that the presence of second phases is a regular issue when using the solid state method. Characterizations are needed to determine in which temperature the material is obtained with the desired purity. However, as aforementioned, there is no evidence of any correlation between oxygen permeability and the occurrence of second phases and further studies need to investigate if there is no correlation [39]. The higher porosity mentioned by Waindich et al. (2009) is another issue that might lead to lower oxygen permeation flux [42]. Despite its disadvantages, conventional powder method is a simple and fast method for the synthesis of perovskites when compared to other methods.

2.5.2. Co-precipitation

Essentially, this method involves the induction of supersaturation state of certain species soluble in the solvent. The supersaturation conditions necessary to the precipitation of the species is usually induced by the result of a chemical reaction when the solution with soluble metal cations is mixed with another solution called precipitation agent. Parameters such as temperature, mixing rate, pH, and concentration are adjusted to reach the desired products and physical properties, such as product size, morphology and particle size distribution [64]. To separate the solid precipitated phase from the liquid a filtration step takes place, followed by the drying and heat treatment of the obtained solid

material. The resultant material requires a lower sintering temperature when compared to solid state reaction because of the higher dispersion of different cations in the precipitate. A material with good homogeneity and purity is generally formed, but special attention is needed to the precipitation rates since different precipitation rates of each compound may lead to material with low microscopic homogeneity. It happens because each cation needs different optimum parameters (pH and temperature) to precipitate in solution, thus a fine control of these parameters is essential to obtain compounds without deficiency of metal cations [5,36]. The addition of some doping agents in the liquid phase can be used in specific applications, for instance, suitable surfactants and capping agents are used to obtain materials with particle sizes of few nanometers [36].

Other methods can be used for inducing the supersaturation conditions, such as chemical reduction, photoreduction, oxidation and hydrolysis. Also, some other parameters related to the solubility can be used for this purpose, for instance temperature and concentration of species in solution. Simple induction of precipitation do not guarantee the production of a nanoparticulate material, since when precipitation begins, small crystal formed in the nucleation step starts to quickly aggregate and form larger, more thermodynamically stable particles (growth step). Only precise control the synthesis parameters will guarantee accurate management of each specific stage and result in a final product with desired properties. [64].

It is known that this method involves stages of nucleation, growth, coarsening, and agglomeration, usually occurring simultaneously. However, to isolate each stage for independent study is still a challenge. Consequently, fundamental mechanisms of co-precipitation is not thoroughly understood. A review of the theory and thermodynamics of the process was detailed by Cushing et al. (2004), together with an extensive list of several inorganic materials synthesized by this method [64].

The use of the co-precipitation method for synthesis of perovskite powders was done by Zeng et al. (1998) in which the nitrate precursors for the synthesis of $La_{0.8}Sr_{0.2}Co_{0.6}Fe_{0.4}O_3$ were dissolved in water. The addition of potassium hydroxide caused the co-precipitation, and the gel obtained was washed to remove the potassium salt, dried and calcined at 800°C. Finally, the material was sintered to form disk-shaped membranes. It is pointed out that the lower strontium hydroxide solubility under a large range of pH may be a

problem due to the drain of strontium in the washing steps used to remove alkaline impurities, which leads to the production of a perovskite material with lack of strontium, estimated in less than 10 % [65]. Also, a LSCF compound was prepared by Qi et al. (2000) with a similar procedure. Molar ratios were measured by elemental analysis and strontium content was found to be 0.03, while it was expected a molar ratio of 0.20, due to the same causes of low strontium hydroxide solubility. Optimization is still necessary in order to achieve a material with the desired stoichiometry [66]. Other experimental data are reported for successful production of nanocrystalline perovskites by the co-precipitation methods [67,68].

2.5.3. Sol-gel technique

The sol-gel technique can be classified in two general routes. The first one consists in the colloid chemistry of aqueous media, whereas the second one consists in the formation of polymeric chains connected with the metal ions in solution. Both methods are able to produce porous membranes and each step involved in the synthesis has a great influence on the porous structure. In this way, a fine control of the process variables can lead to a porous structure suitable for each application [3].

Many inorganic membranes have been successfully obtained by this technique since it was developed in 1940's [5]. Basically, the first step is the formation of a sol by the mixture of molecular precursors that are either metal salts or metal organics. Condensation reactions are carried out in the sol stage, forming colloids or clusters, which lead to the formation of a gel when they agglomerate and cross-link each other. After the gel stage, there is a heat treatment stage when drying and calcination steps take place. The heat treatment stage determines the nature of the membrane, since the used temperature may lead to a material containing residual organics (80-350 °C) or pure inorganic membranes (generally above 350 °C) [3]. The following step is the sintering process in which densification occurs and the final form of the membrane is consolidated. Depending on the temperature profile used, the final material may show different volume fractions of pores [69]. The most important advantages of this method is the low temperature required for the calcination process, high purity and accurate control of the composition of the final material [36]. A detailed description of the sol-gel theory and models used to describe and quantify the process may be found elsewhere [3,69].

A variety of sol-gel techniques are used for preparing perovskites, including alkoxide, alkoxide-salt, and Pechini methods. The latter has derived a variety of routes using the same principles, with small differences between the chemicals used. For this work, the Pechini methods discussed are the complexation method with EDTA-Citrate and a method in which a posterior stage is carried out with the addition of ethylene glycol in the EDTA-Citrate solution.

2.5.3.1. Alkoxide route

In this route, metal alkoxides are used as precursors. The incompatibility of water with a non-polar solvent gives rise to regions where the concentration of water is very high resulting in reactions of hydrolysis and condensation with formation of hydroxides or oxides [36]. Organic by-products are easily removed by volatilization resulting in very pure products. The hydrolysis and condensation reactions are:

$$M(OR)_X + xH_2O \rightarrow M(OH)_X + xROH \quad \text{Equation 8}$$

$$2M(OH)_X \rightarrow M_2O_X + xH_2O \quad \text{Equation 9}$$

Complex perovskites materials have been synthesized by this technique, showing lower reaction temperatures (around 100 °C) when compared to other conventional methods, as well as calcination temperatures [70].

2.5.3.2. Alkoxide-salt route

This variance of the alkoxide route uses metal salts, or hydroxides, of some of the starting materials instead of metal alkoxides, since metal alkoxides of groups I and II are solid and non-volatile, making their purification difficult. Furthermore, metal salts are easily converted to metal hydroxides and oxides and these are more soluble in organic solvents. A solution with the metal alkoxides is prepared followed by the addition of metal salts in an alcoholic solution or in an aqueous solution, which can be used to enhance the hydrolysis reaction. Compounds dissolved in the system are uniformly distributed throughout the volume and gelation immobilizes them in a rigid network [36]. The different reaction rates between the mixed metal alkoxides and salts is a point of attention

when using this technique, which gives rise to the need of a precise control of the hydrolysis reaction [5].

2.5.3.3. Pechini method

The Pechini method is a widely used option for the synthesis of many mixed oxides. It has been idealized on the ability of some compounds, such as, lactic, glycolic, citric, and ethylenediaminetetraacetic (EDTA) acids, to form polybasic acid chelates with cations dissolved in the system [71]. Chelating agents are used to prevent the partial segregation of metals in the final compound, which may be caused by different interactions between metal ions present in the solution [5]. The addition of a polyhydroxy alcohol, allied with heating the solution, leads to the polyesterification of the chelates, creating a cross-linked chain of metal atoms bonded to organic radicals. The heat treatment, which requires lower temperatures than conventional methods, leads to the removal of organic material and formation of the mixed oxides. These oxides are finely divided and exhibit high purity as well as high homogeneity. As a consequence, the system is in a highly desirable state for successfully sintering into a dense membrane [71].

Some groups have shown that the use of two chelating agents may be an interesting alternative in order to guarantee the absence of unbound metal cations [72,73]. In other words, the cooperation of the chelating agents guarantee the complexation of all metal ions, causing the formation of a precursor solution with all metal ions completely bound [72]. Consequently, a more stable chelate complex system is formed, requiring even lower temperatures as observed when compared to the thermal behavior during the heat treatment of compounds obtained with only one chelating agent [73].

The citrate-EDTA complexation method is an example of route that consists in a solution of metal nitrates as precursors in an aqueous solution with addition of citric acid and ethylenediaminetetracetic acid (EDTA) as chelating agents. Complexation of metal ions with EDTA and citric acid occur while the pH is controlled by dosing NH_3H_2O. Finally, the evaporation of water solvent and posterior heat treatment of the complex are carried out with the formation of perovskite structures showing high relative density and chemically homogeneity [5]. A fine control of pH in the precursor solution exerts a great influence in the purity of the final material, since it is directly related with the degree of

complexation [74]. Recommended pH values depend on the desired properties for each application.

A subsequent step may be performed with the addition of a polyol, such as ethylene glycol, promoting the polymerization with the chelating agent. It has been reported that the use of ethylene glycol can result in a material with increased homogeneity and high surface area when compared to samples prepared using only chelating agents; since a polyester net can minimize further segregations of particular metals during the decomposition process at the required temperatures in the heat treatment [5,75].

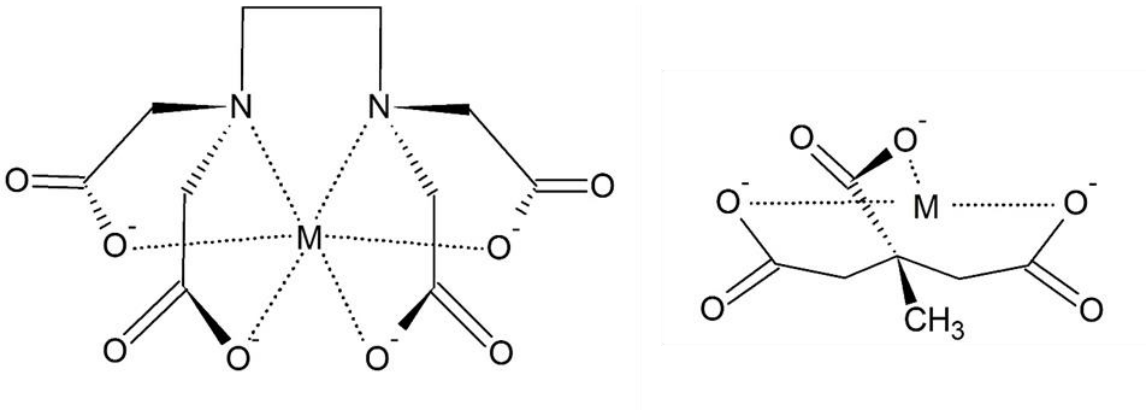

Figure 10 – Complexes formed between metal ions and chelating agents: EDTA on the left and citric acid on the right

Analyzing the complex formation of metals with EDTA or citric acid, it is known that the metal is bonded by six bonds with EDTA, since it has two types of electron donating groups, carboxylic and aliphatic amine, and with the citric acid the metal cation is bonded by three bonds, as shown in Figure 10. Comparing both chelating agents, EDTA exhibits a stronger chelating power than citric acid. However, the co-addition of EDTA and citric acid creates a more stable system. Abdullah et al. (2012) tested perovskite-type oxides by three different routes: using citric acid as chelating agent, using EDTA as chelating agent and using both, all followed by the addition of ethylene glycol. DTG analysis showed a reduced amount of heat release during the calcination step when both chelating agents were used, due to higher effectiveness of the chelation process. The loss of mass assessed by TG was used to calculate a parameter to measure the progression of impurities degradation, called by the author as degree of conversion. This parameter is used to determine the development of the pure perovskite phase and results demonstrated that

when using only citric acid the time required to reach 5 % of conversion was significantly longer than for the other routes, which were very similar. It is pointed out that this fact occurs because of the different number of possible bonds formed between the molecule and metal. Therefore, EDTA is a more efficient chelating agent than citric acid. Finally, FTIR showed that a lower amount of impurity s usually present in materials obtained by that route where both chelating agents are used, suggesting that this is the best choice between the studied chelating agents [73].

Another advantage of using two chelating agents is that one of them might partially contribute to the polyesterification of the other components, without the use of a polyhydroxy alcohol. Each chelating agent exhibit different tendencies for complex formation with a specific metal ion, which reveals that they have distinctive complex formation constants (K). Table 2 summarizes the complex forming constants of EDTA and citric acid with cations used for BSCF production and it is clear that EDTA shows a more intense tendency of forming complexes than citric acid.

Table 2 – Complex forming constants (log K) for cations used for BSCF production [76,77]

Cations	Complex forming constants (K)	
	EDTA	**Citric acid**
Ba^{2+}	7.86	2.73
Sr^{2+}	8.74	3.02
Co^{2+}	16.3	5.00
Fe^{3+}	15.1	11.2

On the basis of these values, Feldhoff et al. (2008) suggested that most cations in the solution will probably bind with EDTA, while citric acid molecules are free to form a polymeric network. This network is formed by a condensation reaction, with the esterification of the alcohol group of the citric acid with the carboxyl group of another citric acid or an EDTA molecule [78]. Figure 11 exhibits a possible structure formed in the Pechini method by the polyesterification between the metal-EDTA complex and the citric acid.

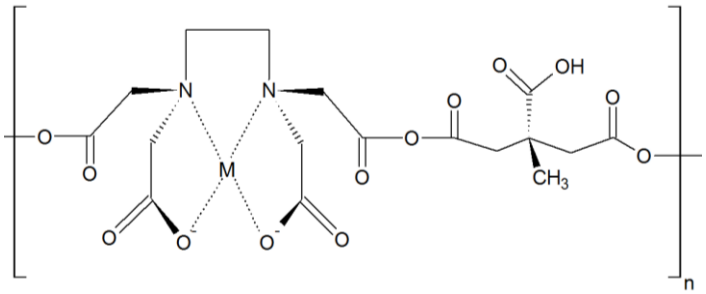

Figure 11 – Structure formed by the polyesterification between EDTA and citric acid

Perovskite-based materials have been extensively produced by the Pechini method. Kakihana et al. (1999) synthesized $LaMnO_{3+\delta}$ compounds by using the polyesterification reaction between citric acid and ethylene glycol. The heat treatment at 700 °C for 6 hours was sufficient to produce a high purity powder with a specific surface area of 20.2 m^2/g. For the sake of comparison, the same powder was produced without the use of ethylene glycol, cited as non-polymerizable amorphous citrate route, and the result was a powder with 18.5 m^2/g. Some unknown impurities were found by XRD analysis for powders obtained at temperatures below 500 °C for the method without the use of ethylene glycol. However, for temperatures above 700 °C the collected XRD pattern was similar to those obtained by the ethylene glycol-based method. The specific surface areas exhibited by materials obtained by both methods were compared with powders prepared in other studies by other routes, such as solid-state and co-precipitation. It was observed that samples obtained by these methods showed higher surface areas than those reported elsewhere [75]. An investigation of the calcination temperature required for successful production of $SrCe_{0.95}Yb_{0.05}O_{2.975}$compounds was done by Liu et al. (2001) using citric acid and glycine. For the determination of the required temperature to obtain the powder, TG, DTA and XRD tests were carried out. TG tests were performed under either nitrogen or air flow. It was reported that the mass loss assessed by TG is smaller when nitrogen is used as testing atmosphere. The complete absence of impurities, evaluated by XRD, was achieved only for heat treatments carried out at temperatures above 950 °C. Further analysis of the obtained powder presented particle sizes in the range of 293-556 nm, a successful result for this specific application, in which hollow fiber membranes were produced, and a crucial enhancement of this parameter when compared with powders produced by the solid state reaction [79].

The ratio between metal precursors and chelating agents can play an important role on the heat treatment used in the synthesis process. Liu et al. (2002) suggested that this ratio should be high enough to guarantee that all metal ions are strongly bonded to their structure and to avoid the precipitation of these metals during the drying process of the solution used. On the other hand, it is interesting to minimize the amount of chelating agents used in order to produce the desired material with minimal costs. The authors discussed about the method used to calculate the mentioned ratio, and also which is the best chelating agent (EDTA, glycine or citric acid) for the synthesis of a perovskite with the general formula $SrCe_{1-x}M_xO_{3-\alpha}$ (M = Yb, Y, In, Ga, La). Due to the presence of carboxylate and aliphatic amine groups on EDTA and glycine, the ratio required for these reactants were lower than for citric acid. Powders synthesized with each reagents were characterized by TG analysis, with all three methods exhibiting its final weight loss stage at about 800 °C. The structural evolution of $SrCe_{1-x}M_xO_{3-\alpha}$was examined by XRD. Powders obtained at temperatures in the range of 800-950 °C exhibited the presence of perovskite and impurities such as SrO and for temperatures above 950 °C there was only the perovskite phase. Therefore, the authors suggested a heat treatment at temperatures above 950 °C for preparing materials with only the perovskite phase. As already discussed, samples obtained by the solid state reaction method need to be calcined at temperatures as high as 1400 °C for long times. At last, SEM analysis of ceramic powders obtained using glycine revealed that the resulting structure was more porous, probably because of the explosive reaction during the heat treatment. Synthesis using EDTA and citric acid produced larger, harder and denser powders agglomerates that are connected each other. Average particle sizes were measured by SEM and the results are that when using citric acid, average particle sizes were smaller than the other methods. However, this behavior was noticed only for sintering temperatures below 1100 °C [80].

Another investigation about the synthesis parameters of BSCF powder was developed by Patra et al. (2011), focusing on parameters such as the molar ratio of chelating agents and pH of the precursor solution. Again, only above 950 °C pure phase perovskites were identified by XRD analysis for all the produced powder. For the same temperature of 950 °C, BSCF powders were synthesized in the range of 1-8 hours, and it was evidenced that for times below 4 hours the XRD peak related with the position (1 1 0) shifted towards lower angles. Besides all tests resulting in a cubic perovskite phase of BSCF, only for

tests performed at 950 °C for at least 4 hours it was possible to obtain a phase with lattice parameter similar to the usually found in the literature, indicating absence of disorder. When comparing all compositions and process parameters used, the conclusion is that all powders synthesized at 950 °C for at least 4 hours were similar, therefore final perovskite phase formation is independent of these parameters. However, for temperatures below 900°C some impurity peaks were found in the XRD patterns, and the powder with lower impurities was the powder obtained at pH 7 and a EDTA / metal cation ratio of 1.0 [81].

For deeper discussion about the influence of composition on the final powder, FTIR spectra were taken for each composition. Absorption bands related to the twisting and stretching vibration of CO_3^{2-} were observed in all spectra, but they exhibited different intensities. It is clear that the higher the EDTA content, the smaller are these peaks. Nonetheless for citric acid the relation is opposite; the peaks become stronger with increasing the citric acid concentration. No evidence was found for the influence of the solution pH on the intensity of the aforementioned bands. Results obtained by SEM and BET showed that the agglomerate size decreases when EDTA content is increased, as well as specific surface area increases with increasing the solution pH. The particle shape was independent of EDTA and citric acid contents, but a higher number of spherical particles were noticed for powders prepared at high pH's. Best results for particle morphology were obtained with the proportion of 1.0/1.5/1.0 (metal ions/citric acid/EDTA) with pH 9, with specific surface area of 18.57 m^2/g and particle size of 0.056μm. Tests to measure the membrane sinterability showed that the highest shrinkage between samples was found for the perovskite obtained by these parameters, due to the highest surface area [81]. Further discussion on pH influence on properties of perovskite materials are detailed elsewhere [74,82].

Other important aspect of the sol–gel method is that several intermediate compounds were detected during the synthesis of perovskites with the sol-gel route, indicating that the formation of perovskite structure involves many intermediate phases very temperature dependent [78-81]. The possible complex process of pure perovskite formation for the specific case of BSCF is schematically represented by Patra et al. (2011) [81].

The results from the mentioned studies are evidences of the strong influence that the synthesis parameters have on the materials properties, and it represents a strategic advantage of the sol-gel method. Several different parameters can be controlled in order to achieve the best properties for the desired application, making the method adaptable for each situation. This accurate control associated with advantages such as low temperature required for the calcination process, high purity and accurate control of the composition of the final compound, make the sol-gel route one of the most used and studied chemical routes for preparing perovskites [83-91]. It is worth to mention the study by Chen et al. (2014) showing that the presence of some impurity ions, in small amounts, does not interfere on the performance of a BSCF membrane making it possible to use raw materials with lower purity, thus lowering the costs of production of the sol-gel route and increasing the competitiveness of BSCF for industrial applications [92].

2.5.4. Hydrothermal

This technique operates at temperatures between the boiling point of water and the material critical temperature is generally used combined with high pressures (15MPa), so that the calcination step can be eliminated. It can be associated with sol-gel technique to control the particle size [5]. Production of $CaTiO_3$ by this method was reported using pressures in the range of 2.5-15 atm and the lowest temperature that the powder was produced was 150 °C for at least 6 hours [93]. X-ray patterns were used to compare the as-prepared powder to that obtained after a heat treatment at 1300 °C. No significant differences were observed in either the phases (no impurities were observed in the samples) or in the cell parameters, validating that the calcination step is not necessary [93].

Since complex oxide powders are formed directly, it is considered a potentially superior method due to its low costs and production of very fine and highly reactive ceramic powders. Inexpensive raw materials are usually used as precursors and for specific cases it is possible to control the particles shape. Considering that an accurate control of particle size is obtained, impurities associated with the process of milling the powders are eliminated [36]. Furthermore, it is possible to reduce or even eliminate the presence of

aggregates. Another crucial advantage of this method is the capability for continuous production of materials by the hydrothermal method, making it particularly useful in industrial continuous fabrication of ceramic powders [94]. Most systems synthesized by this method have utilized the trial-and-error method, an approach that is extremely time consuming. However, thermodynamic modeling to design hydrothermal synthesis is becoming a trend, but only when the system is well known [94].

Some recent effort has been made in studies about the synthesis parameters of perovskites using the hydrothermal method [95-97]. However, it is not widely used yet. Its high potential for low cost production of perovskite powders still has to be completely explored.

2.5.5. Spray and freeze drying

These two techniques use specific rates for phase change of the solvent used to form the solution containing the metal cations. Spray drying uses a fast vaporization of the solvent contained in small droplets of the solution. Taking into account that this is a well-established industrial process, scale up for the production of complex materials can be easily performed. On the other hand, freeze drying uses a slow rate of sublimation of the solvent where the solution is sprayed in fine droplets into liquid nitrogen, with subsequential sublimation of the solvent in the absence of liquid phase [36]. The first step of rapid freezing allows minimum segregation of diluted salts and results in intimate mixing of the ions [98]. Both methods produce homogeneous fine particles with a high control of the morphology and composition [36].

Perovskites powders based in cobalt and nickel were synthesized by the freeze drying method for catalytic applications. It is known that the specific surface area plays an important role on the catalyst activity. Therefore, several compounds were produced using different metals in order to optimize the specific surface area of the final material. Values were within the range of 8.0 – 22.7 m^2/g and all samples showed significant catalytic activity, concluding that the freeze drying method were recommended by the authors as the method of choice for the preparation of novel combustion catalysts [99].

Examples of perovskite production by spray [100] and freeze drying can be found elsewhere [101,102].

2.5.6. Novel methods

In an attempting for improving the powder properties, novel methods for perovskite production have been developed over the past 2 decades. Each application has its own specificities and requirements, such as for catalytic applications, in which the surface area plays a key role on the materials performance. In this context a method known as spray pyrolysis was recently developed. This method involves a solution with metal precursors that is nebulized into an oxy-hydrogen flame and the nanometric particles are collected in an electrostatic precipitator. The resulting material exhibited high thermal stability and sub-micron spherical particles with specific surface areas as high as 40 m^2/g [103]. High drying rates, induced by the low pressures and high temperatures inside the flame, are the main factor causing the formation of nanoparticles [104]. One interesting application of this method is the ability to form regular particles with hollow and thin walls, since a simple milling process of these particles can result in nanoscale particles [105].

The apparatus for spray pyrolysis is designed in a way that the production of the material is continuous, increasing the production rate [104], as well as readily scaled up for commercial production of nanopowders [105]. Additionally, accurate investigation of the experiment is required, since powder morphology strongly depends on process parameters such as temperature of the diffusion flame and residence time inside the high temperature flame, which are easily controlled [105] [106]. Other authors have also shown this strong correlation with several process parameters [107-111].

Another option recently studied is the synthesis of ceramic powders using electromagnetic waves from a microwave furnace, since it overcomes some issues from conventional processes [112]. The microwave has the ability to penetrate into the sample bulk and the energy is uniformly and rapidly absorbed causing a molecular motion by the migration of ions and rotation of dipoles, without changing the basic microstructure of the material. Therefore, sample temperature increases uniformly without the need of heating vessels transparent to microwave energy, and the sample reaches the desired temperature in a reduced time [113]. For ceramic processing, this reduced time for

calcination stages might be extremely important, due to the lack of time available to grain growth and a uniform and fine microstructure is obtained. However, some materials do not absorb well microwave radiation at certain temperature ranges (usually low temperatures) and the need of another heating source is required. In this case, a material with capacity of absorbing the microwave radiation, called susceptor, is placed near to the sample and this material will assist in the heating of the sample until a temperature in which it couples well with microwave radiation [114-116]. When the material to be processed is a ceramic powder, this method is used in most cases and may be called of hybrid microwave heating.

Experimental work by Yan et al. (1997) showed the production of powders of $LiCoO_2$ by hybrid microwave calcination. The result was a powder with grain size of one tenth of the grain size obtained by conventional sintering and further milling was not necessary, since particle coarsening was avoided [112]. In addition, phase purity is achieved with lower temperatures when using microwave heating, suggesting that a different reaction path takes place by this method [5,117-121]. For example, the $LiCoO_2$ powder was produced at temperatures of 600 °C instead of the 800-900 °C usually required for conventional synthesis. Another feature is that volatilization of certain materials is reduced, which inhibits variances and uncertainty in atomic ratios within the final material [112].

An attractive option is the association of wet chemical synthesis methods with the use of microwaves, since water is usually used as solvent and it absorbs well the microwave radiation. For instance, Zhai et al. (2006) used the Pechini method for the synthesis of perovskites using a domestic microwave with basic adaptations for homogeneous mixing of the solution. The evaporation took place until the powder was obtained and it was subsequently calcined in a conventional furnace. Few secondary phases were observed in the samples prepared using the microwave and the particles showed a small grain size [122]. Similarly, complexation of metal cations with PVA (Poly(vinyl alcohol)) was performed in the same adapted microwave and exhibited the advantage of consuming less organic reagents [123]. Hydrothermal synthesis was also performed using a domestic microwave furnace and the result is a $BaTiO_3$ powder with particles showing a uniform distribution of size (150 nm), while for the powder obtained by the conventional hydrothermal the particle size ranges from 0.1 to 1.0 μm [124].

Another alternative is the combustion synthesis, also known as self-propagating high temperature synthesis, in which metal precursors are mixed with a fuel (glycine, hydrazine and urea) and is characterized by fast heating rates, high temperatures (up to 3000 K), and short reaction times [37,125-127]. Highly exothermic and even explosive reactions are used to reach high heating rates and temperatures. Once ignited the system must lose less heat than generates, if not the system will extinguish [37].

Between the conventional methods, the first three methods are commercially well established, whilst the others are still in a demonstration stage. It is clear the trend towards development of synthesis methods in order to obtain improved powders and, consequently, membranes with enhanced properties. Properties such as particle size, homogeneity, purity, specific surface area (surface activity) are the main target in the current scenario (performance properties are extremely correlated with these properties, however they will be discussed in a farther point) and there is strong evidences to support the improvement and utilization of more advanced methods. Another important point of recent researches is the energy and time required for thermal stages within the methods, both strongly interconnected. It is of great interest to produce materials with lower calcination temperature, since it provides savings in the amount of energy demanded by the process, which is already high-energy, although novel methods usually result in higher costs with apparatus [5].

2.5.7. Comparison of synthesis method

A unique microstructure is obtained by each of the methods listed, consequently resulting in different physical properties of the final membrane. It is well known that the membrane performance is strongly correlated with these physical properties [128]. For example, the absence of isolated (closed) pores within the BSCF membrane plays an important role on oxygen transport, since not interconnected pores in the dense layer represent areas in which the ion transport cannot take place. Thus, the absence of isolated pores is important to ensure that the ion transport through the membrane would not be limited by the non-ionic pore domains [15]. According to some results, powders with higher surface area produce denser membranes in similar sintering conditions. Therefore, when the obtained powder has an improved specific surface area, air tight membranes can be obtained under milder conditions (lower temperatures and shorter times on the sintering stage)

[65,81,129]. This is in accordance with the theory about the densification process, since the driving force for the process is the decrease in surface area [26]. In addition to the requirement of eliminating isolated pores, the membrane cannot allow permeation of gases other than oxygen, and a dense layer is required to guarantee an absence of leakage.

Development of perovskite phases are also dependent on the synthesis process, thus different calcination temperatures are required for each one. Comparison of the solid state method and two variants of the Pechini method by XRD analysis within a range of temperatures superior of 700-1000 °C, demonstrated that the Pechini method using citric acid and EDTA results in perfect perovskite phases in lower temperatures (900 °C) than other methods [128]. Therefore, parameters such as powder surface area and calcination temperature are important in order to choose wisely which synthesis process is indicated for each application.

Experimental data comparing several properties for different synthesis methods are vastly reported in literature. For example, Zeng et al. (1998) synthesized a perovskite compound ($La_{0.8}Sr_{0.2}Co_{0.6}Fe_{0.4}O_3$) by four different synthesis methods: hydrothermal synthesis, co-precipitation, spray-pyrolysis and conventional powder method. The hydrothermal synthesis resulted in a system in which the desired reaction was not viable under commercial conditions but further analysis of this method was not performed in this study. Despite some initial issues for the co-precipitation method, due to the complexity of this process with a four component system and partial loss of Sr during washing steps, all three methods resulted in a single-phase perovskite. A comparison of surface area of each method have shown that the co-precipitation and spray-pyrolysis methods resulted in similar values, about 7 m^2/g, and the conventional method exhibited the lowest values (~2.5 m^2/g). They were pressed into disk-shaped samples and sintered at a temperature range. Higher densities were found for the co-precipitation method and the low density for the spray pyrolysis was associated with the fact that the powder particles were not completely dense [65].

Another investigation of the relation between the synthesis method and properties of the powder and of the membrane was performed with the synthesis of $La_{0.8}Sr_{0.2}Co_{0.6}Fe_{0.4}O_{3-\delta}$ by the Pechini method (mentioned in the original article as citrate), solid state, spray-pyrolysis and co-precipitation methods. All the studied methods resulted in membranes

with improved mechanical resistance and the grain size within the membrane increased in following order: spray-pyrolysis, co-precipitation and solid state. However, no clear grain boundary was found for materials produced by the citrate method. Similar results of relative densities of about 97 % of the theoretical density were found for the four membranes, and they were composed of a single-phase structure, as evidenced by XRD. Elemental analysis pointed out that the loss of Sr in the co-precipitation method due to washing steps must be a point of concern; the final amount of Sr was 0.03, while the desired amount was 0.20. This fact arises from the considerable solubility of strontium hydroxide in aqueous solutions utilized in the washing steps. Further optimization of the process is required, since differences in the stoichiometry of the material might lead to inaccurate results. A fine control of the final stoichiometry was obtained by the other three methods. Data of electrical conductivity of the membranes revealed how this control is important; the membrane produced by the co-precipitation method exhibited an electronic conductivity one order of magnitude lower than the other three. The electronic conductivity improved in the following order: co-precipitation, solid state, citrate method and spray-pyrolysis. However, no clear correlation between the electronic conductivity and microstructure was observed. The highest oxygen permeation was evaluated for the spray pyrolysis method but only for high temperatures. Activation energy for oxygen transport followed the same behavior and it was influenced by the grain size [66].

A comparison of the solid state method and two variants of the Pechini method (modified citrate and citrate-EDTA) was performed by the synthesis of BSCF. XRD analysis showed that the perovskite phase is initially observed at 700 °C for the solid state method and was completely developed at 950 °C, while for the two variants of the Pechini method the phase first appeared at higher temperatures. However, the complete development of the perovskite phase was achieved at 900 °C, as noticed by DSC. Different morphologies were found for each of the three methods after the powders were calcined at the same temperature of 950 °C. The main cause is because the temperature used for the solid state method only results in the formation of the perovskite phase, while in the citrate-EDTA the perovskite phase is already formed at lower temperatures and the grains start to grow and merge at higher temperatures, as the value used in the experiment. For this reason the powder synthesized by the solid state method is isolated and the powder synthesized by the citrate-EDTA method is connected together and no clear grain boundary can be seen

in the structure. The modified citrate method resulted in different morphology due to differences in the pyrolysis process. Milling of the calcined powders resulted in similar grain size distributions however the shrinkage and relative density of the membrane during sintering was different for each method. Best results were found for the powder produced by the solid state method and oxygen permeation fluxes were found to increase in the order of citrate-EDTA, modified citrate and solid state, confirming the influence of the microstructure in the performance of the membrane [128].

With respect to the technique of freeze drying, powders of $SrTiO_3$ for production of H_2 by photochemical decomposition of water were produced by the freeze drying method and compared with powders obtained by the sol-gel method. The final material exhibited smaller particle diameter (120 nm) than the material fabricated by sol-gel (209 nm) and specific surface area was also smaller, 12.7 m^2/g for the freeze drying process and 40.0 m^2/g for the sol-gel. In the particular case of H_2 production, performance tests showed that particle size is the most important parameter controlling the process, therefore, the results were much better for freeze dried titanates [98].

In conclusion, the synthesis method is the determining factor to the microstructure, due to different paths of the crystal phase development. As described in the studies comparing more than one synthesis methods, it is clear that the microstructure plays an important role on the performance of each material. The synthesis is the first process in the production of a material and requires significant analysis to understand the requirements of the final material and desired performance, and then accurately define the synthesis route. Moreover, some systems might not be stable under the reaction conditions and this might lead to misinformation when analyzing the results. Thus, the synthesis method must be well suited with the desired compound [37]. Other technical factors must be considered in order to determine which method will be used, in particular the technical complexity of each method, availability of technical devices and related costs. The main points of each method already discussed are listed Table 3 as general advantages and disadvantages for fast comparison of the mentioned methods used for ceramic powders, focusing on experimental data of production of perovskite compounds.

Table 3 – Advantages and disadvantages of methods commonly used in the synthesis of ceramic materials

Method		Advantages	Disadvantages	References
Solid state reaction		• Known as the simplest method for solid preparation • Oxide precursors readily available • Well established method for preparing perovskites	• Demands high temperatures (typically around 1200°C) for long times (8-24 hours) • High amount of energy required • Technically difficult to produce fine particles • Broad size distribution • Poor homogeneity and purity • Difficulties on avoiding second phases • Laborious mechanical mixing • Possibility of vaporization of toxic compounds	[5,36-38]
Co-precipitation		• Higher dispersion of the different elements in the solution • Significant homogeneity and purity • Well established method for perovskite synthesis	• Requires accurate control of process parameters because of the precipitation ratio of each cation • Different precipitation rates might lead to low homogeneity • Washing of specific cations in the filtration steps, creating a material deficient in the washed elements	[5,35,36,64]
Sol-gel		• Excellent control of volume fraction of pores • High purity due to high dispersion of the elements in the solution • Accurate control of the composition of the final compound • Production of fine particles • Well established method for perovskite synthesis	• High costs of the raw materials [130] • Intense shrinkage of the powder due to the degradation of organic compounds [130]	[3,5,36,69,71]
Hydrothermal		• Calcination step can be eliminated • Low costs (inexpensive raw materials) • Production of very fine particles • Superior potential method for ceramic synthesis • Elimination of the milling step and possible contamination during this treatment • Can be used for continuous material production, making it particularly useful for industrial fabrication of ceramic powders	• Still in its early stages of development • Requires high pressures, thus demanding specific apparatus	[5,36]
Spray and freeze drying		• Production of homogeneous fine particles • Accurate control of the composition and morphology	• Still in the demonstration stage	[36,98]
Novel methods	Spray pyrolysis	• High specific surface area • High thermal stability • Production of finer particles • Continuous production	• In general are associated with high costs due to specific apparatus and techniques required for processing ceramic powders • Still in early stages of development	[103-105]
	Microwave assisted method	• Uniform heating of the sample • Reduced time required for production of ceramic powders		[112,113]

	• No time available for grain growth, producing finer particles • Lower temperatures required • Lower volatilization of certain compounds	

2.6. Membrane consolidation

The next step after obtaining the calcined powders is the sintering process, in which the powders are conformed to the desired geometry and then it is heated in order to achieve the demanded densification, which minimizes the pore volume and produces a dense membrane. Some aspects, such as the heating rate, maximum temperature of the process, and dwell time rule the evolution of the densification process, determining the pore volume, pore shape, shrinkage of the membrane and final density. Sintering theory is extensively described by Kingery, Bowen and Uhlmann (1976) [26] as well as models used to describe the process. The sintering step is important for the final performance of the membrane, since it determines a series of the membrane properties, such as porosity, relative density, surface and pore morphology, and grain size.

During the sintering process the grain size changes considerably, but it increases mostly in the final stage of the process and grain growth is strongly affected by higher temperatures and longer dwell times. In other words, the use of high temperatures and long dwell time might lead to grain growth in excess and, by the contrary, the use of low temperatures and short dwell time might result in insufficient grain growth [131]. Therefore, proper understanding of the compound that is used for membrane production and its particular behavior in the sintering process is a necessary start for optimizing the membrane performance. Different geometries also requires specific sintering techniques, for instance, production of asymmetric membranes may lead to formation of cracks in the system, due to differences in the thermal behavior of each layer, if the sintering process is not well understood.

Correlation between performance and grain size is extremely dependent on the material under investigation and key properties for the performance measurements are the ionic and electronic conductivities for applications in solid oxide fuel cells or oxygen separation membranes. This correlation is explained by the distinct electrical resistances

showed by the grain bulk and grain boundary. This behavior is ascribed to the existence of impurities segregation, dopants and secondary phases. Pore trapping and formation of glassy compounds at the grain boundary also explain the different resistances for the transport of ions and electrons. [132].

Because of these imperfections, the grain boundary has higher resistivity for the ionic conductivity when compared with the grain bulk. Hence, an increase in the grain size results in an increase in the total ionic conductivity, since the concentration of grain boundaries is lower. This effect is reasonable even in theoretical cases. Nevertheless, the mechanical stability is highly dependent on grain size limiting the increase of grain size to certain values. Examples of materials following this behavior are $LaCoO_{3-\delta}$ and $SrCo_{0.60}Fe_{0.25}Cu_{0.15}O_{3-\delta}$, in which increasing the sintering temperature resulted in larger grain sizes and greater oxygen fluxes. There are exceptions to this general behavior and each case must be carefully examined [132].

One example of perovskite that several reports validate the fact that larger grain sizes lead to higher oxygen permeation is the BSCF membrane. Significant data was reported in the relative density and linear shrinkage of disk-shaped membranes sintered within the range of 1000-1200 °C, when sintered at 1000 °C the relative density was around 79 % and at 1200 °C it was 96 %. Linear shrinkage increased until 1150 °C, beyond this point it was constant, proving that the densification process dominates the experiment at temperatures below 1150 °C and at temperatures higher than this value the more intense event was grain growth. Analysis of grain size of membranes sintered at 1150 °C, with dwell time of 5 hours, was 50-60 µm and at 1200 °C was 70-90 µm, confirming this hypothesis. The influence of the sintering time was also investigated and for times longer than 5 hours the linear shrinkage remained constant and only relative density increased. For comparison purposes membranes were sintered at 1150 °C for 50 hours and final grain size was in the range of 60-90 µm. Oxygen permeation test showed that the grain size has a strong impact on the membrane performance, since permeation values were obviously higher for disk-shaped membranes with larger grain sizes. The membrane sintered at 1150 °C for 50 hours and that sintered at 1200 °C for 5 hours exhibited similar results [133], which reveals that both parameters studied may be used in order to produce different performances.

Similar results were reported by Mosadeghkah et al. (2007) for BSCF membranes. They showed the influence of the sintering temperature, dwell time, and pressing pressure. The impact of the sintering time on the relative density was more significant for shorter times, probably because of the first stage of the sintering process, in which the densification is the first stage followed by grain growth. Higher values of pressing pressure also results in higher values of relative density. However, the values obtained for samples obtained at pressures above 2000 bar were essentially constant. All these parameters can be compared by SEM and it was clear that the effect of sintering time on crystal growth is more significant when compared to the effect of pressing pressure Nevertheless, the latter is a key parameter for preparing a crack-free membrane [134].

Another study have shown the same behavior for the BSCF membrane [135], in which a strong dependence of the grain size on the oxygen behavior was found for the range of 12-18 μm. However, other groups found that there is no significant influence of the microstructure on the oxygen permeation rate [129,136]. Klande et al. (2013) produced BSCF membranes with sintering times in the range of 2-32 hours at 1100 °C. Relative density was almost constant for dwell times above 4 hours and average grain size changed for different sintering times. Results of oxygen permeation showed that the performance was independent of the grain size in the range of 24.1-41.3 μm, but for the sample sintered for 2 hours (with grain size of 13.9 μm) the oxygen flux was extremely lower than the other results [137].

There are three possibilities for the effect that grain size exerts on oxygen permeation. If the grain boundary has higher resistivity for the oxygen diffusion, having greater grains is favorable to the performance of the membrane and the major effect is the bulk diffusion. Otherwise, if the grain bulk has higher resistivity for the oxygen transport, than it is favorable to have smaller grains and the major contribution for the overall oxygen transport is the grain-boundary diffusion. At last, there is the possibility that the grain size does not influence the oxygen permeation, probably because of limitations on surface exchange rates. On the basis in these findings, Klande et al. (2013) suggested that there is a limit value in the grain size in which after that value the microstructure influence on the oxygen permeation flux is insignificant, for the specific case of BSCF membranes [137].

Each perovskite compound follows a specific behavior in the correlation between microstructure obtained in the sintering process and the performance. Zeng et al. (2007) produced gas tight disk membranes from LSCF powders with sintering temperatures in the range of 1000-1300 °C. They reported that there was a substantial grain growth with increasing the sintering temperature. A strong correlation was found between the oxygen permeation and concentration of grain boundaries, with best performance results for the smaller concentration of grain boundaries, in other words, for the membrane with higher grain sizes. Electrical conductivity was also examined and increasing the sintering temperature led to higher values, with sharp increases in the electrical conductivity for temperatures below 1200 °C. This correlation between electrical conductivity and sintering temperature was attributed to the different grain boundary conductivities, since only negligible differences were found for bulk properties and oxygen nonstoichiometric between the sintered membranes [138]. Therefore, it is reasonable to conclude that the grain boundary has a much lower electrical conductivity than the bulk phase.

It is important stressing that the perovskite membrane for oxygen separation modules requires a dense and airtight layer in order to avoid leakage of other gases and guarantee the theoretical infinite selectivity. Hence, absence of cracks in the dense layer is ideal for this application and a fine control of the final porosity (both percentage and morphology) should be desirable, since interconnected pores in this layer would lead to transport of other gases through these paths [2,139]. Most studies use a certain value of relative density for measurement of the oxygen flux, which is calculated by the theoretical density (constant for each compound) and the total porosity of the membrane, and this value generally ranges from 90 % to 95 % [45]. Other interesting property for oxygen separation modules is high packing density, in other words, high surface area per volume ratio, in order to reduce plant footprint and the amount of membrane needed [2].

Above all these different behaviors and properties for each compound in the sintering process, there is another point of concern and it needs to be well addressed, which is the choice of the methods to be used to shape the membrane and the heating method. Two main methods are used for membrane shaping, extrusion and tape casting [3], but several other methods are extensively found in literature, such as dry pressing [134], slip-casting [140], phase inversion technique [9,141-143], isostatic pressing method [144],freeze-

casting [145-147], pressure filtration, centrifugal casting [148], with some of them with variations from the main method. Geometry of the final membrane is an aspect that needs to be well matched with the choice of conformation method. For instance, tubular membranes usually are produced by the extrusion method [3], while production of asymmetrical membranes might require addition of additives for support (porous substrate) production [30].

In addition to the membrane shaping, choosing heating techniques for the membrane sintering is another point of investigation, since different methods are found in literature. The most used is conventional furnace heating, but other sources of heating have also successfully produced dense membranes, such as microwave heating [149] and Spark Plasma Sintering [150].

2.7. State of Art

The technology of dense membranes has been attracting a great interest from the research community and capital investments from governments and industries. However, some drawbacks must be overcome before these materials can be widely used commercially. Many research groups have made considerable efforts in order to improve the MIEC membranes. These studies have been mostly focused on the following aims [4]:

- To obtain expressive oxygen permeation fluxes through perovskites at high temperatures;
- To enhance the chemical and mechanical stabilities of perovskite membranes for enabling their long-term operation at high temperatures and pressures;
- To decrease the capital costs associated with the production of these materials;
- To reduce the high temperatures commonly used for preparing gas-tight membranes.

In order to address these issues some strategies have been used to obtain perovskite membranes with improved properties. As aforementioned, asymmetric membranes is an attractive alternative for preparing ultrathin membranes with a high mechanical stability.

In addition, experimental results revealed that asymmetric membranes usually deliver high oxygen fluxes. For instance, Baumann et al. [16] compared the oxygen permeation through dense and asymmetric BSCF membranes. They observed that asymmetric membranes showed a higher oxygen permeation rate when compared to the dense ones. This finding reveals that the support porosity has a great influence on the membrane performance. Similar results were described by other authors [53,151,152]. It has also been reported that asymmetric membranes usually exhibit longer operation times than dense membranes [153].

It is well established that a support must show a low resistance to the permeate flow. As a result, the support must show a highly interconnected pore structure. The intermediate layers bridge the gap between the large and small pores observed, respectively, in the support and dense layer. Rachadel et al. [15] studied asymmetric membranes and obtained membranes with improved mechanical stability. They also observed that the support thickness plays a key role on the oxygen flux, since thin supports led to higher values of permeability than thick supports. However, the asymmetric membranes displayed a reduction of the oxygen permeation when compared to dense membranes. This behavior was attributed to the formation of closed pores in the membrane structure, which represents a limitation for the transport of oxygen ions.

Results of asymmetric membranes with interconnected pores were reported by Shao et al. (2013). Using the phase inversion process and a stainless steel mesh the authors prepared a membrane with a layer with uniformly interconnected pores, or microchannels, and a thin dense layer. A remarkable improvement was achieved when this membrane was used in oxygen separation applications, showing oxygen fluxes about five times higher than dense membranes [154]. In a further study Shao and co-workers prepared a dual phase membrane, using perovskite and fluorite materials to match the high electronic conducting ability of perovskites with the high ionic conducting ability of fluorites. As a result, the oxygen flux was 57% higher for the dual phase membrane and the obtained membrane exhibited an improved chemical stability. They also coated the membrane with Pt particles in order to improve the surface-exchange reactions. It was possible to coat the membrane surface, even inside the microchannels, giving rise to enhanced results for the oxygen separation [9]. In addition, oriented pores can also be obtained by the freeze

casting technique, with noticeable improvements on the oxygen permeation for asymmetric membranes. Nevertheless, recent works based on this method showed considerable potential for enhancing the control of pore formation, especially on an intermediate layer where random and non-oriented pores are observed [146].

Thin tubes and hollow fibers are also a promising alternative, since this geometry leads to separation modules with a larger membrane area per unit volume [155]. In fact, recent works have shown that the use of hollow fibers with thin walls increased the oxygen flux by a factor of three when compared to flat membranes [156]. Additionally, there is the advantage that in tubular geometries the area to be sealed is smaller, which minimizes the risk of gas leakage [5]. However, these membranes create significant pressure drop over the system, which could decrease both the oxygen flux and separation efficiency. Much effort has been made to obtain asymmetric membranes with hollow fiber geometry in order to avoid their mechanical failure under operating conditions [13].

Many research groups have focused on improvements on the surface exchange to enhance the oxygen flux. This is usually made by coating the surface with a catalyst, such as metal particles or other ceramic oxides [156-158]. It is important to notice that improvements on the surface exchange of MIEC membranes can only result in higher oxygen flux when the surface reaction rates become a limiting step. For instance, bulk diffusion in ultrathin membranes may become negligible and in this case the predominant step for the overall kinetic is the surface reactions. Thus, the surface modification approach is more likely to be used on ultrathin membranes.

Regarding the improvements on the membrane properties, such as oxygen flux and stability, it is a common strategy to incorporate a dopant into the perovskite crystal. If the doping of the original material creates a compound with higher oxygen vacancy concentration, it is expected that the oxygen flux through a dense membrane will be increased. In general, the enhancement of the ionic conductivity is obtained by the substitution of A-site cations with larger and lower valent cations. On the other hand, the substitution of B-site cations can improve the electronic conductivity of the material [5]. However, in some cases the incorporation of elements into the B-site can also result in improvement of the ionic conductivity, as shown elsewhere [20,159,160]. For instance, Haworth et al. (2011) doped the b-site of a BSCF compound with yttrium. The prepared

samples exhibited the following chemical formula: $Ba_{0.5}Sr_{0.5}Co_{0.8}Fe_{0.2-x}Y_xO_{3-\delta}$. The doping was successful when x was smaller than 0.2 and resulted in samples with a higher concentration of oxygen vacancies. As expected, they observed that the higher concentration of oxygen vacancies, the higher oxygen fluxes. This finding reinforces that doping the B-site cation can also improve the oxygen flux [20]. An extensive list of several perovskite compounds with many different formulas is detailed by some authors together with respective oxygen flux results obtained for each compound [4,5].

The long-term stability of perovskite materials is still a challenge for oxygen separation applications due to their reaction with CO_2 and water vapor. Several research groups have been worked on the enhancement of perovskites stability, and four techniques are mainly used for this purpose: the production of cobalt-free MIEC compounds, the substitution of zirconium at the B-site cation, the substitution of high valence cations at either the A- or B-sites, and the partial incorporation of large cations into either the A- or B-sites. These approaches led to materials with improved stabilities. However, the oxygen flux decreased for cobalt-free MIEC compounds and material prepared by the substitution of high valence cations at either the A- or B-sites. Samples obtained by the substitution of zirconium at the B-site cation showed a moderate potential for particular compositions. No gain on the oxygen permeation was observed for specimens prepared by the partial incorporation of large cations into either the A- or B-sites. Nonetheless, some of these materials exhibited an improved chemical stability [5,85,161]. Another approach recently studied is the production of dual-phase membranes using materials that present an enhanced chemical stability [162,163].

The long-term stability is essential for perovskite membranes, since the oxy fuel process may recycle CO_2, using this gas as the sweep gas. Therefore, it is necessary a detailed understanding of the CO_2 reaction with the perovskite membranes [162]. Many research groups have performed oxygen permeation tests using CO_2 as the sweep gas in order to simulate the operation conditions used in the industrial scale. Klande et al. (2013) reported the formation of a dense layer composed essentially by $SrCO_3$ and CoO at the sweep side when using $SrCo_{0.8}Fe_{0.2}O_{3-\delta}$. As a consequence, the oxygen permeation through the membrane strongly decreased with time and almost stopped after 3 hours of testing. By partially substituting Sr for La, it was obtained a membrane that could withstand a CO_2

stream for long times with only small amounts of impurities formed at the sweep side. It is possible that doping the material with La led to a perovskite phase thermodynamically favored over the carbonate formation [161]. Also, the partial substitution for Nb on some perovskite has been studied [164,165]. Yi et al. (2013) reported an enhancement on the CO_2 resistance of a $BaCo_{1-x-y}Fe_xNb_yO_{3-\delta}$ membrane evaluated by chemical, morphological, performance evaluation tests. The recovery of the initial properties was assessed and the oxygen permeation was largely recovered, while the initial perovskite structure was not regenerated [164]. Intense research effort has been focused in the last five years towards further understanding of the mechanism in which CO_2 decrease the membrane performance and improving the CO_2 resistance of the perovskite membranes [166-168].

Among the key topics aforementioned, the preparation of gas-tight modules of perovskites has become the major engineering challenge to be faced for the commercial application of these materials and much work has been made for decreasing the sealing area in order to obtain a leak-free system. High temperatures are required for sealing the membranes (about 1,000 °C), which may lead to chemical interactions at the interface and reduce the efficiency. On the basis of these observations, it is essential a special design of sealing techniques and materials to match the required properties for further improvements, and to make solutions become more technically and economically feasible [13].

These key topics observed for perovskite membranes still represent a challenge for the commercial application of this technology and there is a great potential for improvements. However, these membranes have already been used for oxygen separation on membrane modules on pilot and industrial scales. One research group have already reported a membrane module produced with $La_{0.6}Sr_{0.4}Co_{0.2}Fe_{0.8}O_{3-\delta}$ hollow fibers operating for more than 1167 hours at about 960 °C, with the highest values of oxygen flux obtained at 1070°C. Interestingly, they found that the energy consumption per unit of oxygen production decreased with increasing the temperature of the system [169]. The state of art of oxygen separation are the plants operated by Air Products and Chemicals Inc. On these plants the membrane modules utilize perovskite membranes with a wafer-like geometry. The first plant was a pilot plant that has successfully operated for more than

1,000 days, producing 5 tons of oxygen per day (TPD O_2), with demonstrated stability on the O_2 purity and flux. Also, tests of pressure and temperature cycling were successful. After scaling-up the process, the first large scale oxygen production plant with capacity for 100 TPD O_2, was completed on 2015 and is operating at ¼ of the nominal capacity so far. The next step is to reach the maximum capacity of this plant and then build a 2,000 TPD O_2 plant up to 2020. This wafer-like geometry reduces the sealing area per membrane area and also provides a large membrane packing density, resulting in high oxygen fluxes per unit volume. Information about the perovskite compound, module design and specific technical details are proprietary information of Air Products & Chemical [13,170-173]. The first report on the scientific literature has been published in 2015 detailing some of the achievements with this technology [174]

2.8. Overview

Perovskite compounds are materials with great potential for future research due to the suitability for industrial applications allied with some major challenges that still need to be overcome. In this work, the intention is to study synthesis optimization and assess the possibility of producing perovskite partially substituted with specific cations in order to obtain compounds with improved properties. The chosen material was the BSCF perovskite, since it has shown the best oxygen permeation results.

Between the synthesis methods, the sol-gel seemed to be most suitable because the accurate control of the stoichiometry was extremely important for the second part of this work. Specifically, the Pechini method was studied for the first part of this work and two variations were selected for study of the synthesis parameters and correlation with the compound properties. The two variations of the Pechini method were compared by studying the parameters involved on the heat treatment for formation of the perovskite compounds.

The second part of this work involved assessment of the ability of the cubic perovskite phase to accommodate partial substitution with certain cations. Oxygen permeation of this class of materials is directly proportional to the concentration of oxygen vacancies. Thus, increase of the oxygen vacancy concentration may lead to material with improved performance. It is known that introducing a large cation in the A or B-site of the

perovskite crystal might lead to this outcome. Therefore, cesium was chosen for partial substitution on the A-site, while yttrium was picked for the B-site. This partial substitution allowed assessment of the perovskite phase stability, along with the properties of the produced perovskites. A third option was selected since some reports have shown excellent improvement of the perovskite stability by incorporation scandium on the structure. This cation was substituted on the B-site and an experiment was idealized for assessment of the material stability under CO_2 atmosphere.

3. Objectives

3.1. Main objectives

The main objective of this work is to study the synthesis of the BSCF perovskite by two variations of the Pechini method in order to assess the correlation between the synthesis parameters and physicochemical properties of the final material. The second part of this study intends to assess the ability of the perovskite structure to accommodate partial substitution with different cations and assess the material properties and final structure.

3.2. Specific objectives

The first part of this work consists on the comparison of synthesis routes and synthesis parameters, with the objectives listed below:

- Compare the two variations of the Pechini method;
- Study the influence of both temperature and the time in the calcination stage.

The second part involves the partial substitution of certain cations on the perovskite structure with the listed objectives:

- Partially substitute cesium on the A-site in order to measure the structure stability and assess the material properties and final structure;
- Partially substitute yttrium on the B-site of the cubic perovskite structure, in order to measure the structure stability and assess the material properties and final structure;
- Partially substitute scandium on the B-site of the cubic perovskite structure in order to measure the structural stability and assess the material properties and final structure, along with assessment of the resulting material stability under CO_2 atmosphere.

4. Methodology

4.1. Perovskite synthesis

In this study, the chosen synthesis method was the Pechini route, since it has exhibited outstanding control on the composition of the final material. The chemicals used in the synthesis method are listed in Table 4.

Table 4 – Reactants for synthesis of MIEC membrane

Reagent	Formula	Function	Purity	Supplier
Citric acid	$C_6H_8O_7H_2O$	Chelating agent	98 wt%	Sigma-Aldrich
Ethylenediaminetetra acetic acid (EDTA)	$C_{10}H_{16}N_2O_8$	Chelating agent	98,5 wt%	Sigma-Aldrich
Ethylene glycol	$C_2H_4(OH)_2$	Polymerizing agent	>99 %	Sigma-Aldrich
Ammonium hydroxide	NH_4OH	pH control	97 wt%	Sigma-Aldrich
Barium nitrate	$Ba(NO_3)_2$	Metallic precursor	>99 wt%	Sigma-Aldrich
Cesium nitrate	$CsNO_3$	Metallic precursor	>99 wt%	Sigma-Aldrich
Cobalt nitrate	$Co(NO_3)_2.6H_2O$	Metallic precursor	>98 wt%	Sigma-Aldrich
Strontium nitrate	$Sr(NO_3)_2$	Metallic precursor	98 wt%	Sigma-Aldrich
Scandium nitrate	$Sc(NO_3)_3$	Metallic precursor	99 wt%	Sigma-Aldrich
Iron (III) nitrate	$Fe(NO_3)_3.9H_2O$	Metallic precursor	>98 wt%	Sigma-Aldrich
Yttrium nitrate	$Y(NO_3)_3.6H_2O$	Metallic precursor	99.9 wt%	Sigma-Aldrich

The Pechni method, as shown in Figure 12, consists essentially on mixing EDTA and NH_4OH in an aqueous solution until the complete dissolution of EDTA (pH around 8). During the entire experiment, the pH was controlled by a pHmeter (Digimed DM23-V1.0). Precursor nitrates are added to this solution, followed by addition of citric acid. At this moment the solution became turbid since some metals form precipitates. The NH_4OH was then added to control the pH to 6 and form the precursor solution. Posteriorly, the precursor solution was dried with continuous stirring at 100 °C. Posteriorly, the dried gel is thermal treated in subsequential steps: , pre-calcination at 450 °C for 8 hours and

calcination at the specified temperature and time. These heat treatments were executed with a 5 °C/min heating rate.

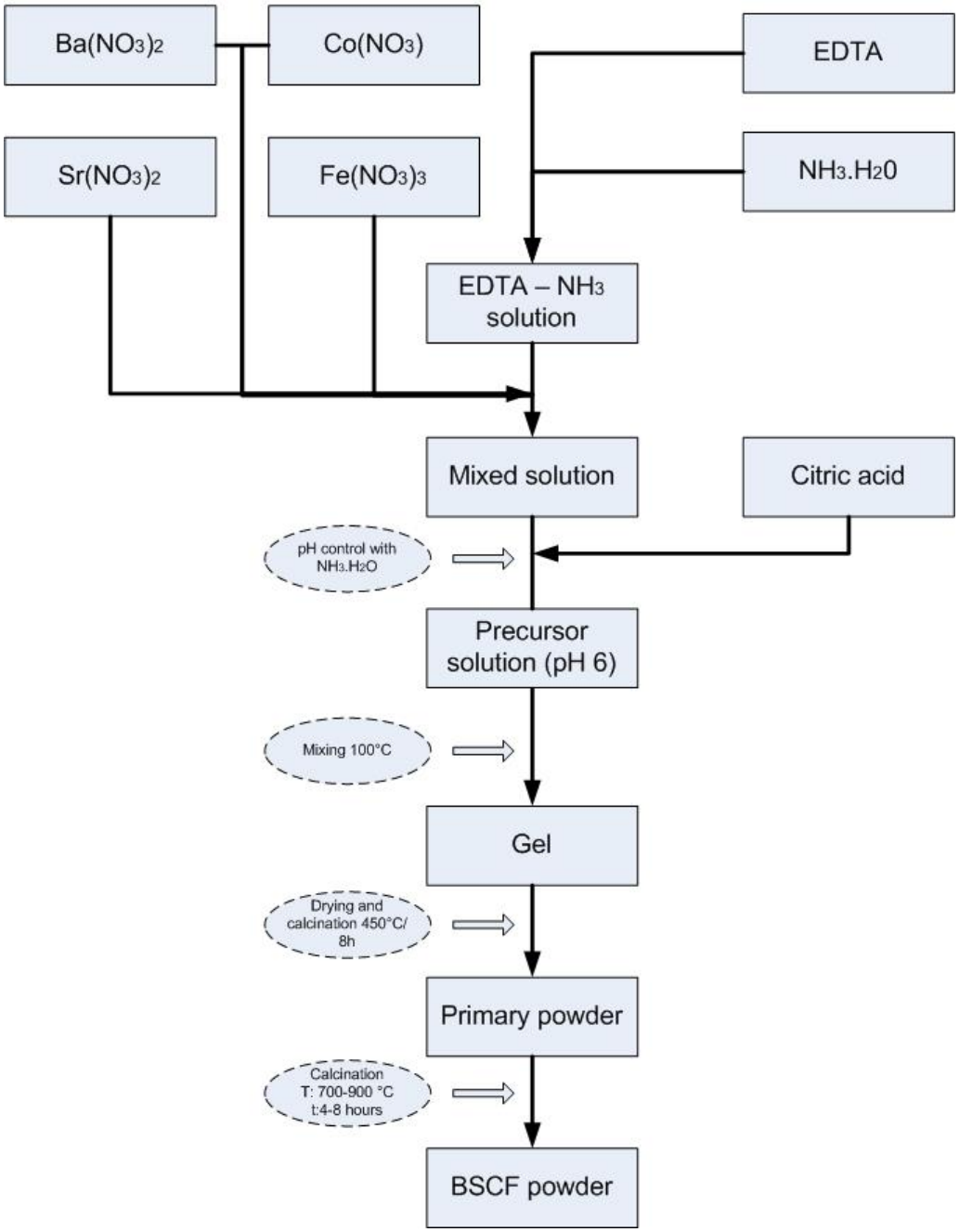

Figure 12 - CA-EDTA complexing method

For the microwave assisted synthesis, a household microwave model Electrolux MEF33 23L was adapted to carry out the experiments with control of the radiation power, external

agitation and measurement of the sample temperature. The microwave allowed control of the radiation power, varying from 10 % to 100 %, with 100 % representing the maximum power of 800W. For agitation of the sample, a mechanical stirrer (Fistaom 713-73W) was attached to the system, along with an orifice to insert a K-type thermocouple (Ecil) in the sample. The temperature control was performed with a digital thermometer (Digital Instruments – DM6802B). Finally, and outlet for gases formed during the synthesis was built with attachment of a simple computer cooler. All adaptations considered safety issues, and a wire screen (the same used in the microwave doors) was used for complete isolation of the system. A scheme of the adapted system is shown in Figure 13.

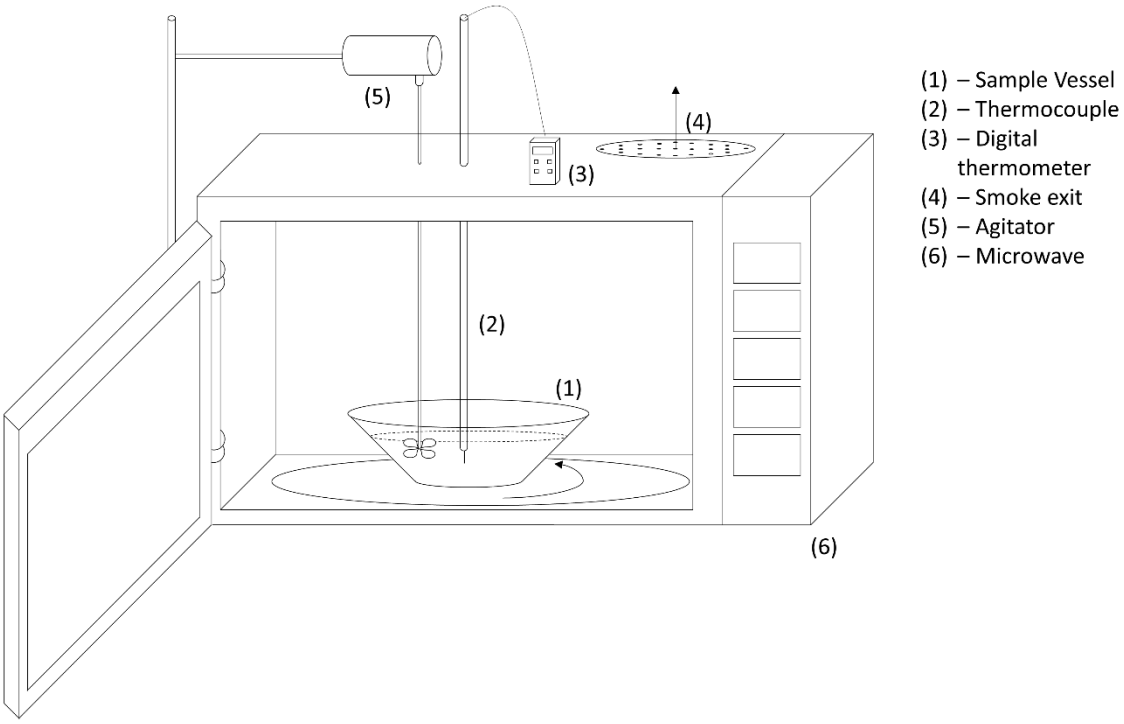

Figure 13 – Adapted household microwave

Microwave experiments were performed using the classic Pechini method, as shown in Figure 14, in which the precursor solution was dried under the microwave radiation. The calcination steps of the dried gel were performed inside the adapted microwave. After noticing that the thermocouple was causing an instability on the system, a few experiments were performed without the thermocouple.

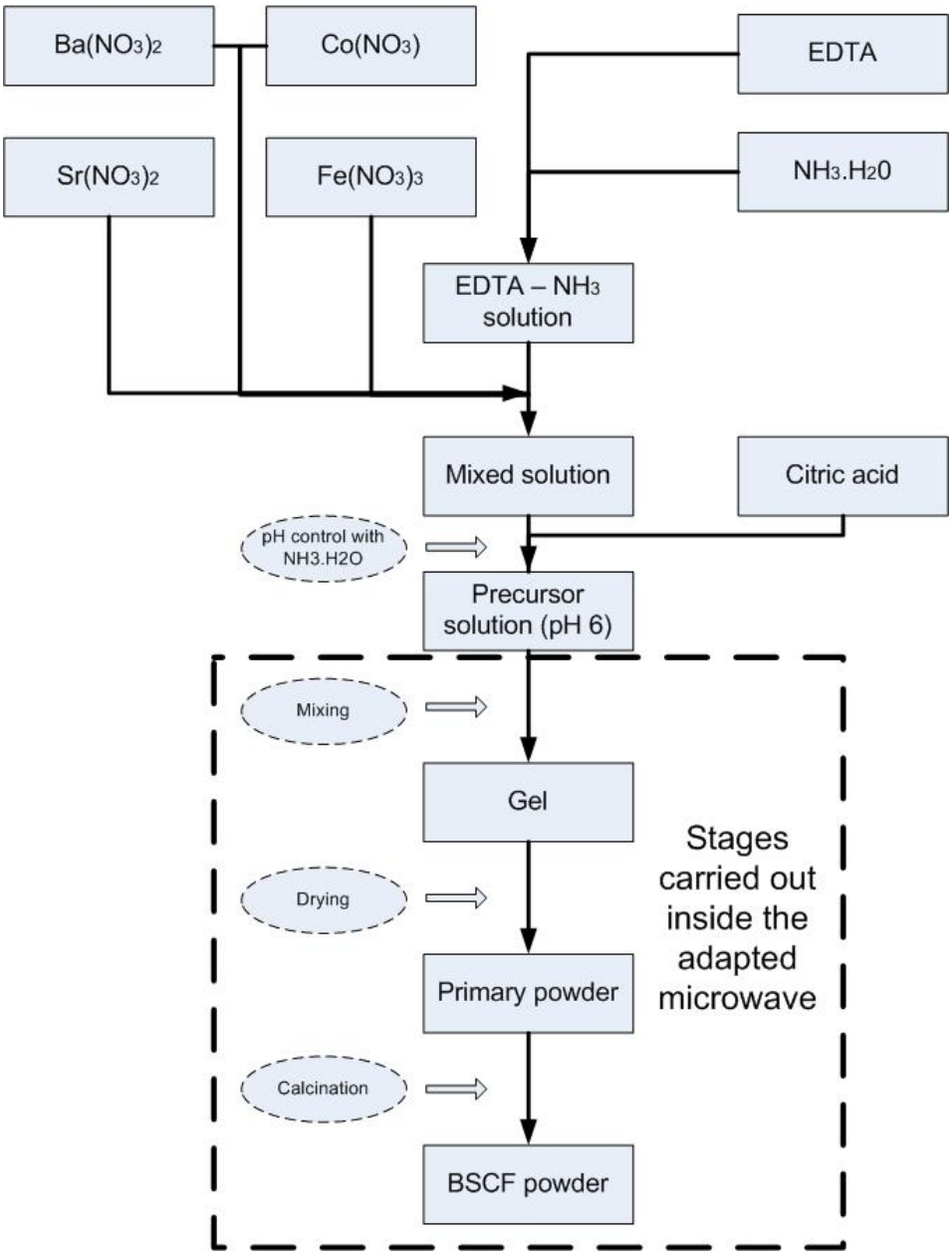

Figure 14 – CA-EDTA complexing method microwave assisted

For the study of the synthesis route and optimization of the synthesis parameters, a variation of the Pechini method was used for comparison of BSCF synthesis with the route detailed in Figure 15. The main difference between the two routes (Figure 12 and Figure 15) is the polymerization step, in which ethylene glycol is gradually added to the precursor solution to aid on the polymerization and formation of the gel. The posterior steps were performed similarly. The optimization of the synthesis parameters was studied for both routes by variation of the calcination temperature and the holding time at the

target temperature. The selected values were 700 °C, 800 °C, 900 °C and 1,000 °C for the calcination temperature and 4 h, 6 h and 8 hours for the calcination time.

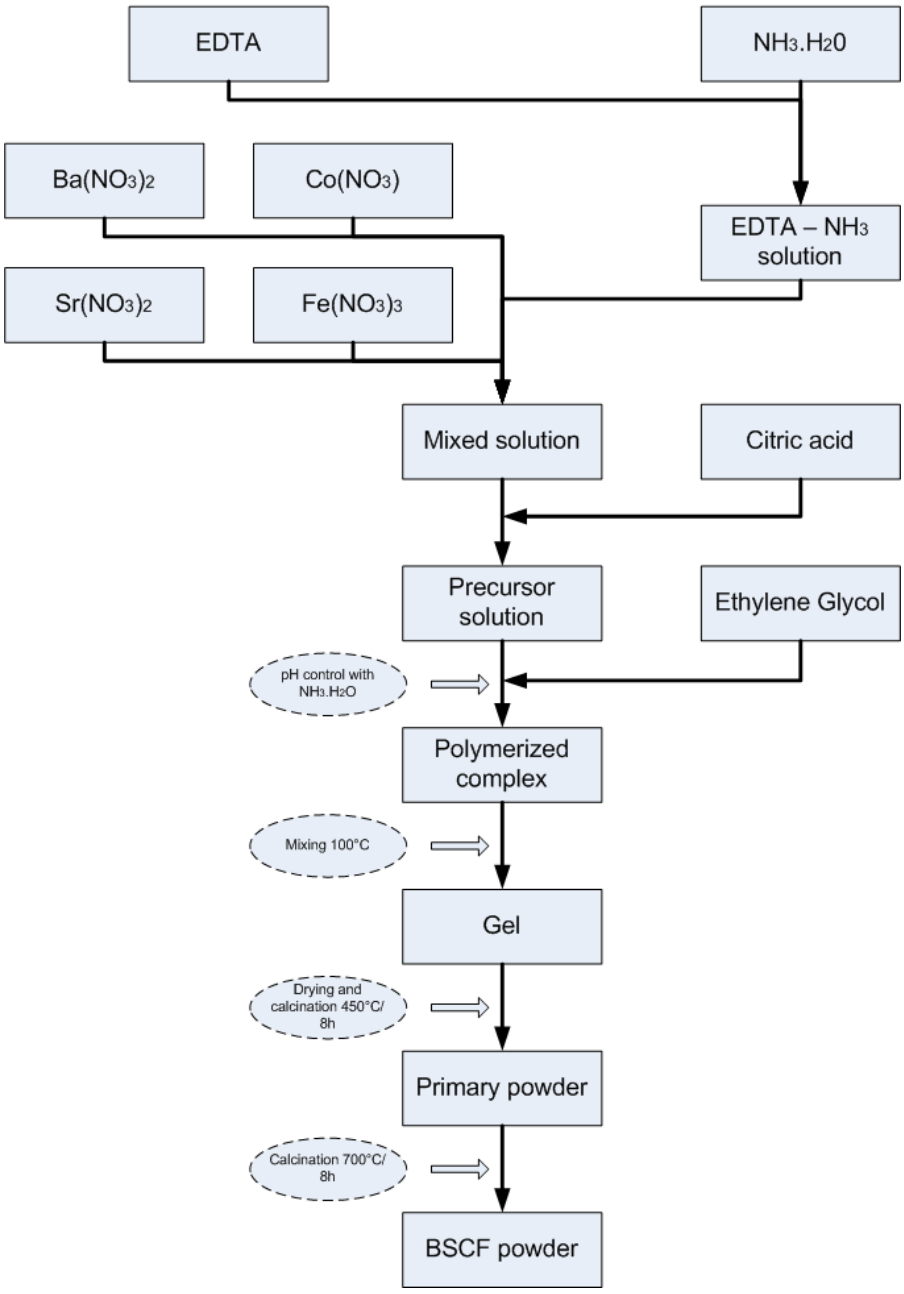

Figure 15– CA-EDTA-EG complexing method with polymerization subsequent step

Production of perovskites with partial substitution was performed using the CA-EDTA route. The used method consisted on partial substitution of all cations on the A or B site, and the formula used will be $Cs_x(Ba_{0.5}Sr_{0.5})_{1-x}Co_{0.8}Fe_{0.2}O_{3-\delta}$, $Ba_{0.5}Sr_{0.5}(Co_{0.8}Fe_{0.2})_{1-x}Y_xO_{3-\delta}$ and $Ba_{0.5}Sr_{0.5}(Co_{0.8}Fe_{0.2})_{1-x}Sc_xO_{3-\delta}$ respectively. Selected values for X were 5 %, 10 %,

20 % and 40%. All samples were calcined at 900 °C for 8 hours, to guarantee that the material would be as pure as possible.

4.2. Characterization

Samples produced on the microwave experiments were characterized by an X-ray diffractometer (XRD) (Phillips-Panalytical – PW 1710) with a scan step size of 0.067 ° and a scan step time of 4.45 s, and a scanning electron microscope (Aspex - Explorer) were used. The JCPDS number #01-075-6980 was used as basis for BSCF structure on the XRD analysis.

For the study of the synthesis route, an initial analysis of both routes was performed in order to completely understand the procedures involved in each method and specific characteristics of the obtained materials. Thermogravimetric analysis of the obtained gel was performed in a Perkin-Elmer STA 6000 thermal analyzer under synthetic air (20 mL/min) and with a 10 °C/min heating rate. Simultaneously, the gases evolved during the TG experiments were analyzed by a mass spectrometer (Hiden – HPR20). Samples were characterized by XRD and SEM microscopy. An EDS system (Omegamax) allowed determination of the elements present on the particles. The samples calcined at 900 °C were hydraulic pressed using a dye for production of pellets with 13.0 mm diameter and thicknesses between 1.2-1.8 mm. The pellets were sintered in a conventional furnace (Thermolab – Thermocouple Pt30%Rh/Pt6%Rh) at 1,000 °C and 1,100 °C for 8 hours with a heating rate of 2 °C/min.

The optimization of the synthesis parameters used data obtained by XRD, Fourier transform infrared spectroscopy (FTIR) (Perkin-Elmer – Frontier), and N_2 adsorption tests (Quantachrome Autosorb 1C). For the XRD and N_2 adsorption tests, all samples were powdered for 5 minutes in an industrial vibratory disc mill.

Perovskites with partial substitution with Cs, Y and Sc were characterized by XRD and thermogravimetric analysis (TG). The X-ray XRD patterns allowed the estimation of the unit cell size by Bragg's law [175]. Also, SEM micrographs of the powders (FEI – Quanta 200 and FEI – FIB – Quanta FEG 3D) were used to verify the morphology of the resulting material.

The compounds that resulted in perovskite phase were further analyzed. To assess the oxygen vacancy concentration, samples were analyzed in the TG equipment. For this experiment, they were heated until 900 °C with a 10 °C/min heating rate under an inert atmosphere. This temperature was maintained until all samples were stable enough, in this study the temperature was maintained for 5 hours. Finally, the samples were cooled to room temperature under synthetic air atmosphere with a cooling rate 2 °C/min. Measurement of the samples' weight for estimation of oxygen vacancy concentration was performed during the cooling step, since the heating step might result in mass loss attributed to adsorbed compounds. This analysis was performed with constant gas flow of 20 mL/min. The same samples were pressed and sintered in a conventional furnace at 1,100 °C for 8 hours with a heating rate of 2 °C/min. SEM images of the membranes (JEOL – JSM 6360LV) were used for assessing the surface morphology, presence of pores and densification of the membrane.

Finally, the samples $Ba_{0.5}Sr_{0.5}(Co_{0.8}Fe_{0.}2)_{1-x}Sc_xO_{3-\delta}$ were tested by thermogravimetric analysis for assessing the stability of this compound under CO_2 atmosphere. A first step of this experiment was performed to guarantee that there is no water adsorbed on the material. Thus, it was heated until 200 °C with a heating rate 10 °C/min and kept at 200 °C for 30 min. The sample was then cooled to room temperature. The final step consisted on heating the sample with a heating rate of 1 °C/min under CO_2 atmosphere until 900 °C. It was possible to measure the rate of mass absorption (or carbonate formation rate) by using the samples weight. In addition, determination of specific surface area, assessed by BET, allowed estimation of the mass absorption rate per surface area.

5. Results and discussion

5.1. Microwave assisted synthesis

After adaptation of the household microwave system, trials of fast production of BSCF powder were unsuccessful. In the first stage of the method - drying the solution until the formation of a gel - the system worked as planned, the mechanical agitator was vigorously agitating the system and the thermocouple was reading the temperature of the solution precisely (solution started boiling around 100°C). The obtained gel was dried with the production of a tremendous amount of white smoke. About 8 minutes were necessary to dry all the gel and form a huge framework structure of the resulting powder. Since expansion was intense during the gel drying, it was necessary to turn off the microwave, crush the formed mass and then start the calcination stage. At first the system heated rapidly and without further occurrences. However, after 2 minutes it was observed intense sparks from the tip of the thermocouple that was inside the sample. These sparks were extremely bright and the digital thermometer reached tremendous heating rates. They usually maintained for a few seconds (5–10 s) and a strong sound of electrical current was observed.

Due to the high temperatures reached while these sparks were observed (about 1.000°C), the thermocouple could not endure the aggressive parameters and it melted. This was possible to observe because the digital thermometer stopped reading temperature data after any intense spark. At this point, the experiment was discontinued and it was possible to see that the tip of the thermocouple melted and the internal components were exposed. A series of modifications on the adapted microwave were done, however the same phenomenon was observed in the experiments.

In a specific experiment, a spark too intense was observed 5 minutes after starting the calcination step. Since the digital thermometer stopped reading the temperature, the experiment was suspended. When checking the sample the powder at the top had melted and formed a compacted and hard agglomerate. Since ceramic materials usually have high melting point, there was a possibility that temperatures reached were enough to form the perovskite structure. Thus, an analysis of the XRD pattern of the formed agglomerate revealed that it was formed of a crystalline phase, with characteristic peaks that can be

related to the typical cubic perovskite structure. Moreover, it was possible to distinguish other weak peaks attributed to the presence of impurities, as shown in Figure 16. These peaks were detailed by Patra et al. (2011) and attributed to several secondary phases, such as: $BaCO_3$, SrO, Fe_2O_4 and CoO [81].

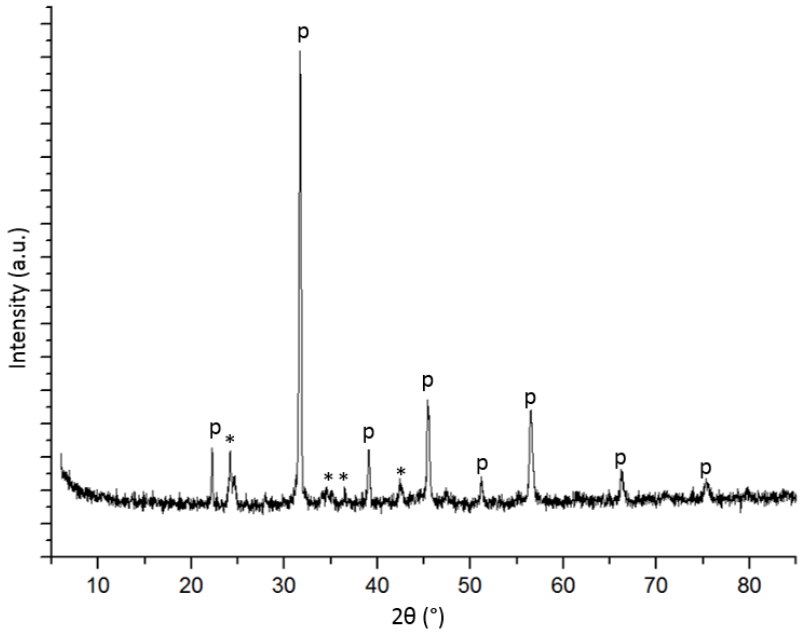

Figure 16 – XRD pattern of the agglomerate in which (p) represents the perovskite peaks and (*) represents the impurities present in the sample

In order to understand better the formation of this agglomerate and try to visualize and further understand the impurities present on the XRD, a morphology analysis was necessary. SEM micrographs revealed that the solid had a smooth surface and it was not possible to see grain boundaries. Figure 17 shows the surface of the obtained agglomerate. It is possible to see some powders in the surface, however EDS revealed that they have the same composition than the rest of the sample. Hence, it is reasonable to suggest that this powder found in the surface is due to the precursor powder and it may not be the cause of the impurity peaks found in the XRD pattern.

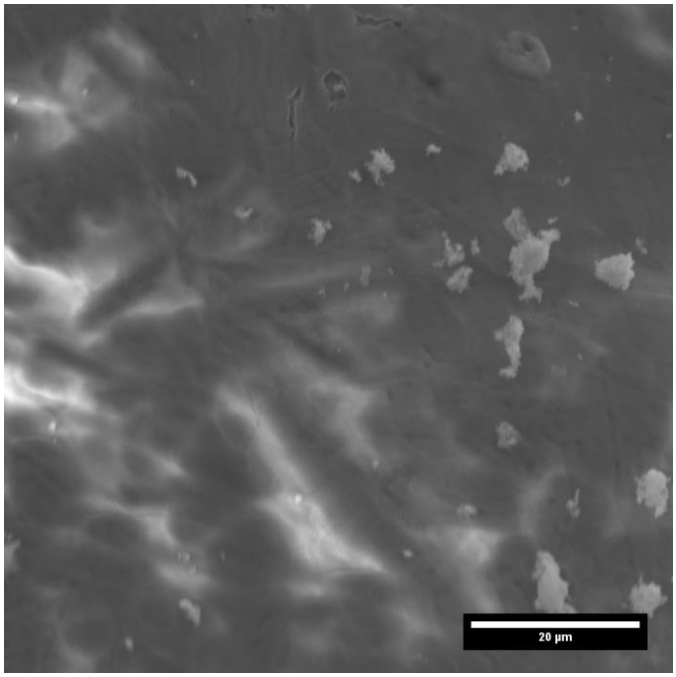

Figure 17 – SEM image of the agglomerate formed in the microwave

The powder in the bottom of the vessel was also analyzed to check if it had the same phases present in the top agglomerate and similar peaks were found in the XRD pattern displayed in Figure 18. Nonetheless, in this case, the impurity peaks were relatively more intense and it was possible to identify additional peaks. These peaks were attributed to the same phases visible on Figure 16, however in this case it was possible to distinguish peaks typical of $BaFe_2O_4$.

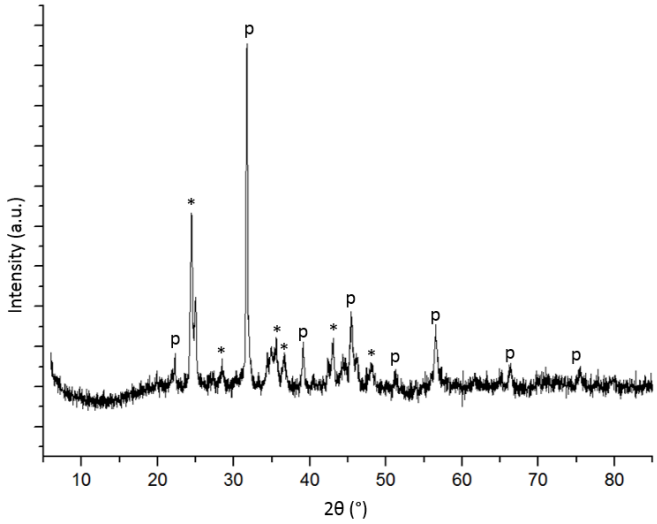

Figure 18 – XRD pattern of the powder at the bottom of the sample

The fact that the experiments destroyed the thermocouples, allied with the difficulties of buying improved thermocouples that would endure the high temperatures, new experiments without the thermocouples were carried out. Similar procedures were used, the solution was heated to form a gel, followed by the drying of the gel and finally the obtained powder was calcined for times of 10, 20, 30 and 40 minutes. The first two samples were calcined without further occurrences, however the third sample, started releasing intense smoke and it became incandescent after 22 minutes. It remained incandescent and after 2 minutes it was possible to see some weak flames coming out of the sample. The fourth experiment was similar to the first two samples, without becoming incandescent or releasing smoke.

XRD patterns of each sample were compared with the XRD pattern of a pure perovskite synthesized by conventional method. As one may notice in Figure 19, they were essentially amorphous and only the sample that stayed in the microwave for 30 minutes exhibited weak peaks that were attributed to the same impurity found in previous samples. Also, it was not possible to notice any trace of the perovskite phase in any of these XRD patterns.

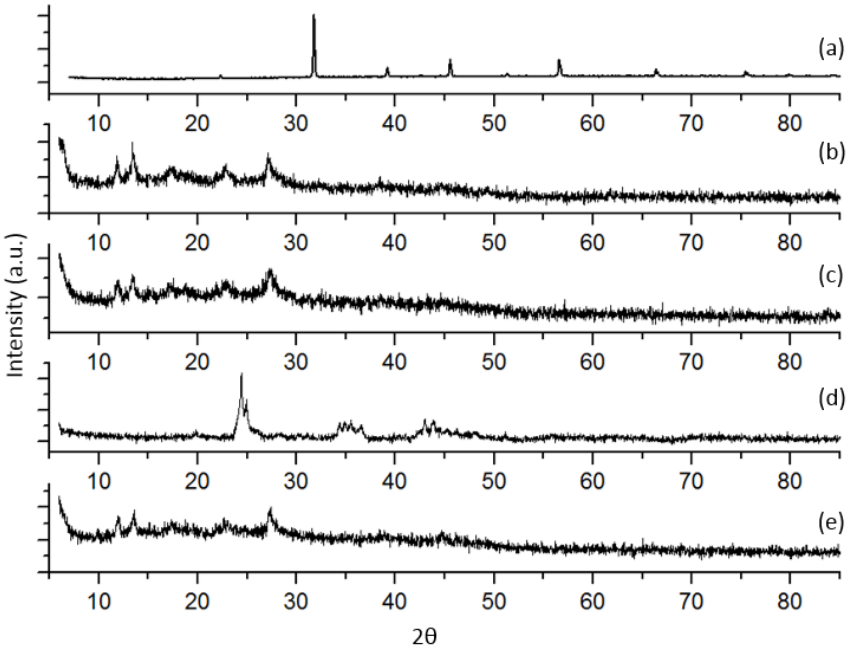

Figure 19 – XRD patterns of the samples calcined for: (a) 8 hours on the conventional furnace; (b) 10 min; (c) 20 min; (d) 30 min and (e) 40 min on the microwave

Expectations were that the sample that was calcined for 40 minutes would behave similar to the sample that was calcined for 30 minutes, becoming incandescent and release some smoke, or even exhibit a more developed crystalline phase in the XRD pattern. Taking into account that the results were extremely different from the expectations, it was possible to conclude that the microwave radiation was not interacting well with the sample, and the temperatures reached for the sample calcined for 30 minutes were due to heating through conduction, instead of radiation.

The idea behind this hypothesis was that after processing the first two samples for 10 and 20 minutes each, the ceramic sheet used under the samples (for safety purposes) were already hot and with the incidence of the microwave radiation on this sheet, this apparatus was hot enough to heat the sample through conduction. To prove this hypothesis, the ceramic sheet was irradiated with microwave radiation for a few seconds and it heated tremendously. Another test to check the interaction between the perovskite samples and the microwave was performed without any support of a ceramic sheet. Impressively, the sample was not heating enough, even after several minutes inside the microwave.

Despite obtaining somehow a crystalline phase when using the thermocouple attached to the microwave, the system was considered unstable. Sometimes the sparks were too intense to produce a powder with strong peaks of the perovskite phase and with few impurity peaks, but sometimes the sparks were not intense enough and only an amorphous phase was obtained. The idea of buying a thermocouple that would endure the temperatures was discarded, since it would be too expensive to buy. Without the thermocouple, the microwave radiation was not heating enough the precursor powder and the conductive mechanism was predominant. Thus, the use of the adapted microwave for calcination of the precursor powder was interrupted due to all these facts.

A brief analysis was done in the powder obtained by drying the solution on the microwave and posteriorly heat treating the gel on the conventional furnace. By doing this, the process of drying the solution took only 15 minutes, instead of the 2-4 hours needed to dry it by the conventional method. However, the powder exhibited lower values of specific surface area (0.644 m^2/g) when compared to the powder formed by the conventional synthesis method (0.858 m^2/g).

Therefore, all tests on the household adapted microwave were suspended due to the results obtained. Creating a stable system that would allow the rapid production of pure perovskite would represent a great advance on the commercial deployment of perovskite membranes for use on the industrial scale. Considerable effort is required for successful adaptation of a household microwave, however it possesses a great potential yet to be explored.

5.2. Synthesis optimization

5.2.1. Initial analysis

The first stage for synthesis optimization was carried out by comparing both chosen synthesis routes. Initial analysis was performed to understand the studied system and the synthesis mechanism. Several works used temperatures of 900°C in the calcination stage in order to obtain BSCF powder, with the majority heat treating the precursor powder for times as long as 8 hours. Thus, for this first analysis it was used times of 8 hours for the calcination of the powders.

Addition of the ethylene glycol on the precursor solution was idealized with the intention to support the formation of the cross-linked chain of organic-metal complexes. In this path, it is suspected that all organic-metal complexes in the solution will be strongly bonded to the whole chain and, as a result, avoid any segregation. In the absence of segregation within the solution, the primary powder obtained by drying the gel will be in a well mixed state, which is highly desirable for the calcination. Ideally, a powder with even distribution of metal cations in the submicron range will benefit the reaction between particles, because of shorter length that each cation has to diffuse, and the pure perovskite structure might be obtained at lower temperatures.

However, the addition of ethylene glycol increases the amount of organic matter on the solution. This can represent a limitation for the complete burnout of the organics and posterior degradation of intermediate phases. Predictions of which factor will be more predominant are difficult and thermogravimetric (TG) analysis were carried out in order to detail to what extent each factor is more or less predominant.

The thermogravimetric profile of the gel drying obtained by the CA-EDTA method, Figure 20, exhibited a curve with four major peaks of mass loss. The first at 59°C is probably due to the evaporation of H_2O, NO_x and NH_4, and the second at 229°C attributed to the degradation of organic matter and release of CO_2, which was confirmed by mass spectrometry. The third and fourth peaks of mass loss were also because of release of CO_2, but this time probably because of degradation of intermediate carbonates. Mass loss stopped at about 760°C and maintained stable until 900°C, indicating complete decomposition of these carbonates at 760°C. At the end of the analysis, the final mass was 8.8% of the initial value.

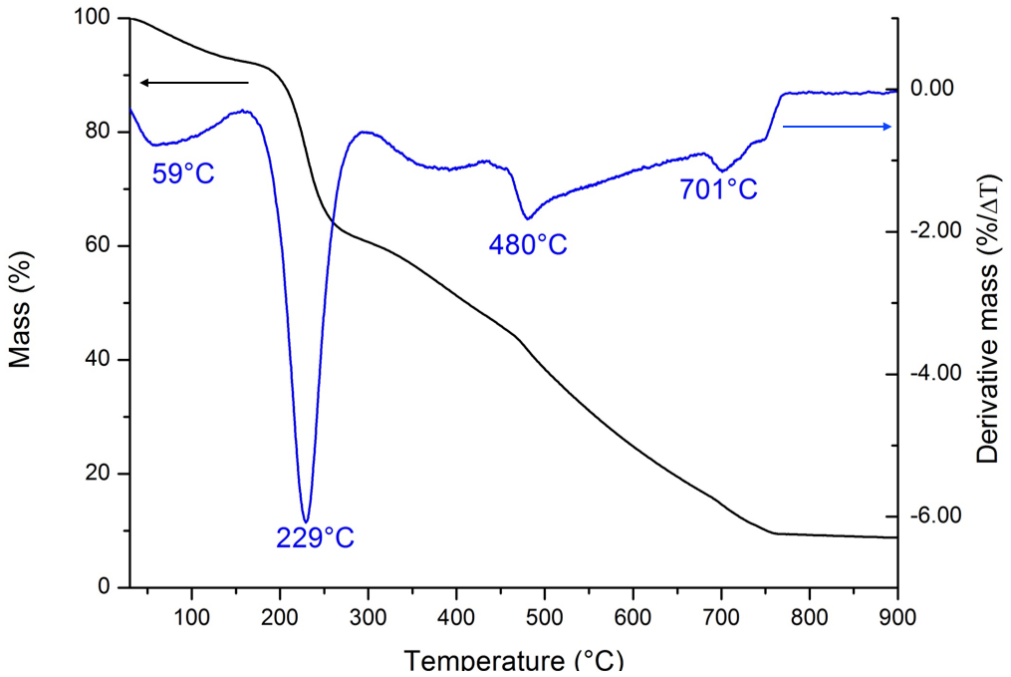

Figure 20 – Thermogravimetric profile of the powder synthesized by the CA-EDTA method

The gel obtained by the CA-EDTA-EG method resulted in a similar TG pattern, but with small differences that indicate the interference of ethylene glycol on the system. One may notice in Figure 21 four mass loss peaks, all very similar to the peaks found in Figure 20, and mass spectrometry confirmed that the same gases were released. The first two peaks were dislocated to higher temperatures, which can be attributed to the higher amount of organic matter in the sample. However, the third and fourth peaks were shifted towards lower temperatures while they appear to be narrower and more intense. This might indicate that there is a more intense degradation of carbonates at lower temperatures.

Nonetheless, the main difference here is that in this case the compound kept losing mass until the temperature reached 900°C, in other words, the carbonates were not completely decomposed. In this case, the mass loss does not stabilize at any temperature, and the sample keeps loosing significant mass even at 900°C. The final mass is 12.8% of the initial mass, which might indicate that there were a few intermediate compounds yet to be decomposed.

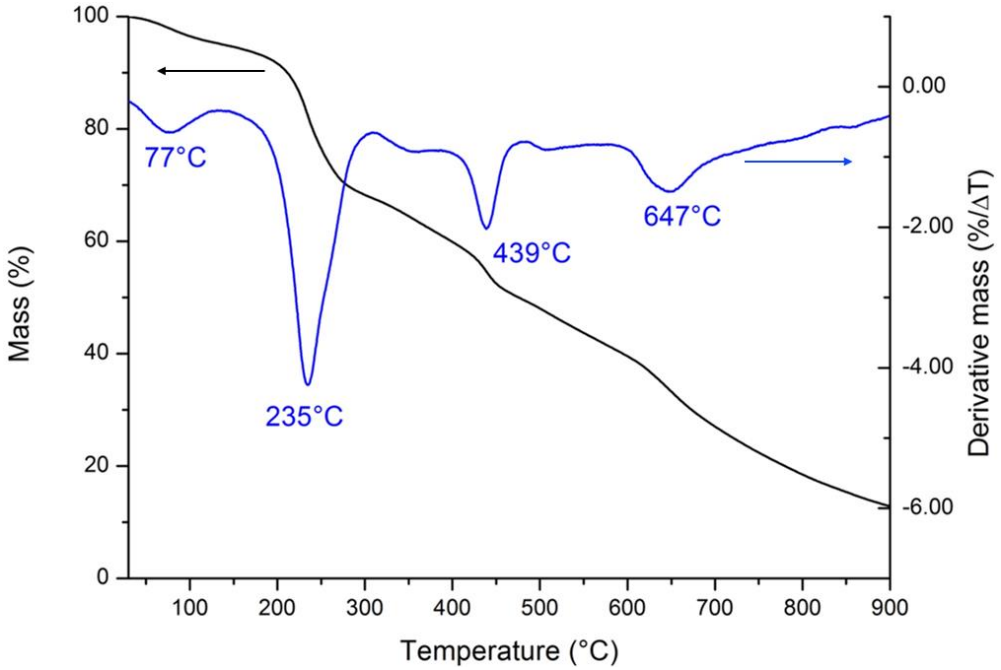

Figure 21 – Thermogravimetric profile of the powder synthesized by the CA-EDTA-EG method

Assessment of phase development of each synthesis route was achieved by comparing XRD patterns of powders calcined at 700°C, 800°C and 900°C. For both routes, the patterns were almost identical, as observed in Figure 22 and Figure 23. Pure perovskite phase was obtained for the powder calcined at 800°C and 900°C, with no clear difference on the results for each calcination temperature. The powder calcined at 700°C exhibited a few less intense peaks that were attributed in previous works to a series of intermediate compounds of carbonates and oxides of present cations, as detailed on both XRD patterns [81].

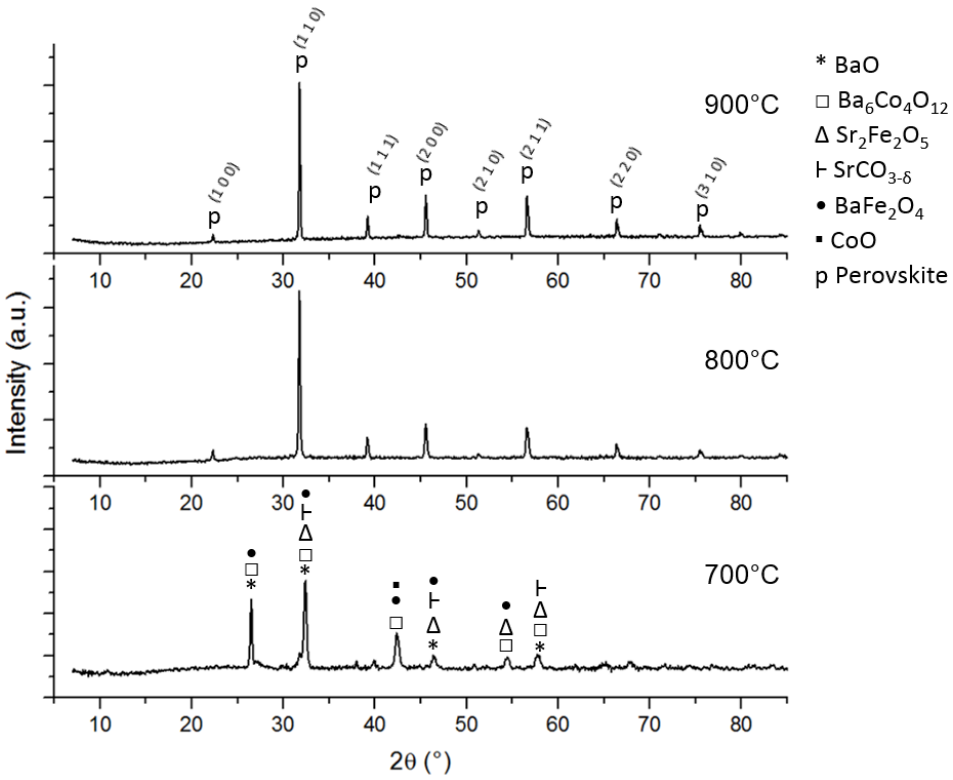

Figure 22 – XRD patterns of the powders synthesized by the CA-EDTA method and at different calcination temperatures

The idea that there would still be some impurities at 900°C for the powder produced by the CA-EDTA-EG route could not be proven by the XRD pattern. It is known that XRD analysis is not accurate for assessment of impurities phases with concentrations lower than 5%, thus, it is reasonable to estimate that there are only traces of impurities on the material synthesized by the CA-EDTA-EG route. Despite the successful production of pure perovskite phase at 800°C and 900°C, the chosen calcination temperature for further analysis was 900°C in order to avoid that any possible impurities might compromise the other results.

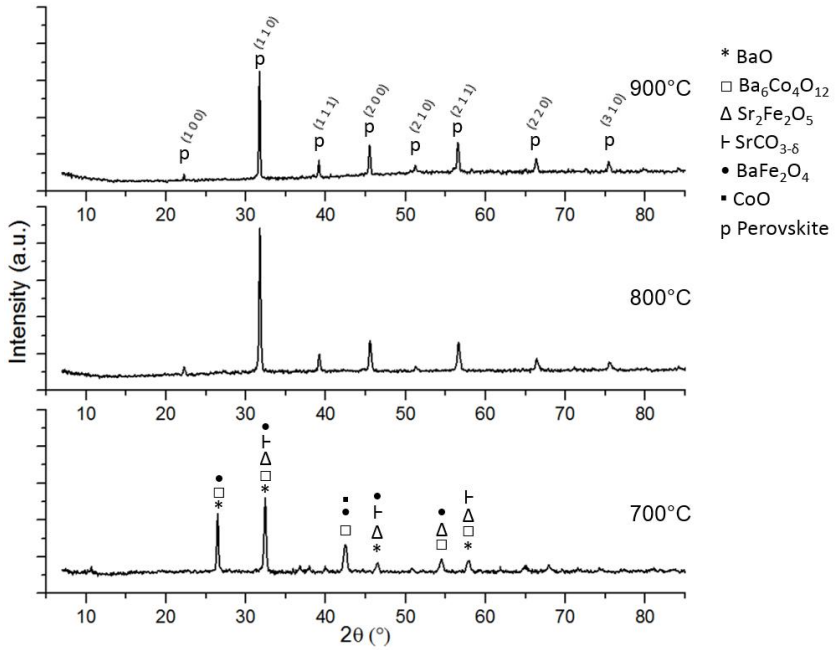

Figure 23 – XRD patterns of the powders synthesized by the CA-EDTA-EG method and at different calcination temperatures

Membranes sintered at 1,000 °C and 1,100 °C, both for 8 hours, were also analyzed by SEM micrographs to understand the densification mechanism of the BSCF material synthesized by the two different routes. From Figure 24, it is clear that the densification was not enough for disks sintered at 1,000°C, since it is possible to notice a high concentration of pores on the membrane surface. Also, no clear grain boundaries were evidenced, which is sufficient to suspect that the used temperature was not high enough for successful sintering.

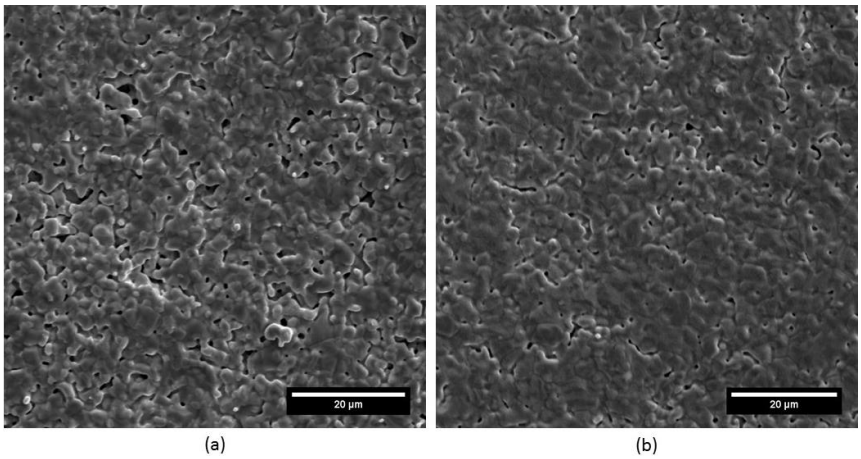

Figure 24 – SEM image of perovskite membranes sintered at 1,000 °C for 8 h, (a) BSCF synthesized by CA-EDTA method and (b) BSCF synthesized by CA-EDTA-EG

On the other hand, membranes sintered at 1,100 °C for 8 hours, as shown in Figure 25, exhibited complete densification with absence of pores on the surface. Grain boundaries are visible on both samples and the grain sizes are clearly increased. Thus, for this material, a temperature of 1,100 °C for 8 hours was enough to guarantee complete densification and posterior grain growth on the last stages of the sintering process. No clear differences on the grain size were found between these samples.

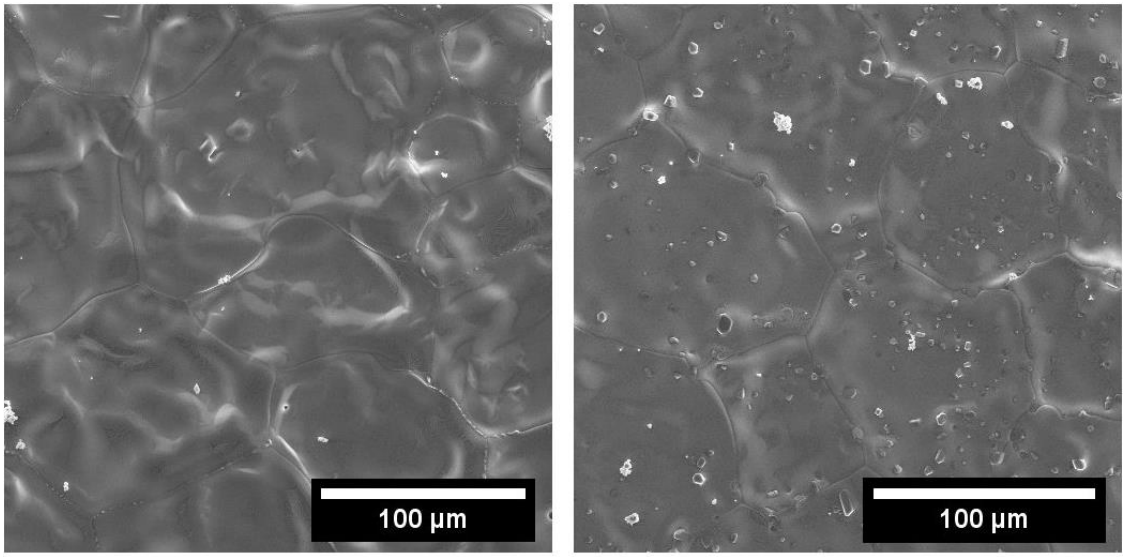

Figure 25 – SEM image of perovskite membranes sintered at 1,100 °C for 8 h, (a) BSCF synthesized by CA-EDTA method and (b) BSCF synthesized by CA-EDTA-EG

As one may notice in Figure 25, it is possible to observe impurities on the surface of both pellets. Figure 25 (a) exhibited a few powders with no typical geometry and EDS analysis showed that they are BSCF powders. The presence of this impurity might be because of the vessel used to hold the sample that could have some remaining powder that broke from the pellet before sintering. Regarding the membrane on Figure 25 (b), a different phase was found on the surface. This phase displayed well defined edges and it could be found above or incrusted onto the surface, as detailed in Figure 26. It was found by EDS that it is enriched with cobalt and oxygen, thus it is possible to attribute this phase to cobalt oxide. However no further information of the crystal phase was possible to obtain with the used characterization methods. No secondary phase was found for disks sintered at 1,000 °C, which might indicate that the formation of cobalt oxide on the surface of the

membrane takes place when the material is processed at temperatures higher than 1,000 °C.

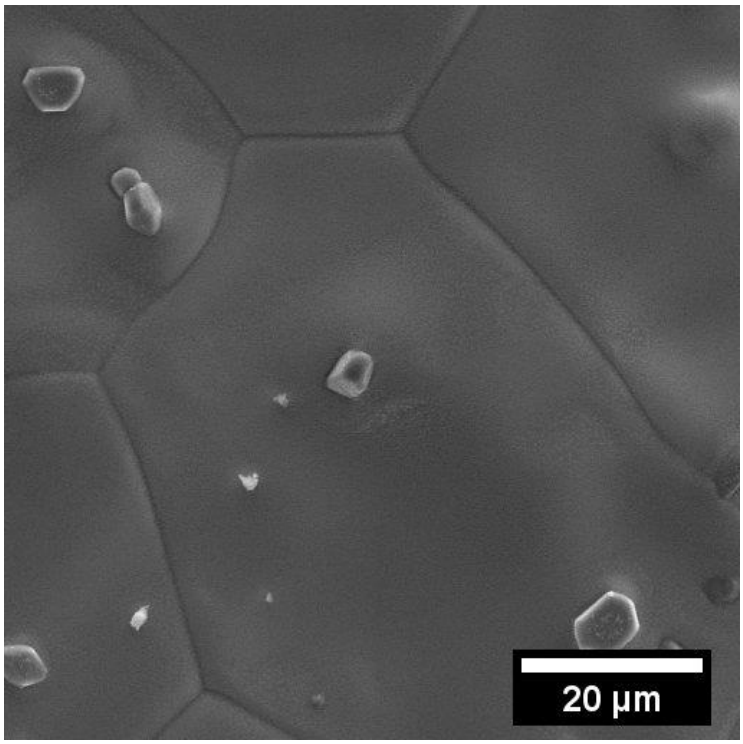

Figure 26 – Detail of the secondary phase found on the membrane sintered at 1,100 °C for 8 h using the powder synthesized by the CA-EDTA-EG method

These initial results were enough to master the procedures of powder synthesis and membrane consolidation, in other words, the purpose of the initial analysis was accomplished. For now, the use of ethylene glycol does not seem to have positive impacts on the synthesis of BSCF powders, as thermogravimetric results demonstrate that higher temperatures are necessary for complete degradation of impurities and that the sintering process at high temperatures lead to the formation of a secondary phase at the surface of the membranes.

5.2.2. Synthesis parameters optimization

It is clear that at calcination temperatures higher than 800°C the perovskite phase is already fully developed. However, the powder synthesized by the CA-EDTA-EG route still loses mass at 900 °C, which is an evidence that there are still some impurities to be degraded. Some authors have reported the calcination of perovskites at temperatures as

low as 700 °C with posterior sintering at 1,100°C [15]. As shown in Figure 22 and Figure 23, the perovskite phase is not present on the XRD patterns at temperatures of 700 °C. Therefore, the calcination at 700 °C might not lead to development of the perovskite phase, but could produce a powder with improved properties that would allow higher and faster densification of during the membrane preparation. Considering that the sintering temperatures are high enough to develop the perovskite phase, using a powder for membrane sintering that is not perovskite yet could not be an issue. This is confirmed by the mentioned report, since they analyzed a XRD pattern of the sample after sinterization and the result was a fully developed perovskite phase [15].

Between the properties that play an important role on the sinterization process, high specific surface area is highly desirable. For other applications that do not involve membrane production, such as catalysis, this is critical for satisfying performance. Thus, the specific surface area was chosen as the property used to determine the optimized route. The calcination temperature and time at the maximum temperature were the parameters to be optimized. Both were chosen due the high amount of energy demanded by the perovskite processing and any improvements on these two parameters would result in less energy required on the process.

Evaluation of the perovskite phase development using powders produced by the CA-EDTA route was checked by XRD analysis, resulting on the XRD patterns on Figure 27. For the powders calcined at 700 °C, peaks typical of perovskite phase were not visible. As detailed in Figure 22, the visible peaks are attributed to a series of intermediate phases: BaO, $Ba_6Co_4O_{12}$, $Sr_2Fe_2O_5$, $SrCO_{3-\delta}$, $BaFe_2O_4$ and CoO. In these XRD patterns there is another peak typical of $BaCO_3$ at 24.4 ° [81], which becomes weaker with increasing the calcination times, and some even disappear for calcination time of 8 hours. Other intermediate phase peaks become narrower and slightly more intense for longer times, which is an indication that their development depends on the calcination time. At 800 °C the perovskite phase is already fully developed and it was similar to the XRD pattern of the powders calcined at 900 °C for 8 h. The peaks of the powder produced at 1,000 °C were typical of the perovskite phase, however one characteristic peak at 75.4 ° is not visible, while the other peaks became wider. This is an indication that at 1,000 °C the crystallite size of the material is increased.

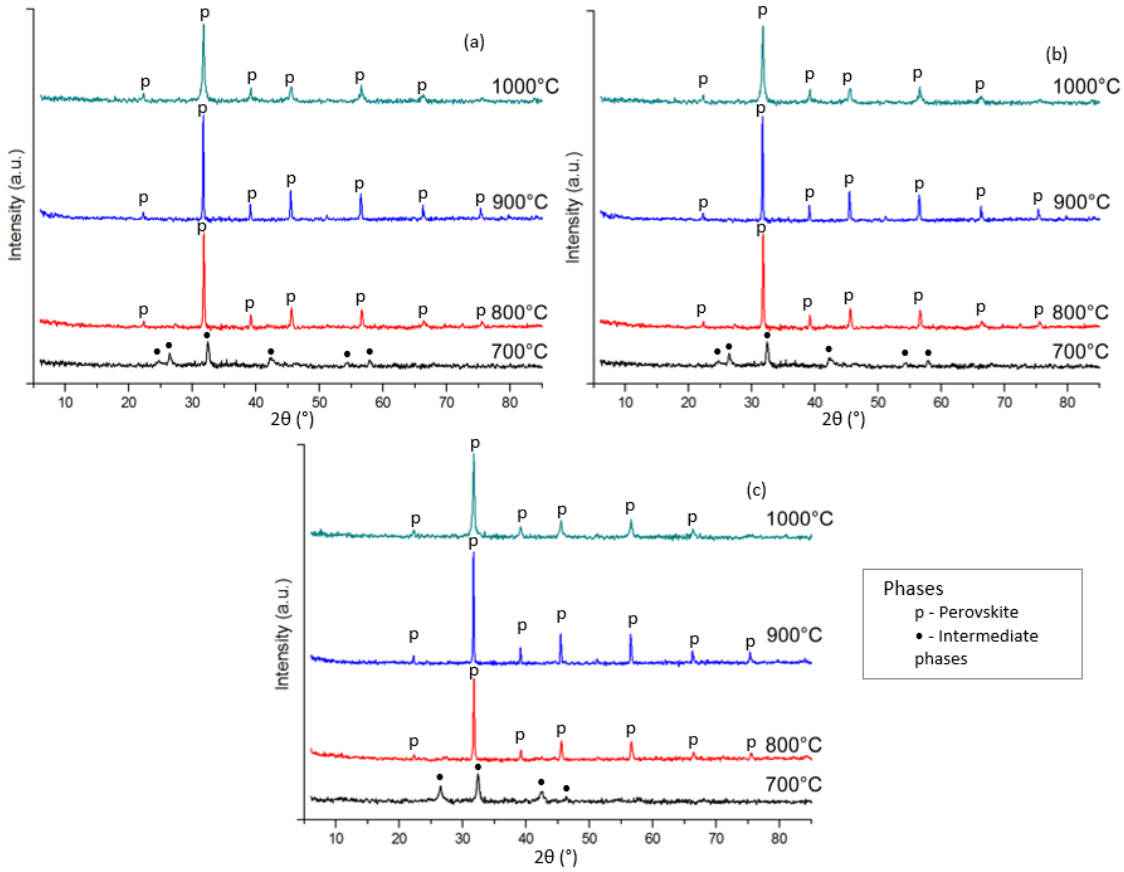

Figure 27 – XRD patterns of the powders obtained by the CA-EDTA route with calcination times of (a) 4 hours, (b) 6 hours and (c) 8 hours

Evidences of the correlation between calcination times and phase development were only found for calcination temperatures of 700 °C. For temperatures higher than 800 °C the XRD patterns resulted from different calcination times were identical. Thus, this finding suggest that perovskite powder could be produced with heat treatments half of the time regularly used on the literature, which is already an improvement on the energy demand of the production process. Moreover, crystalline perovskite could be obtained at 800°C, representing another improvement on the energy demand of the process.

The analysis of the powders synthesized by the CA-EDTA-EG route resulted in the XRD patterns shown in Figure 28. This time the powder calcined at 700 °C for 4 hours exhibited a more intense peak at 2θ values of 24.4 °, attributed to the $BaCO_3$ phase, while the other intermediate phases seem to be suppressed. As the calcination time increased, the intensity of the $BaCO_3$ peak was lowered but did not disappear when calcined for 8 hours, while peaks typical of other intermediate phases became sharper. This could indicate that

the use of the ethylene glycol increases the organic matter in a way that the precursor powders possess higher concentration of residual carbonates, generating more resistance for complete degradation of these carbonates and development of the perovskite phase.

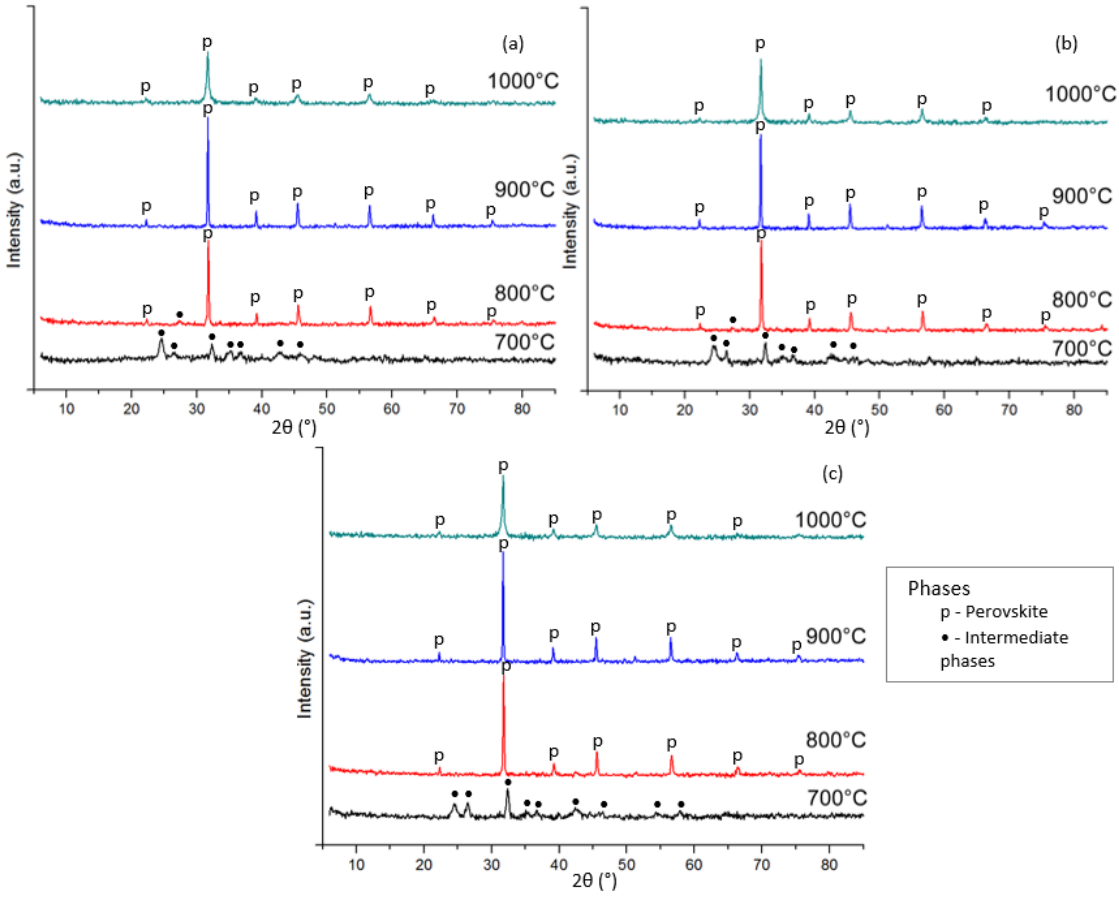

Figure 28 – XRD patterns of the powder obtained by the CA-EDTA-EG route with calcination times of (a) 4 hours, (b) 6 hours and (c) 8 hours

For the powder produced at 800 °C, the perovskite phase was well developed, however for calcination times of 4 and 6 hours it is possible to distinguish a weak peak typical of intermediate phases [81], indicating that the perovskite phase is not pure yet. Only when calcined at 800 °C for 8 hours that the perovskite phase could be considered pure. The XRD patterns of the powders obtained at 900 °C and 1,000 °C are identical to the XRD patterns of the powders synthesized by the CA-EDTA route. At both temperatures the perovskite phase is pure and complete developed, nonetheless the peaks of the samples treated at 1,000 °C are broader, indicating increase on the crystallite size.

According to the XRD patterns on Figure 27 and Figure 28, the addition of ethylene glycol did not help the calcination stage. The idea was that this would create a more interlinked system, which could result on a precursor powder that would require lower energy for complete development of pure perovskite. However, it seems that the increase on the organic matter interfere more intensively on the calcination stage. In fact, higher temperatures and longer calcination times were necessary for pure perovskite production. Therefore, the use of ethylene glycol does not seem to improve any stage of the synthesis process with the results so far.

It is known that FTIR spectroscopy is more precise than XRD to detect the presence of trace carbonates below 5%. Thus, FTIR analysis was also performed for the samples [176]. As demarked in spectra of the powder synthesized by the EDTA-CA method (Figure 29), the main peaks found on the spectra are observed at around 590, 659, 748, 858, 1450 and 1620 cm^{-1}. The two bands at 590 and 748 cm^{-1} are typical of stretching vibration of the metal oxygen bond in the perovskite phase, while the peak at 659 cm^{-1} can be attributed to the stretching vibration of the metal oxygen bond of intermediate oxides [177,178]. Samples calcined at 700 °C exhibited these three bands and, since XRD analysis showed that the perovskite phase was not present on the powder calcined at 700 °C, these bands can be attributed to intermediate oxides, but only for samples calcined at 700 °C. Stretching and twisting vibration of carbonates are attributed to the absorption bands at 858 and 1450 cm^{-1}, and the band at 1620 cm^{-1} is associated with the presence of physically adsorbed H_2O [179].

Essentially, when the calcination temperature is 700 °C, the use of longer times for the calcination results on lowering the amount of intermediate phases. As one may notice, all bands became weaker as calcination time changed from 4 h to 8 h. In fact, most bands are almost not visible for the sample calcined for 8 h, only the band at 1450 cm^{-1} remains distinguishable. Increasing the temperature to 800 °C lead to formation of the two bands typical of the perovskite structure. No intermediate oxides were present, however the other intermediate phases are still visible, with the band at 1450 cm^{-1} being the most visible. No influence of the calcination time was evident for this temperature. Similarly, at 900 °C the calcination time does not have any influence on the FTIR spectra. Regarding the intermediate phases, the band at 1450 cm^{-1} decreases, indicating that there are only

traces of the carbonates. Finally, at 1,000 °C the bands of the perovskite structure became almost flat, while the bands at 1450 and 1620 cm^{-1} slightly increased their intensity. Possibly, this was evidenced due to formation of phases other than the perovskite at the used temperature.

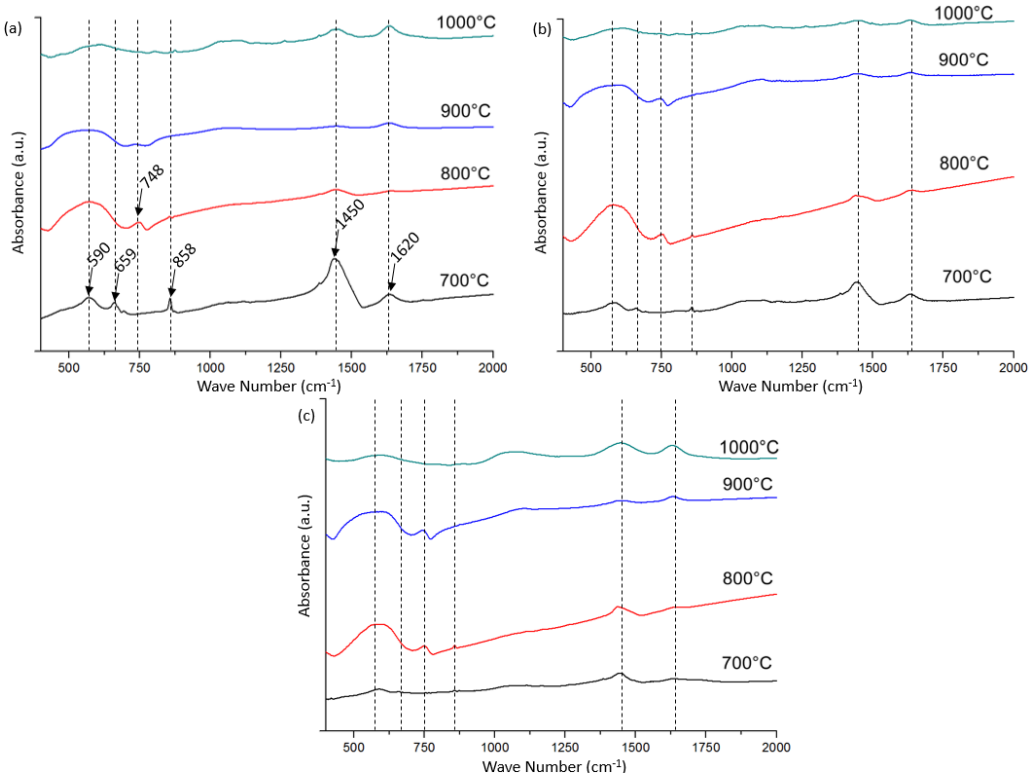

Figure 29 – FTIR spectra of the powders synthesized by the CA-EDTA route, with calcination times of (a) 4 hours, (b) 6 hours and (c) 8 hours

Figure 30 shows FTIR spectra of the powder synthesized by the CA-EDTA-EG route. Both bands typical of carbonates on the spectrum of the powder calcined at 700 °C are more intense, when compared to Figure 29. This is in accordance with results from the XRD analysis, which showed that this route produces a powder with higher concentration of carbonates. Even for calcination times of 8 h the bands remain visible. The samples produced at 800 °C, 900 °C and 1,000 °C exhibited the same results as the powder synthesized by the CA-EDTA route, at 800 °C the perovskite bands are already visible and it is possible to visualize the bands attributed to carbonates. At 900 °C there are only traces of the intermediate phases and at 1,000 °C the bands of the perovskite phase

became almost flat, while the bands attributed to the carbonates slightly increased their intensity, similar to what was observed for the CA-EDTA route.

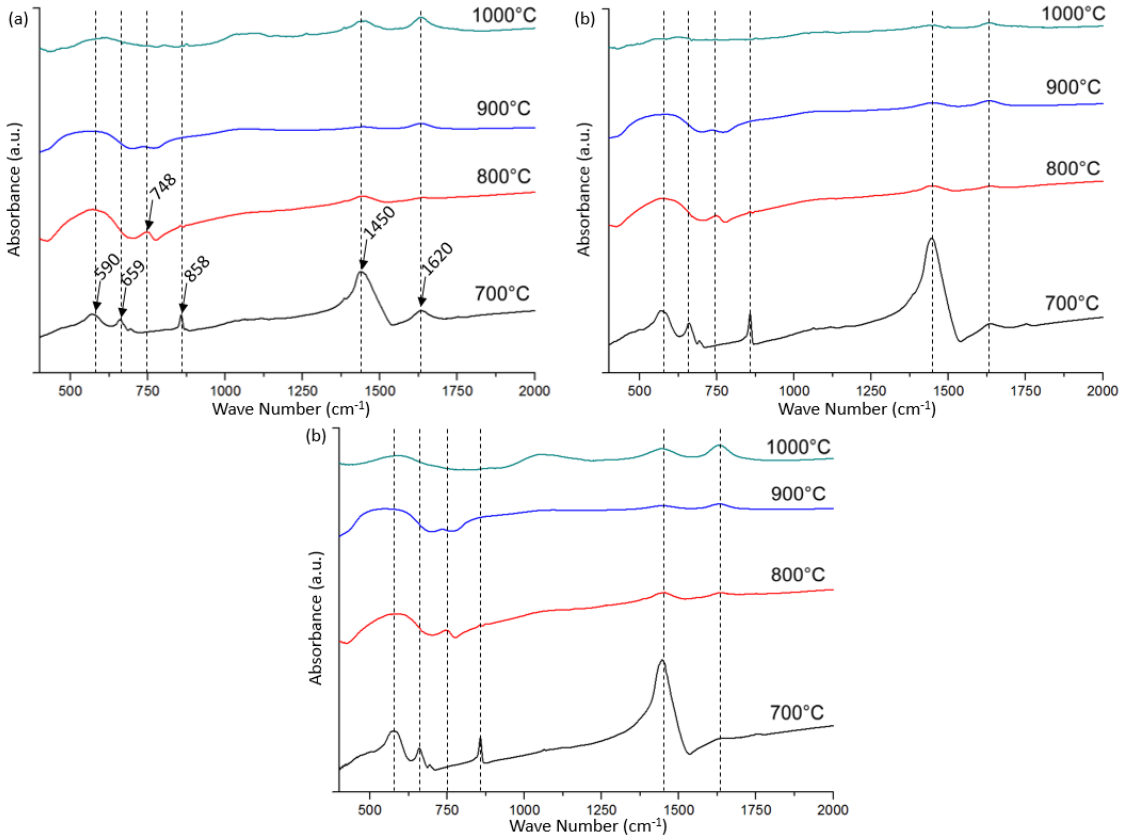

Figure 30 – FTIR spectra of the powders synthesized by the CA-EDTA-EG route, with calcination times of (a) 4 hours, (b) 6 hours and (c) 8 hours

The FTIR spectra confirmed that the samples obtained by the CA-EDTA-EG route and with calcination temperatures of 700 °C exhibit a higher concentration of carbonates when compared to the powder synthesized by the CA-EDTA route. Nonetheless, it was not possible to determine any differences between the two routes when the precursor powder was calcined at higher temperatures, as detailed in the XRD analysis, in which it was found that powders calcined at 800 °C for 4 and 6 hours exhibited traces of impurities.

In conclusion, both routes resulted in samples with least amount of impurities at 900 °C, with no clear influence of the calcination time for this temperature. Curiously, samples calcined at 1,000 °C were not the samples with least concentration of carbonates, as expected and reported on the literature [81]. Perovskite powder could be obtained at 800 °C, however the concentration of carbonates found on the FTIR spectra might interfere

in the properties of the final material. The decrease of perovskite bands and increase of other bands for samples calcined at 1,000 °C is an indication that somehow the perovskite is being consumed and forming other undesirable compounds.

The BET analysis of the synthesized powders allowed the estimation of specific surface area. Comparison of the specific surface area of each powder is shown in Figure 31. It was expected that increasing the calcination temperature, the values would decrease, due to a pre-sintering process in which densification of the particles start to take place with particles merging and forming necks between them. This phenomenon results in decrease of the exposed area per volume, leading to lower specific surface area. Hence, it was expected that higher temperatures would lead in lower specific surface areas.

However, the results (Figure 31) show no clear pattern of the specific surface area related to the studied parameters. One possible reason to understand the absence of patterns on the results is that the values of specific surface area were considered low when compared to the values attributed to materials normally characterized by the BET technique. Thus, the error associated with the results could be considered too high for accurate comparison between all the samples. Nevertheless, an error bar of 5% was adopted for this analysis, since a statistical approach was not performed.

In order to explain the results, it is necessary to understand that the presence of impurities or intermediate phases might interfere on the found values. Specific surface area is extremely dependent on the geometry of the particles, as the ratio between surface area and volume of the particle varies with the geometry. Also the precursor powder was originated from a framework structure, composed of intermediate carbonates and oxides, after burnout of the organic matter. Hence, this structure is initially thoroughly interconnected and the exposed area of the particles could be lowered if these intermediate phases are not fully consumed in the calcination process.

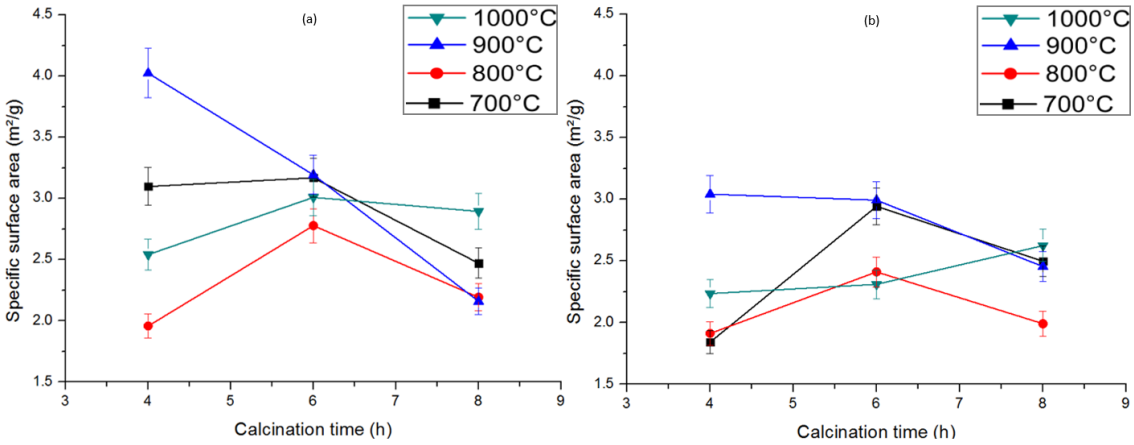

Figure 31 – Specific surface area of the powders synthesized by the (a) CA-EDTA route and by the (b) CA-EDTA-EG route

For instance, samples treated at 700 °C did not exhibit the highest values for specific surface area as expected. However, the presence of impurities and secondary phases make it difficult to compare the samples treated at 700 °C to the others, since only above 800 °C the perovskite phase was obtained. For temperatures higher than 800 °C the samples prepared by the CA-EDTA route displayed specific surface area 12% higher than the ones synthesized by the CA-EDTA-EG route, with an exception for the samples treated at 900 °C for 4 hours, which showed an increase of 68% on the specific surface area. The mean difference of 12 % between the two routes suggests that the CA-EDTA route produced powders in a more desirable state for posterior sintering. For both routes the optimized parameters for calcination was at 900 °C for 4 hours.

The main difference between the two routes is the ratio between the organic matter and precursor metals used for formation of the solution. After the first heat treatment at 450 °C and burnout of the organic matter, the complexed metals form the intermediary phases. Increase on the organic matter resulted in powders with higher amount of intermediary phases, as seen by the previous results of samples calcined at 700 °C. Also, the different ratios affect the properties of the final material. For instance, it is suggested that the higher organic matter to metals ratio on the CA-EDTA-EG route produced a material with agglomerates connected more strongly. Thus, the grinding of this powder requires more energy. In contrast, the CA-EDTA route produced a powder with agglomerates that were easily broken apart. To confirm this idea a simple experiment was performed to assess how much the specific surface area of the powder increased by grinding the samples with

identical parameters in an industrial disc mill. The increase was of 413% for the CA-EDTA route while the increase for the CA-EDTA-EG route was only 53%. Thus, these results confirm that the perovskite synthesized with the use of ethylene glycol produced agglomerates that were more difficult to grind.

Therefore, use of ethylene glycol for higher connectivity between the cations in order to produce enhanced powders was not successful. Indeed the perovskite phase was present at similar heat treatment parameters, however the higher amount of intermediary phases was visible at lower temperatures. In general, the specific surface area was higher without the use of ethylene glycol and it was shown this is due to the lower resistance for grinding of the powder obtained by the CA-EDTA route. Besides all these drawbacks, the main issue of using the ethylene glycol was the presence of the cobalt oxide found on the surface of the sintered membranes. This impurity was always present for membranes produced from the CA-EDTA-EG route and this represents that some of the cobalt used for perovskite synthesis was consumed during sintering, leading to a material with stoichiometry different from the desired. Moreover, the cobalt oxide would probably interfere on the surface reaction with the oxygen and worsen the membrane performance.

In conclusion, the CA-EDTA route was confirmed to be the most suitable for this paper and was the method used at this work from now on. For future work with pure BSCF, it is suggested the calcination of the material at 900 °C for 4 hours.

5.3. Synthesis of BSCF perovskite with partial substitution

Partial substitution of some cations on the perovskite structure might culminate on creation of a novel structure with higher concentration of oxygen vacancies, generating a material with higher oxygen permeation. Additionally, it is known that the use of cations with larger ionic radius for partial substitution on A or B-site of the perovskite structure creates a compound with higher stability. Thus, two cations were chosen for partial substitution on the BSCF structure, cesium to be partially substituted on the A-site of the BSCF and then yttrium was incorporated on the B-site of the BSCF. The used method consists on partial substitution of all cations on the A or B site, and the formula used was $Cs_x(Ba_{0.5}Sr_{0.5})_{1-x}Co_{0.8}Fe_{0.2}O_{3-\delta}$ and $Ba_{0.5}Sr_{0.5}(Co_{0.8}Fe_{0.}2)_{1-x}Y_xO_{3-\delta}$, respectively.

Another approach to create a perovskite compound with higher stability found in the literature was by partial substitution of scandium on the B-site [85]. Thus compounds with the formula $Ba_{0.5}Sr_{0.5}(Co_{0.8}Fe_{0.}2)_{1-x}Sc_xO_{3-\delta}$ were also synthesized and the stability of this compound analyzed by different techniques. From now on, the doped compounds will be named with the general formula: BSCF – M X, with M being the cations Cs, Y or Sc, and X ranging from 0 to 40%.

5.3.1. BSCF – Cs

Cesium is considerably larger than the cations at the A-site, thus substitution of cesium on the perovskite structure might not generate a stable structure, although Goldschmidt factors were within the range recommended for cubic perovskite. Hence, predictions were that the crystal with cesium incorporation would be stable. If the structure is stable enough to maintain the cubic structure with the use of cesium, the final material is suspected to exhibit high concentration of oxygen vacancies. To begin the analysis of the doped perovskite, it was necessary to evaluate the temperature required for formation of pure perovskite phase and complete development of the perovskite phase.

The development perovskite phase of samples produced with different amounts of cesium were investigated by the XRD patterns found in Figure 32. Besides the sample with 40% substitution with cesium, all samples formed pure perovskite phase with peaks of similar intensity and mean length. For the sample BSCF – Cs 40%, the XRD patterns exhibited a few weak peaks of impurities (Co_3O_4 and $Ba_8Fe_8O_{21}$), thus pure perovskite was obtained only for samples with partial substitution less than 20%. Further analysis of the main peaks of the perovskite structure revealed that all peaks shifted to higher 2θ values, indicating changes on the unit cell size.

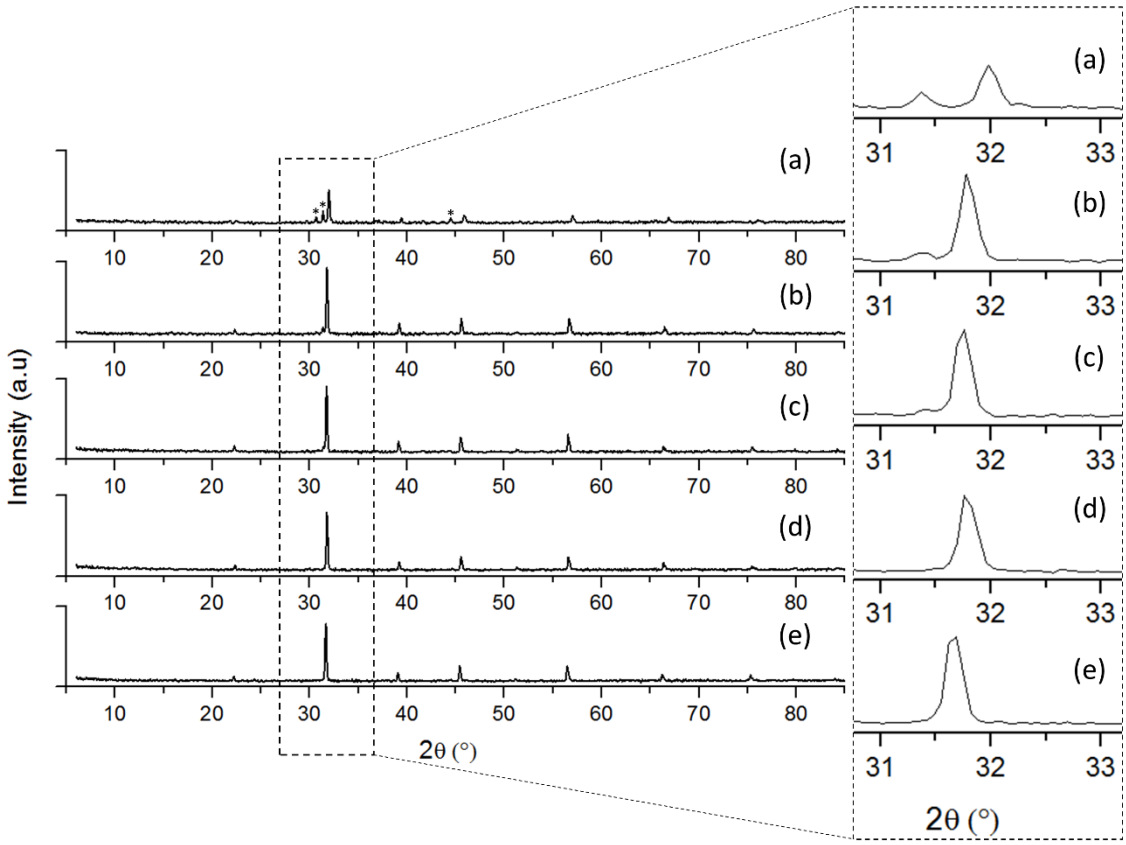

Figure 32 – XRD patterns of BSCF – Cs X% with X values of (a) 40%, (b) 20%, (c) 10%, (d) 5% and (e) 0%. Impurities and intermediary phases are shown with *.

Analysis of the cell unit size is shown in Figure 33. Since cesium is a larger cation than barium and strontium, expectations were that substituting Cs on the A-site would produce a material with higher values of cell unit size. Curiously, the results were not as expected, since higher values of partial substitution of cesium on the BSCF structure produced a material with smaller cell unit size. In fact, the values found for cell unit size followed an almost linear profile.

A possible explanation for this unexpected outcome might be the method chosen for production of doped perovskites. As explained before, the partial substitution was performed in a way that all cations on A-site were partially substituted for cesium, one may notice this by the formula used for this compound $Cs_x(Ba_{0.5}Sr_{0.5})_{1-x}Co_{0.8}Fe_{0.2}O_{3-\delta}$. Thus, if somehow the cesium was not successfully inserted into the crystal structure, there would be a system with deficiency of A-site cations. In other words, the system exhibits an unbalanced stoichiometry between A and B-site cations. It is well known that the A-site cations have the larger ionic radii and a system with deficiency of this A-site cation

would form a final structure composed predominantly by cations with smaller ionic radius and the cell unit size would be relatively smaller. Therefore, it is reasonable to suspect that somehow cesium was not incorporated in the structure.

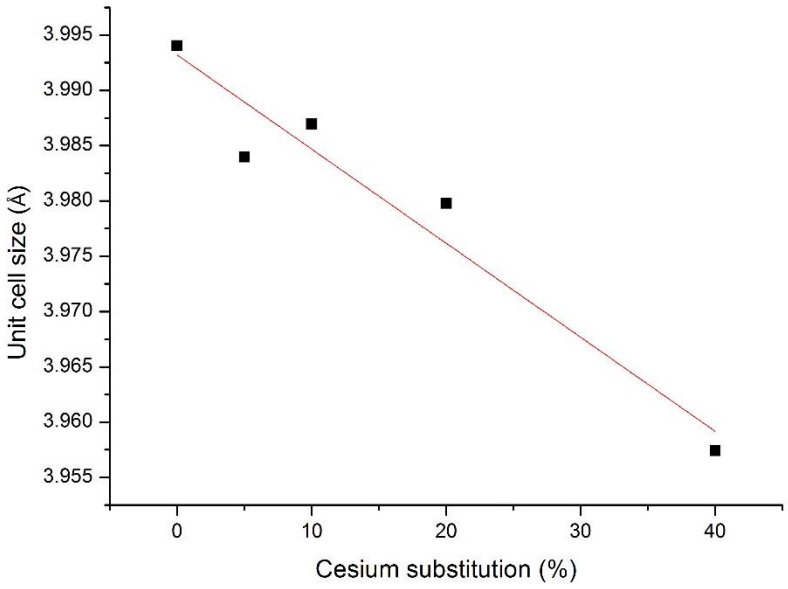

Figure 33 – Unit cell size as a function of cesium substitution on the BSCF structure

Cesium has a boiling point of 678°C, very low when compared to other metals [180]. Consequently, it is possible that cesium was lost on the heat treatment of the dried gel. To confirm this hypothesis, thermogravimetric analysis were performed, as seen in Figure 34, together with mass spectrometry. No major differences were found in the TG profiles, only that the BSCF without dopants exhibited a more intense mass loss until 200 °C, probably due to variances on the amount of water, NH_4 and NO_X that remained in the sample after the gel was dried. A small discontinuity was observed for samples with 5% and 10% substitution at 660 – 670 °C, which might indicate phase transformation with elimination of some compounds.

All samples showed nearly stable mass at temperatures higher than 820 °C. There was no evidence of evaporation of the cesium in the TG profile nor in the data obtained by mass spectrometry. Lack of data from the mass spectrometry is due to the low accuracy of the equipment in the range where cesium compounds were to be detected. In addition, the final mass did not reveal significant difference, it ranged between 8.6 % and 10.8 % of

the initial mass, with no clear pattern. Hence, the TG analysis did not confirm if cesium was lost on the heat treatment or if it remained in the sample.

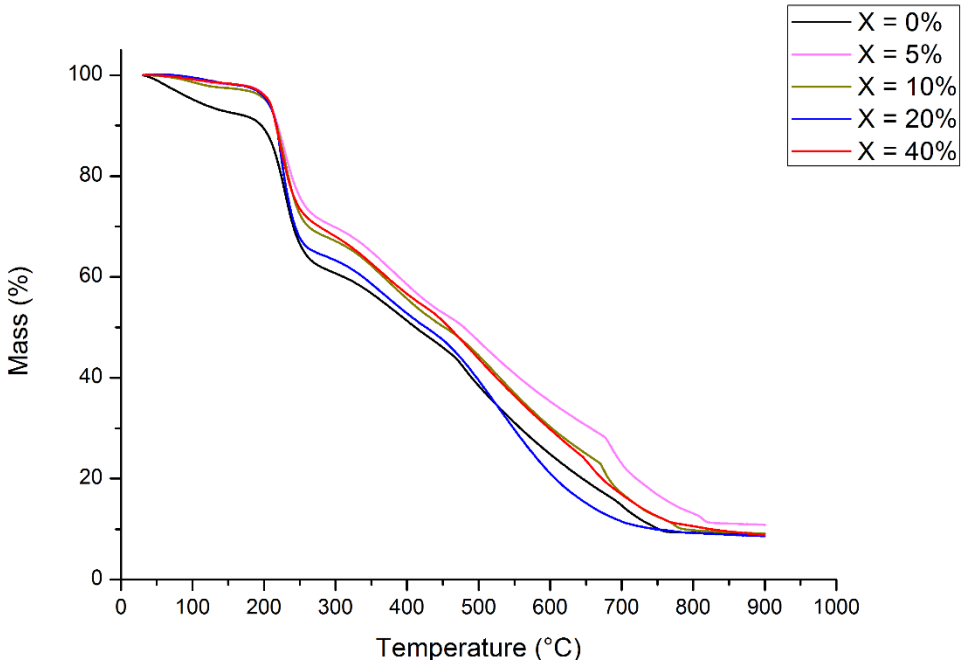

Figure 34 – Thermogravimetric analysis of the BSCF – Cs X precursor powders

In order to check if the cesium created traces of a secondary phase, SEM micrographs were analyzed in Figure 35. All micrographs displayed two different particle morphologies, one amorphous with a tendency to form rounded particles with rough surfaces, and the other morphology with a smooth surface and well defined edges. The presence of the this secondary phase with well defined geometry could be noticed in all BSCF-Cs samples, however in Figure 35 c and d they are more evident. Assessment of chemical composition of both kinds of particles by EDS did not lead to any conclusion because this technique utilizes an electron beam that interacts with a great volume of the sample. In other words, the particles are too small to be precisely measured by this technique. Thus, it was not possible to determine the composition of each particle. Additionally, EDS analysis was performed in order to determine if cesium cations are present, however, the characteristic peak of cesium on the EDS spectrum was not distinguishable from the peak attributed to barium. Consequently, it was not possible to determine if cesium was present on the sample after heat treatment.

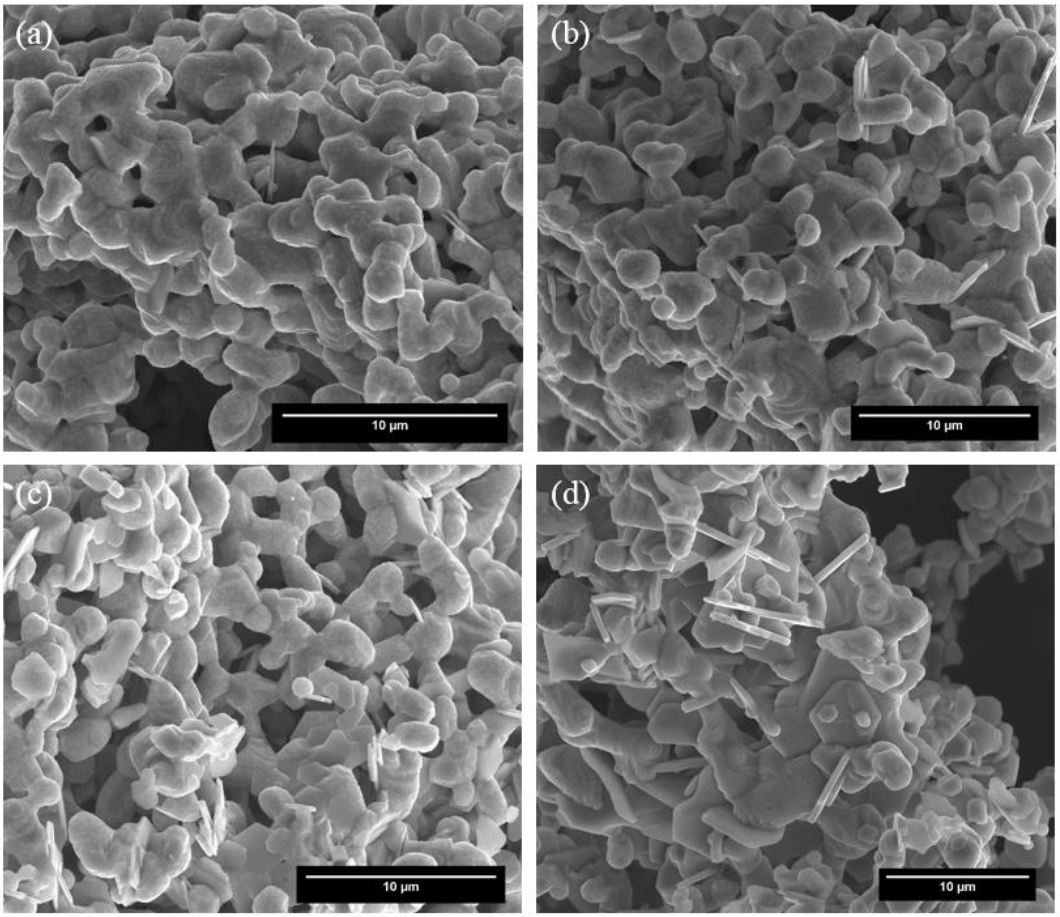

Figure 35 – SEM micrographs of the BSCF-Cs X samples, with X corresponding to (a) 5%, (b) 10%, (c) 20% and (d) 40%

When compared to a micrograph of pure BSCF, it is clear that incorporation of Cs on the synthesis of the BSCF led to the formation of these particles with well defined geometries. Moreover, it seems that the concentration of these particles increase for higher values of partial substitution with cesium, due to a brief analysis of the amount of particles per area of the obtained images. However, they were always present on the sample, regardless of the cesium concentration. These particles are shown in detail in Figure 36.

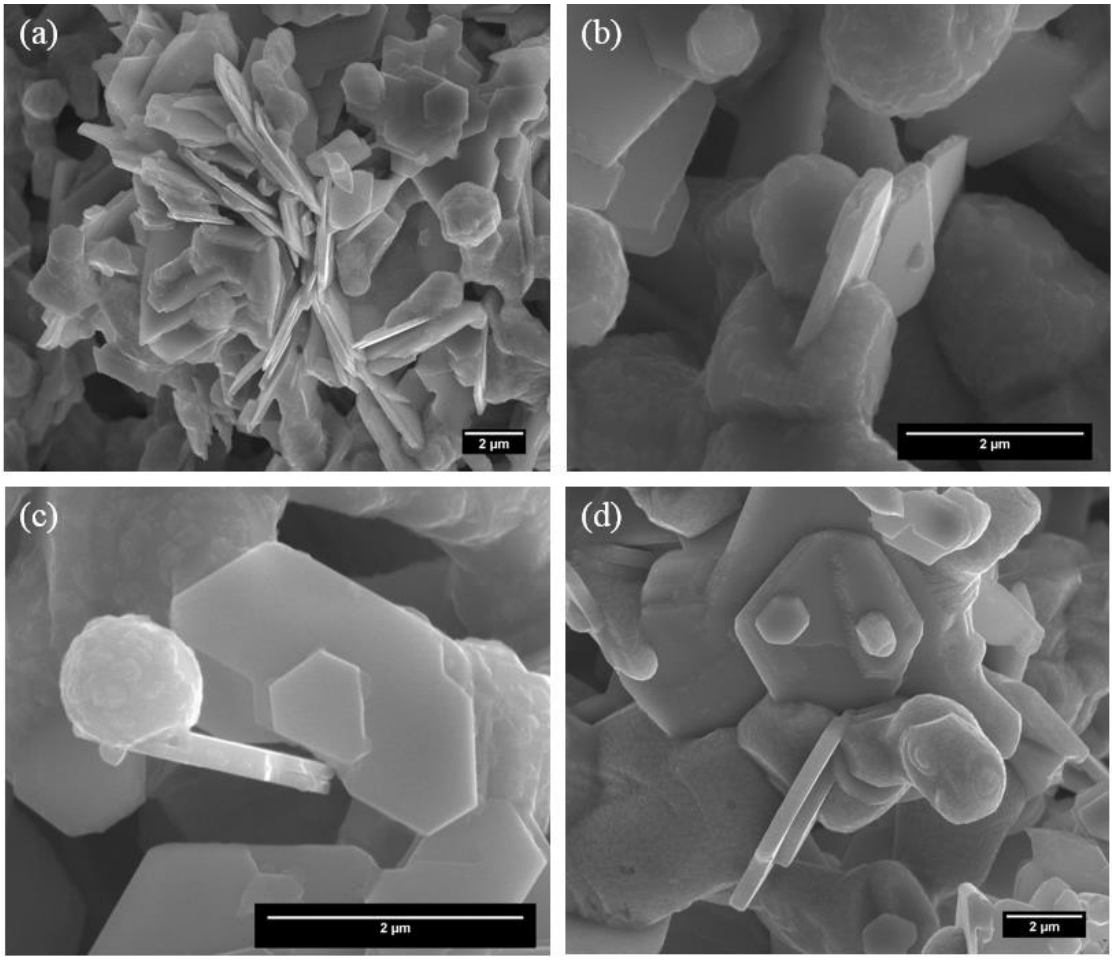

Figure 36 – SEM micrographs showing details of the unknown phase found on the BSCF-Cs X samples, with X corresponding to (a) 5%, (b) 10%, (c) 20% and (d) 40%

Curiously, further analysis of the samples revealed that the rounded particles, without a defined geometry, display a certain pattern on the surface, as shown in Figure 37 (a). It seems that the particle is composed of several layers strongly connected across their faces. This pattern is further detailed in Figure 37 (b). It is clear that these layers consist of sheets with straight and well defined edges, similar to the morphology of the particles shown in Figure 36. Therefore, it is reasonable to consider that the whole sample might be composed of one single phase with a flat geometry. This phase might be found agglomerated, but sometimes it might peel off and become visible through microscopic techniques. This could be a reason to explain why two geometries are found on the SEM micrographs, while the XRD exhibited formation of impurities only for partial substitution of 40%.

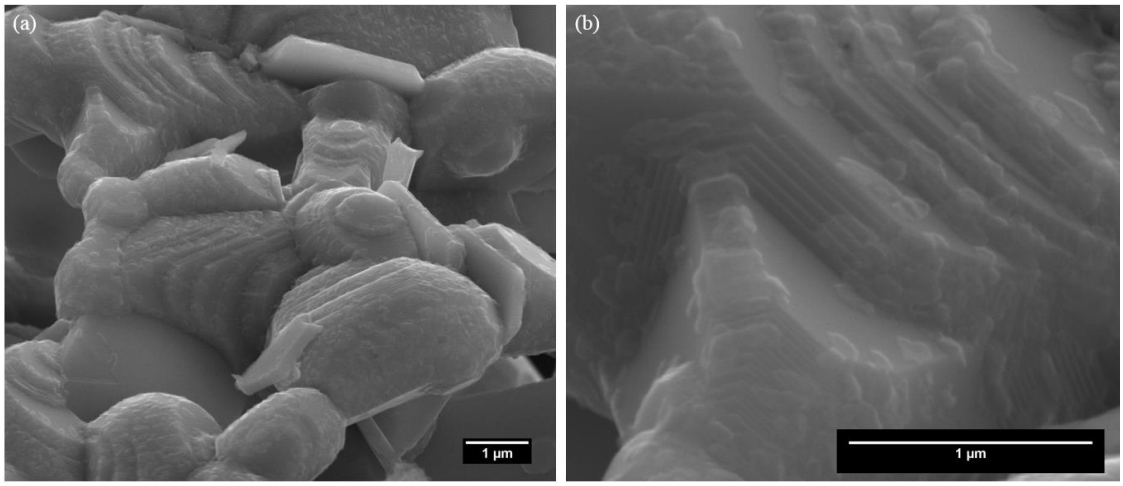

Figure 37 – Details of the pattern found on the BSCF-Cs samples

Since the values of unit cell size decreased when increasing the partial substitution for cesium, it was concluded that cesium was not incorporated on the BSCF structure. The large difference between cesium ionic radius and the ionic radii of the A-site cations would dislocate the structure so intensively that this outcome was expected, although Goldschmidt factor was within the tolerance. It is clear that a pure cubic perovskite phase was formed in which there was an unbalanced ratio between A-site cations and B-site cations. Only at partial substitutions higher than 20% that it was possible to notice impurities. In addition, what was thought to be a secondary phase undetected by the XRD patterns and visible on the SEM images, was further revealed to be the constituent of the grains that somehow pealed off the aggregate. As for the cesium, there were three possible alternatives, it was either incorporated in the A-site of the perovskite crystal, or it would not be incorporated on the crystal and appear as an oxide, or evaporate. Unfortunately, the only possible conclusion is that Cesium was not incorporated in the perovskite crystal, since all other alternatives were not confirmed by the performed tests. Therefore, it is suggested that cesium has probably evaporated during the heat treatment of the BSCF-Cs samples.

5.3.2. BSCF – Y

Another group has already performed partial substitution of yttrium on the BSCF membrane in order to improve the oxygen flux of perovskite membranes. The strategy

consisted on the introduction of a larger cation on the B-site, by substituting only Fe for Y with a general formula $Ba_{0.5}Sr_{0.5}Co_{0.8}Fe_{0.2-x}Y_xO_{3-\delta}$ [181]. In order to maintain the procedures previously adopted, in this work both the cobalt and iron cations were substituted for yttrium. Thus, the used formula is represented by $Ba_{0.5}Sr_{0.5}(Co_{0.8}Fe_{0.2})_{1-x}Y_xO_{3-\delta}$.

XRD patterns in Figure 38 revealed that for partial substitution values below 20% the final powders were composed of crystalline pure perovskite phase, with peaks of similar intensity and length. XRD profile of the sample with partial substitution of 40% exhibited some weak impurity peaks. They were associated with the presence of intermediary phases composed of Y_2O_3 and SrY_2O_4, which is reasonable since both the strontium and yttrium are in excess in this case. It was possible to distinguish peaks typical of the perovskite phase, however it was assumed that only for partial substitution of 20% or less the final samples resulted in pure perovskite phase. Further analysis of the strongest peak of these samples, as displayed on Figure 38, showed that they considerably shifted to lower 2θ angles.

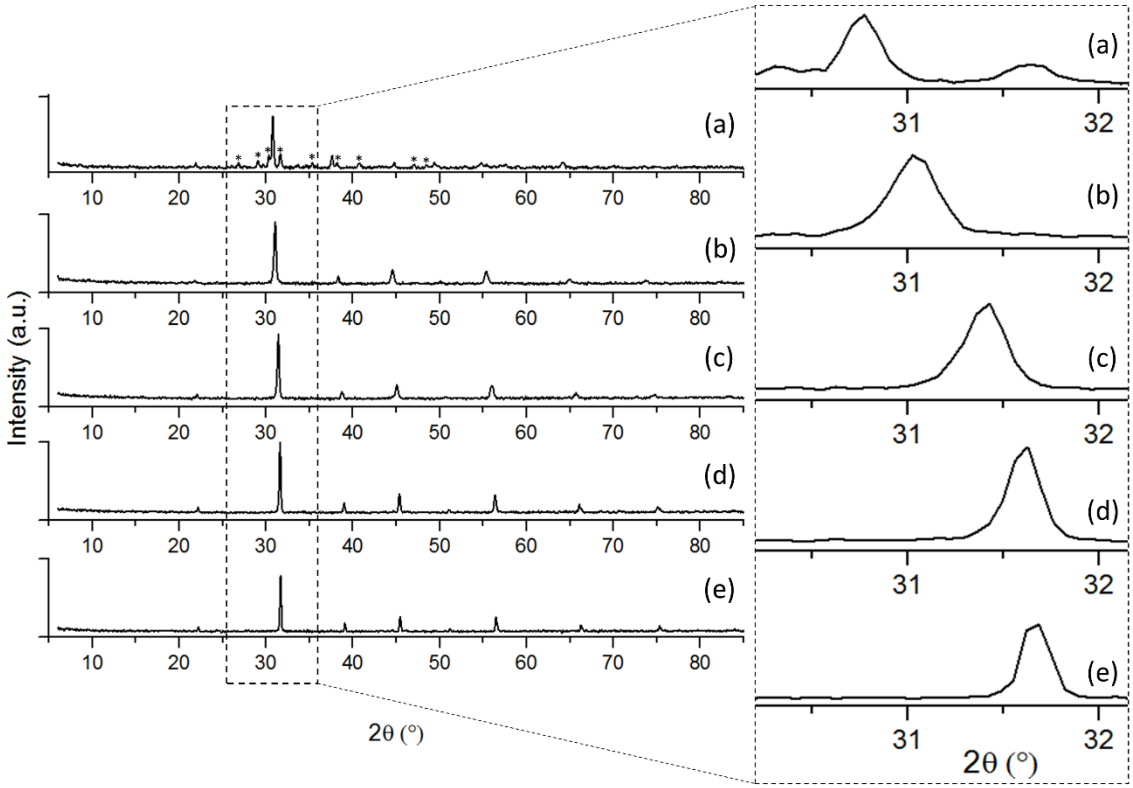

Figure 38 – XRD patterns of BSCF – Y X% with X values of (a) 40%, (b) 20%, (c) 10%, (d) 5% and (e) 0%. Impurities and intermediary phases are shown with *.

The shifted peaks suggested that the unit cell size of the sample is proportional to the partial substitution for yttrium. Determination of the correlation between the amount of yttrium substitution and the unit cell size, as shown in Figure 39, confirm the direct proportion between them. Essentially, this strong correlation between the parameters are enough to estimate that the yttrium cation was inserted on the B-site of the perovskite structure. This is due to the differences on the ionic radii of the present cations. The ionic radius of yttrium is smaller than ionic radii of the A-site cations, thus if barium and strontium were substituted for yttrium, the resulting material would have shown a smaller unit cell size. Therefore, the increase on the unit cell size confirms the hypothesis that yttrium was inserted on the B-site of the perovskite structure.

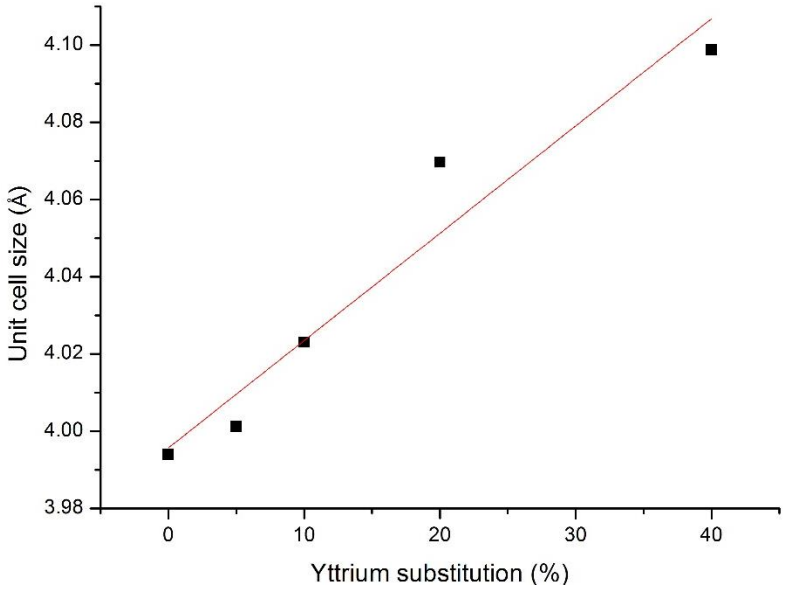

Figure 39 - Unit cell size as a function of yttrium substitution on the BSCF structure

Assessment of the degradation profile of the impurities present on the BSCF – Y samples are shown in Figure 40. Samples with partial substitution of 40% exhibited similar results to the BSCF samples, both showed major mass loss on the same temperatures and the mass remained stable at temperatures higher than 750 °C. Comparison of the XRD analysis with the TG led to the assumption that the intermediary phases were extremely stable, since no mass loss was observed above 750 °C. Thus, further increase of the used temperature probably would not be enough to consume the oxides. In other words, it is believed that small increases on the calcination temperature might not be enough to obtain pure perovskite phase with partial substitution of 40%.

Regarding the samples with partial substitution of 20 % and 10 %, they kept losing mass until the temperature reached 900 °C and the test was concluded. Even though impurity peaks were not visible on the XRD patterns, the TG analysis might indicate the presence of traces of carbonates and other intermediary phases. As for the sample with 5 % partial substitution, the mass remained stable after 870 °C. The mass loss profiles of the samples with 5%, 10% and 20% were more intense at temperatures in the range 240-250 °C. Other than this range, the mass loss was almost constant, with only a slight discontinuity at 670-690 °C, which can be attributed to elimination of compounds related to phase transformation.

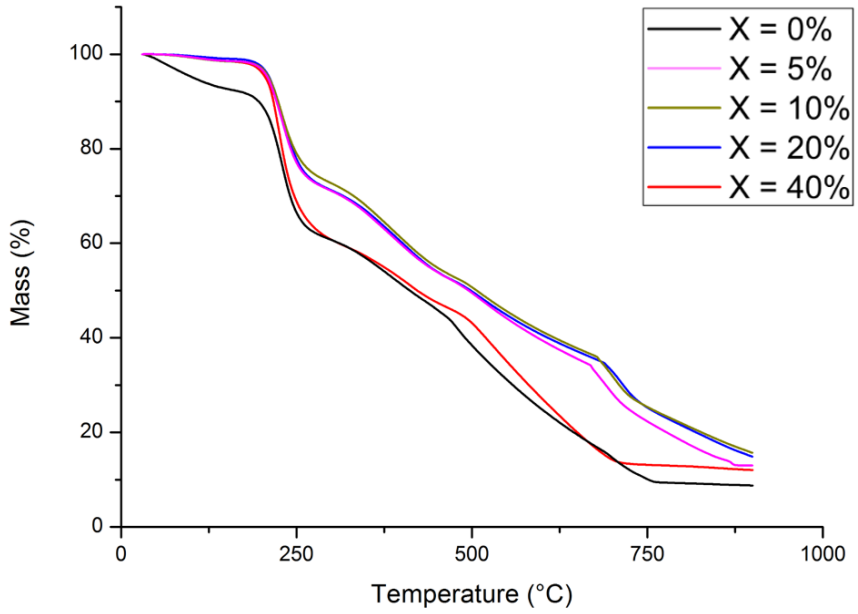

Figure 40 –Thermogravimetric analysis of the BSCF – Y X precursor powders

Essentially, these samples demand further analysis of phase development at different temperatures in order to understand what temperature the mass become stable. In addition, it is necessary to identify what is happening at the discontinuity visible on the thermogravimetric profile of certain samples.

Assessment of the powder morphology, as seen in Figure 41, revealed that the particles are strongly agglomerated and it is difficult to visualize the interface between particles. However, it is possible to assume that the mean grain size was considerably smaller when compared to pure BSCF (~9 µm). Increase in yttrium substitution led to grains in the nanometer scale. For 20% and 40% of partial substitution, the agglomerates displayed a

sponge-like structure, which indicate that yttrium has some influence on membrane densification. This might be a concern for membrane sintering, since the intention is to produce a dense membrane.

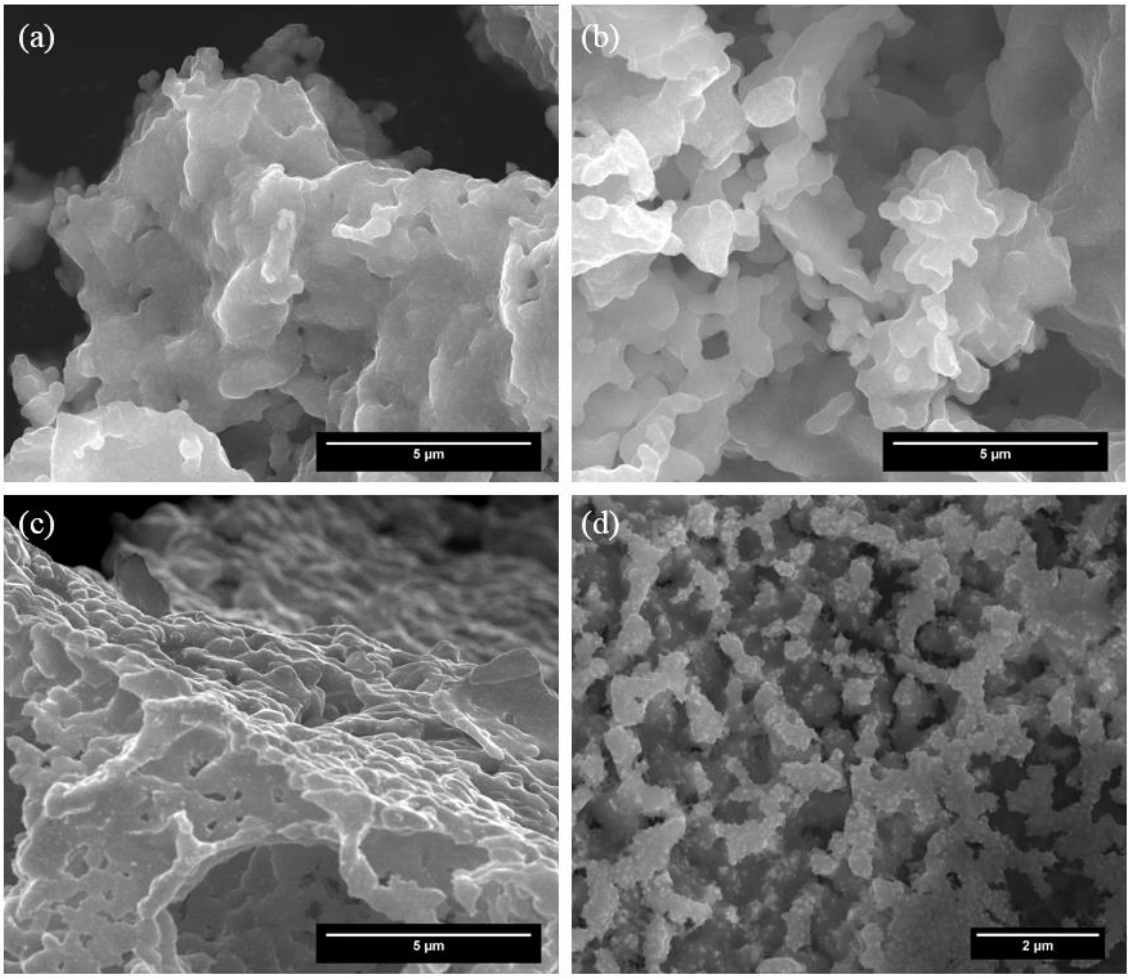

Figure 41 – SEM micrographs of the BSCF-Y X samples, with X corresponding to (a) 5%, (b) 10%, (c) 20% and (d) 40%

Since the perovskite phase with partial substitution was achieved, membranes were produced in order to check if it was possible to successfully produce dense and crack-free membranes. The sample BSCF-Y 40% did not result in pure perovskite phase at 900 °C, nevertheless, membranes of this sample were also produced for evaluation of Y_2O_3 and SrY_2O_4 behavior on the sintering process. Figure 42 displays the SEM micrographs of the membranes and it is clear that in all the samples some amount of porosity was present. For the samples with 5%, 10% and 20% it can be considered that dense membranes were fabricated, however the sample with 40% partial substitution did not exhibit a dense layer.

Again, this is probably because of the influence of the intermediary phases visible on the XRD patterns, which inhibited merging of particles and complete densification. Similar result was reported by Voytovych et al. (2002) in which the presence of yttrium oxide inhibited the densification of alumina [182].

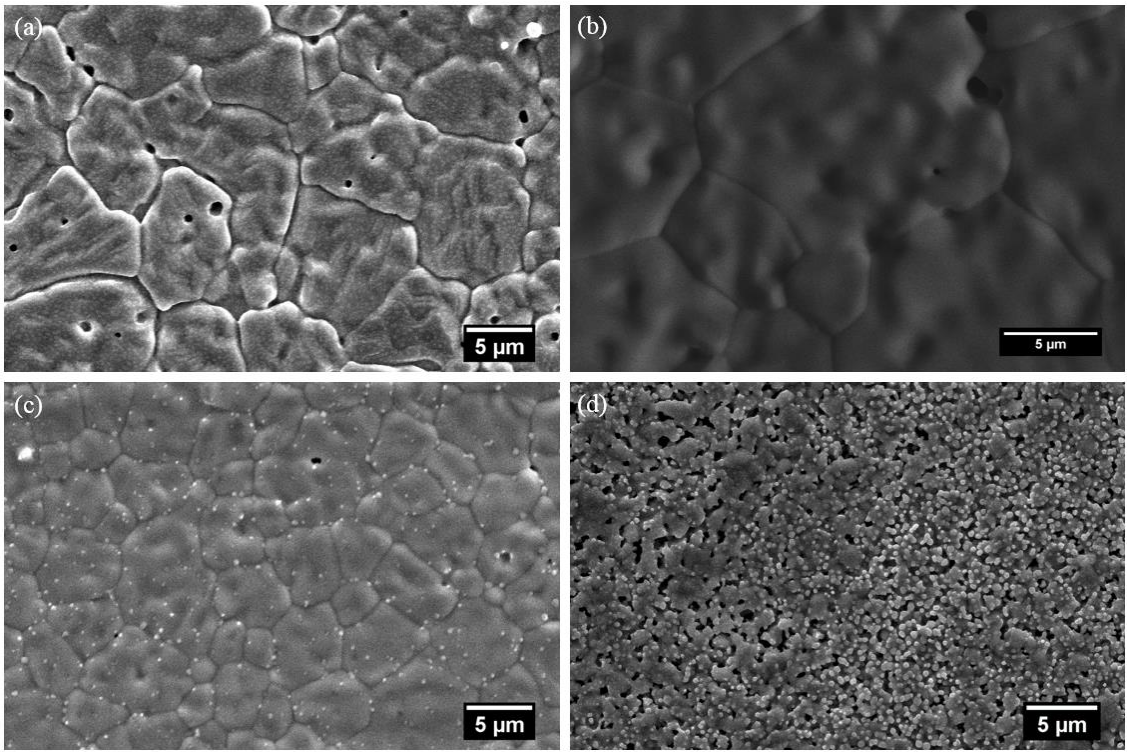

Figure 42 – SEM micrographs of the membranes sintered at 1,100 °C and produced from the BSCF-Y X samples, X corresponding to (a) 5%, (b) 10%, (c) 20% and (d) 40%

Regarding the other samples, the membranes were dense with visible grain boundaries. Some sparse pores were found on the surface, however they were essentially dense. Comparison of the sample BSCF-Y 5% and BSCF-Y 10% the grain size increased with increase of yttrium substitution. This pattern was not observed for the sample BSCF-Y 20%, since the grain size decreased. In addition, as one may notice in Figure 42 (c), there are some particles of a secondary phase on the membrane surface, which might explain why the grain size decreased. For instance, Voytovych et al. (2002) mentioned that the yttrium oxide also inhibited the grain growth, since it is located on the interfaces of the inorganic particles and diffusion between them is suppressed [182]. Therefore, it is reasonable to suggest that the yttrium that was previously inserted in the BSCF crystal at 900 °C somehow managed to segregate at the higher temperatures used for sintering, forming yttrium oxide on the particle interfaces and become an obstacle for grain growth.

After providing confirmation that the yttrium was successfully introduced on the BSCF crystal, and that it was possible to produce dense membranes for the samples BSCF-Y 5%, BSCF-Y 10% and BSCF-Y 20%, assessment of the oxygen vacancy concentration was performed in order to measure the correlation with the yttrium substitution. The sample BSCF-Y 40% was not pure and the presence of other compounds might result in inaccurate results. Thus, oxygen vacancy for this sample was not measured.

The graph presented in Figure 43 show a pattern for the pure BSCF similar to the previously found in literature [15,20], thus, substitution for yttrium on the BSCF crystal resulted in oxygen vacancy profiles very similar to the BSCF structure. The oxygen stoichiometry initially increases until 300 °C and only then starts to decrease until a minimum value 900 °C. Only the sample with 20% substitution exhibited a different profile, since the oxygen stoichiometry decreased from the beginning of the experiment and after 670 °C the oxygen vacancy remained almost stable. Therefore, this sample had low concentration of oxygen vacancies by the end of the experiment. Finally, the highest values for oxygen vacancy concentration were found for the sample, BSCF-Y 5%.

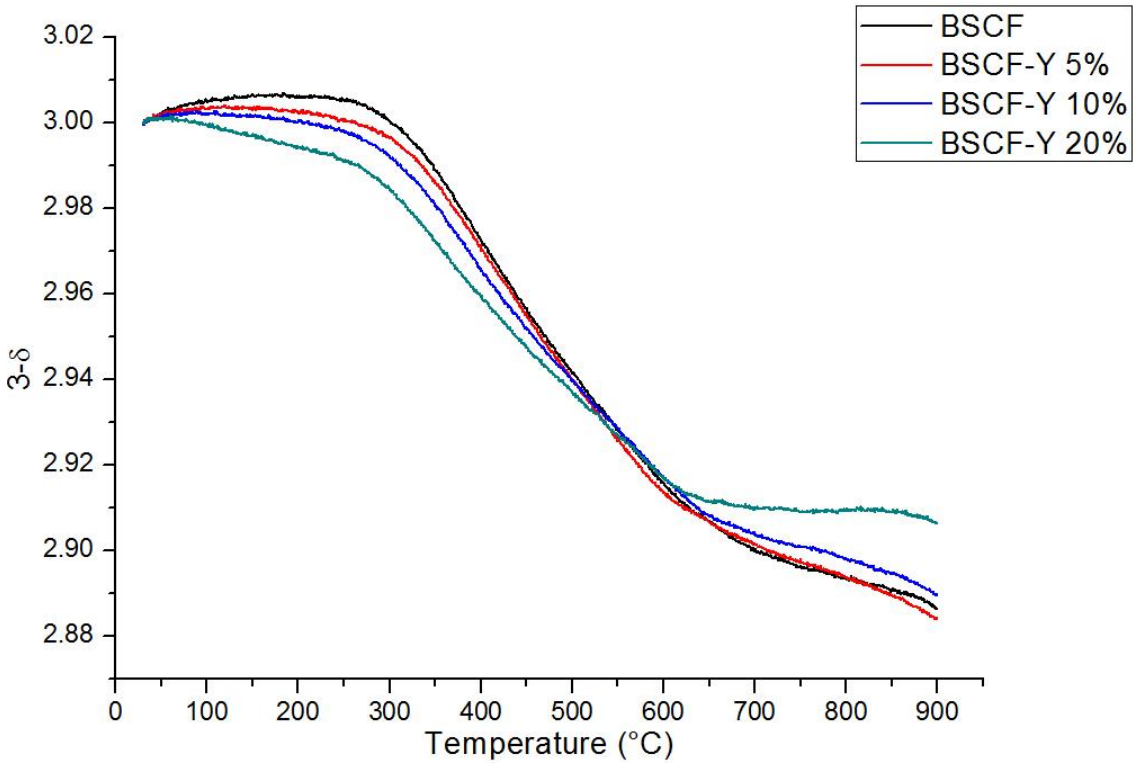

Figure 43 – Oxygen vacancy profile of the BSCF-Y samples measured while cooling the sample

In conclusion, the use of yttrium for partial substitution on the BSCF structure resulted in excellent outcomes. The percentage that was successfully incorporated on the BSCF crystal demonstrates how stable the cubic perovskite structure is. The sample BSCF-Y 5% exhibited outstanding results when compared to the other samples: it was composed of pure perovskite phase, formed dense membrane and had the highest concentration of oxygen vacancies at higher temperatures. Therefore, BSCF-Y 5% is the sample with more potential for further applications. Nevertheless, it is necessary to assess the optimum sintering temperature in order to avoid the sparse formation of pores on the surface, as shown in this work.

5.3.3. BSCF – Sc

Partial substitution of scandium has been proven to efficiently stabilize perovskite compounds, improve certain properties of the material and even increase the oxygen permeation [85,183]. Nevertheless, this approach of introducing scandium on the BSCF crystal has not been studied before. The intention here is to substitute the Sc on the B-site in order to increase the unit cell size and assess the material's properties. For determination of the BSCF-Sc stability, an interesting method was performed by studying the behavior of the material under CO_2 atmosphere.

Figure 44 shows the X-ray diffraction patterns of the partially substituted perovskites. All samples exhibited peaks characteristic of the cubic perovskite phase. There were no visible peaks of impurities or intermediary phases, indicating that the BSCF crystal was able to fully incorporate amounts up to 40% of scandium without forming other phases. Thus, all samples were composed of pure perovskite phase. Comparison of the strongest perovskite peak revealed that they slightly shifted to lower 2θ values, with lowest 2θ values for the sample BSCF-Sc 40%. Similarly to the analysis done for yttrium, this is an evidence that scandium was incorporated on the B-site of the cubic perovskite crystal. The unit cell size increased when the scandium percentage increased and confirmation of this hypothesis is shown in Figure 45, in which it is clear the almost linear correlation between the unit cell size and scandium substitution.

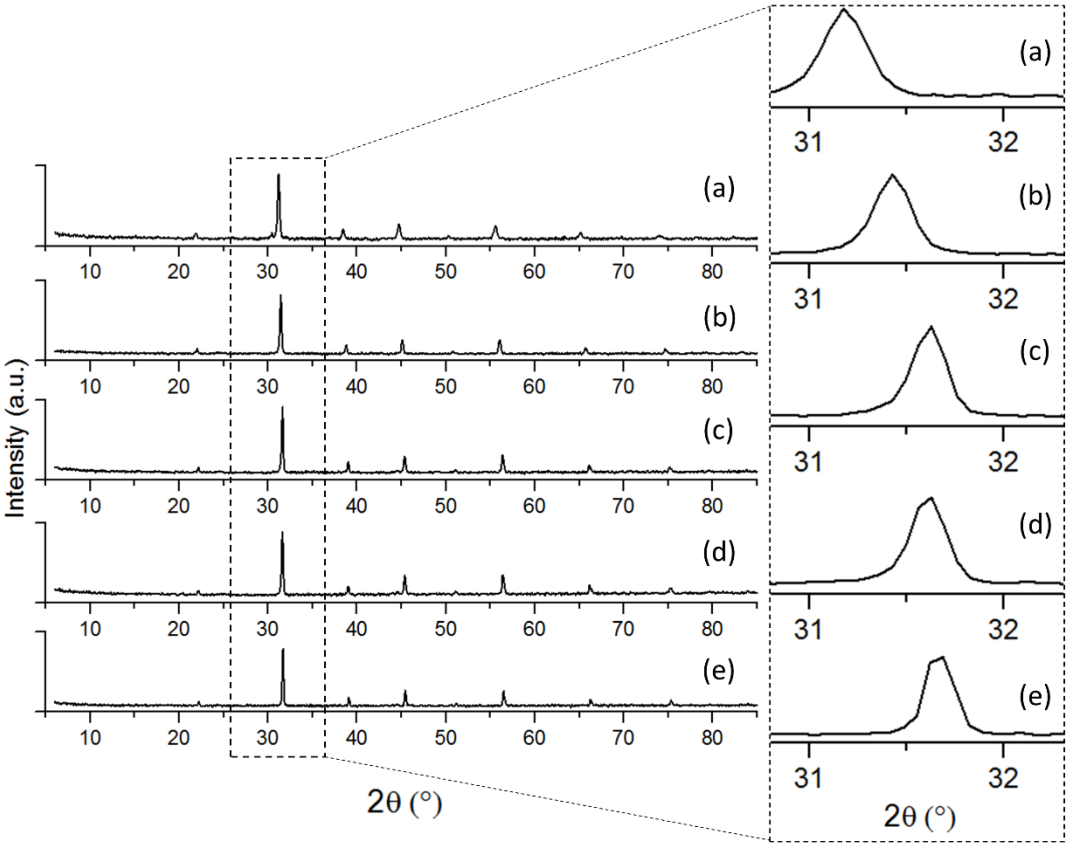

Figure 44 – XRD patterns of BSCF – Sc X% with X values of (a) 40%, (b) 20%, (c) 10%, (d) 5% and (e) 0%.

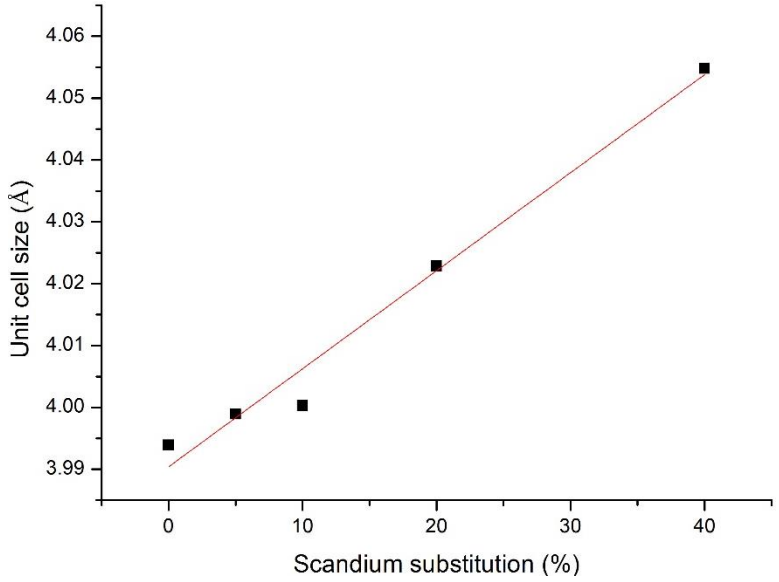

Figure 45 – Unit cell size as a function of scandium substitution on the BSCF structure

When comparing scandium substitution with yttrium substitution, it is clear that the increase of the unit cell size is much more intense when yttrium is incorporated into the BSCF crystal (Figure 46). This happens due to the yttrium higher ionic radius (0.9Å)

when compared to scandium (0.745Å). Thus, incorporation of large cations into the crystal structure on high amounts may become a challenge due to the strong dislocation caused in the structure. This issue might explain why the BSCF structure is capable of accommodating high amounts of scandium without forming secondary phases, while high values of yttrium substitution led to formation of yttrium oxides.

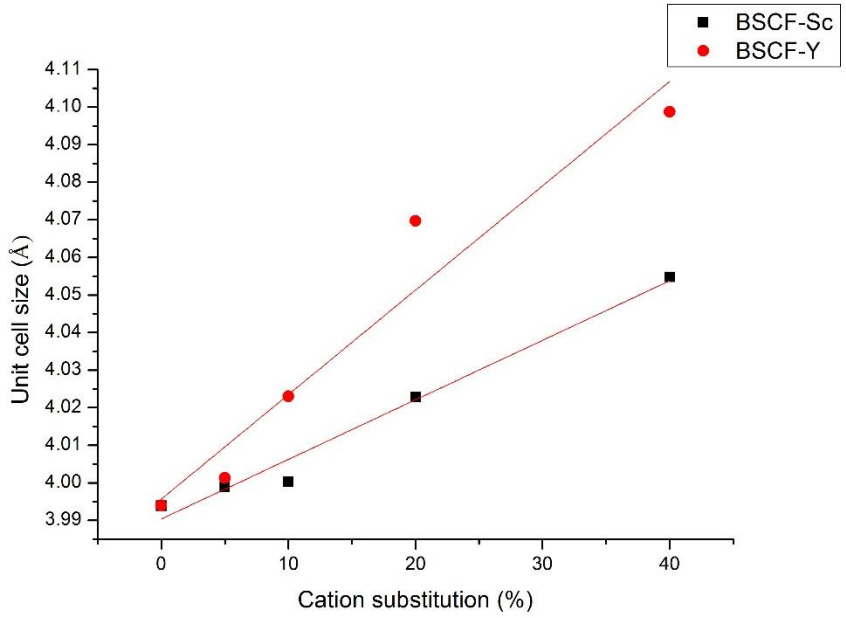

Figure 46 – Differences between the increase of the unit cell size of the BSCF-Y and BSCF-Sc samples

The thermal decomposition profiles of the BSCF-Sc samples revealed that the most intense mass loss of all samples took place in the range of 200-250 °C, similar to the pure BSCF. At temperatures higher than 250 °C the mass loss was almost constant until the end of the experiment. The most different sample was the BSCF-Sc 5% with only moderate mass loss at 200-250 °C. It kept losing mass for the entire temperature range used for this experiment, suggesting that some impurities or intermediary phases might still be present on the sample after calcination. Samples BSCF-Sc 10% and BSCF-Sc 20% exhibited stable mass around 11% for temperatures higher than 750 °C, slightly higher than the BSCF due to the heavier scandium. Finally, the sample BSCF-Sc 40% kept losing mass until the end of the experiment, again suggesting that the sample has some impurities yet and higher temperatures would be necessary for successful calcination.

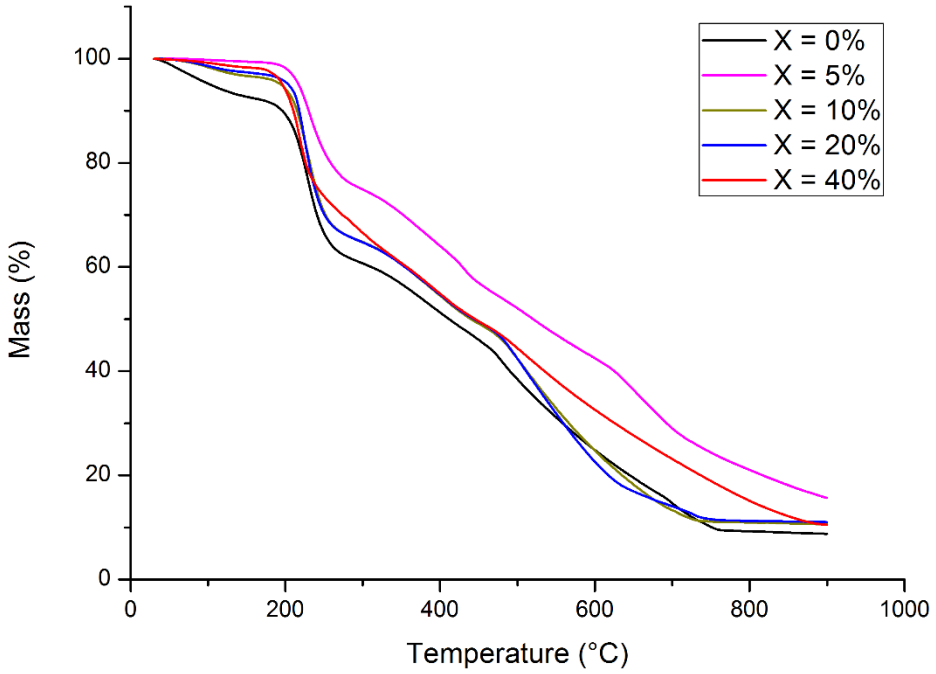

Figure 47 – Thermogravimetric analysis of the BSCF – Sc X precursor powders

Analysis of powder morphology revealed irregular grains with no clear geometry, as shown in the micrographs in Figure 48. Grains were strongly agglomerated and grain boundaries were difficult to visualize, however further analysis revealed that they could be distinguished at higher magnification. Similar to the micrographs of the BSCF-Y samples, the resulting grains have smaller grain size when compared to the BSCF powder; however, a statistical analysis could not be performed using the SEM micrographs. A sponge-like structure was found for the samples BSCF-Sc 10%, BSCF-Sc 20% and BSCF-Sc 40%, with small particles and great pore percentage. This structure seems to depend on the amount of scandium used for partial substitution on the BSCF structure, with the maximum value culminating in small particles in the nanometer scale with great volume of empty spaces. Again, this behavior might represent an issue in the sintering stage, since the sponge-like structure could have developed due to possible difficulties to merge the grains.

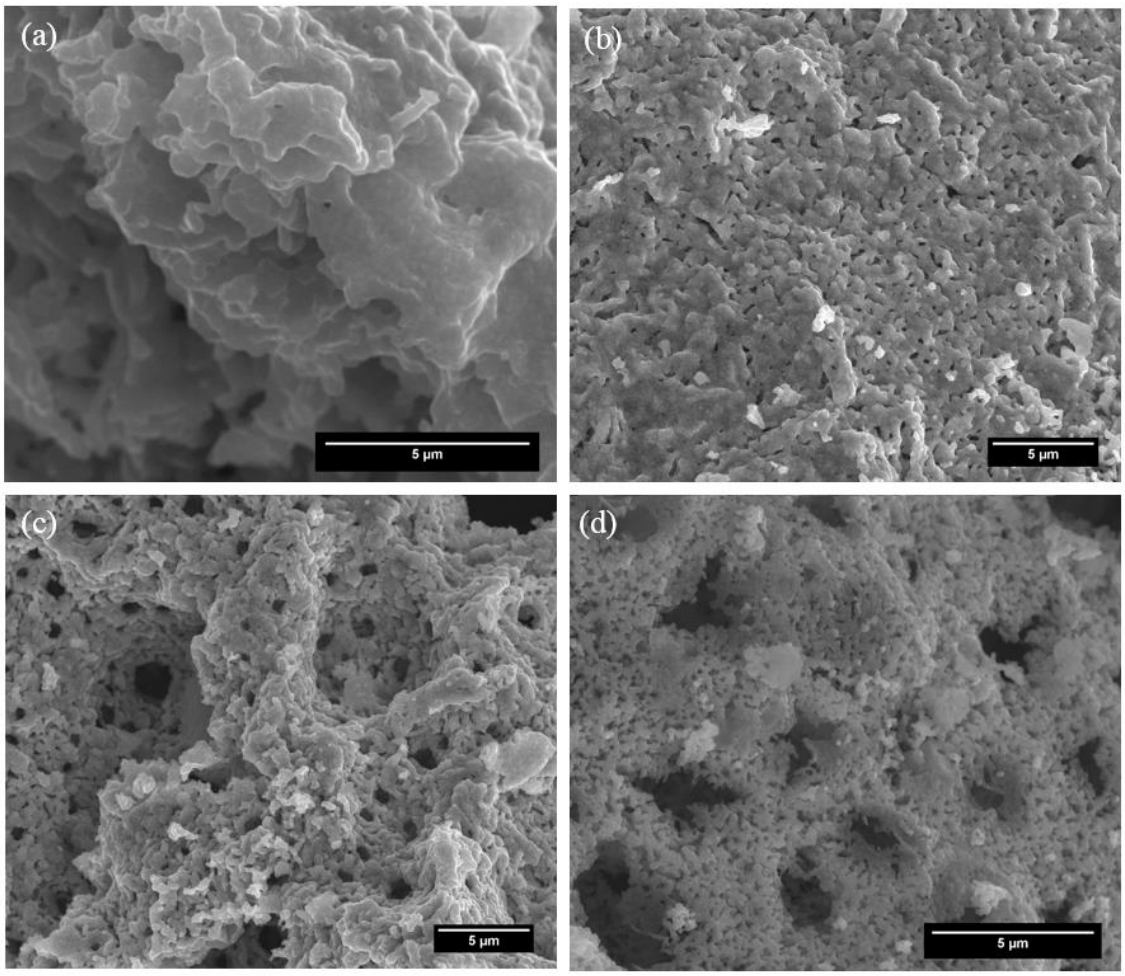

Figure 48 – SEM micrographs of the BSCF-Sc X samples, with X corresponding to (a) 5%, (b) 10%, (c) 20% and (d) 40%

Regarding membrane production (Figure 49), all samples exhibited grain growth and densification in some level. In other words, the sponge-like structure did not seem to interfere on the densification as much as noticed on the BSCF-Y 40% sample. The BSCF-Sc 5% and BSCF-Sc 10% produced dense membranes with a few pores on the surface. Grains are in the order of 10-30 µm and the interface between them seems to be well defined, which can be attributed to higher level of cohesion between them. For the samples BSCF-Sc 20% and BSCF-Sc 40%, the temperature used for sintering (1,100 °C) was not enough to provide energy for complete densification and more intense grain growth. The particles merged and the grains were in the order of 2-5 µm, indicating that grain growth occurred in a small level. However, there was a substantial amount of pores on the surface and the grain boundaries are not well defined, suggesting that the grains are not strongly connected. Therefore, it is expected low mechanical stability for these

two samples. Use of higher temperatures might lead to production of a dense membrane. In addition, the oxygen permeation is extremely dependent on the grain size, and it is known that, for the BSCF, greater grains promote improvements in oxygen permeation. Thus, a higher temperature would also culminate in membranes with better performance due to formation of greater grains.

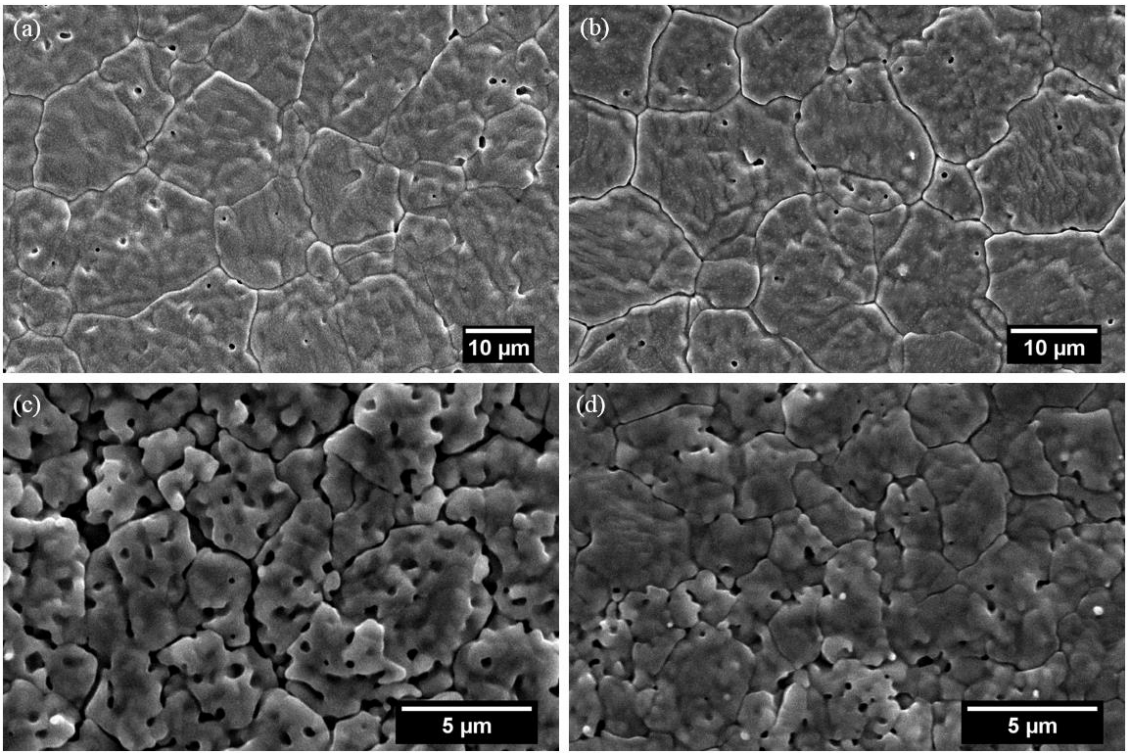

Figure 49 – SEM micrographs of the membranes sintered at 1,100 °C and produced from the BSCF-Y X samples, X corresponding to (a) 5%, (b) 10%, (c) 20% and (d) 40%

Nevertheless, assessment of oxygen vacancy was performed in all samples, since only minor adjustments on the sintering temperature are required for complete densification. The 3-δ profiles exhibited in Figure 50 revealed that in general the BSCF-Sc samples displayed different behaviors when compared to the pure BSCF. For instance, the initial increase in 3-δ of the BSCF lost intensity for higher values of scandium substitution. The BSCF-Sc 5% exhibited similar behavior of the BSCF sample for the whole temperature range used on the experiment. However, the 3-δ values of the sample with 40% partial substitution started decreasing immediately. The BSCF-Sc 10% remained stable until temperatures around 300 °C, after this, the 3-δ values started decreasing. This sample achieved the lowest 3-δ value of all samples, in other words, it displayed the highest

concentration of oxygen vacancy. Indeed all samples had oxygen vacancy concentration higher than the BSCF, except the BSCF-Sc 40%.

The BSCF-Sc 40% showed an unexpected behavior as seen in Figure 50. The 3-δ values started increasing after 650 °C and constantly increased until 900 °C. A possible explanation is the stability of the compound under experiment conditions. It is important to stress that the displayed data was obtained while the sample was cooling. The experiment began at 900 °C, on this basis, it is possible to understand that the BSCF-Sc 40% is actually losing mass at temperatures higher than 650 °C and it is not stable at this temperature range. Only below 650 °C the sample becomes stable. Due to this behavior, this sample exhibited the highest values of 3-δ, thus, the lowest values of oxygen vacancy.

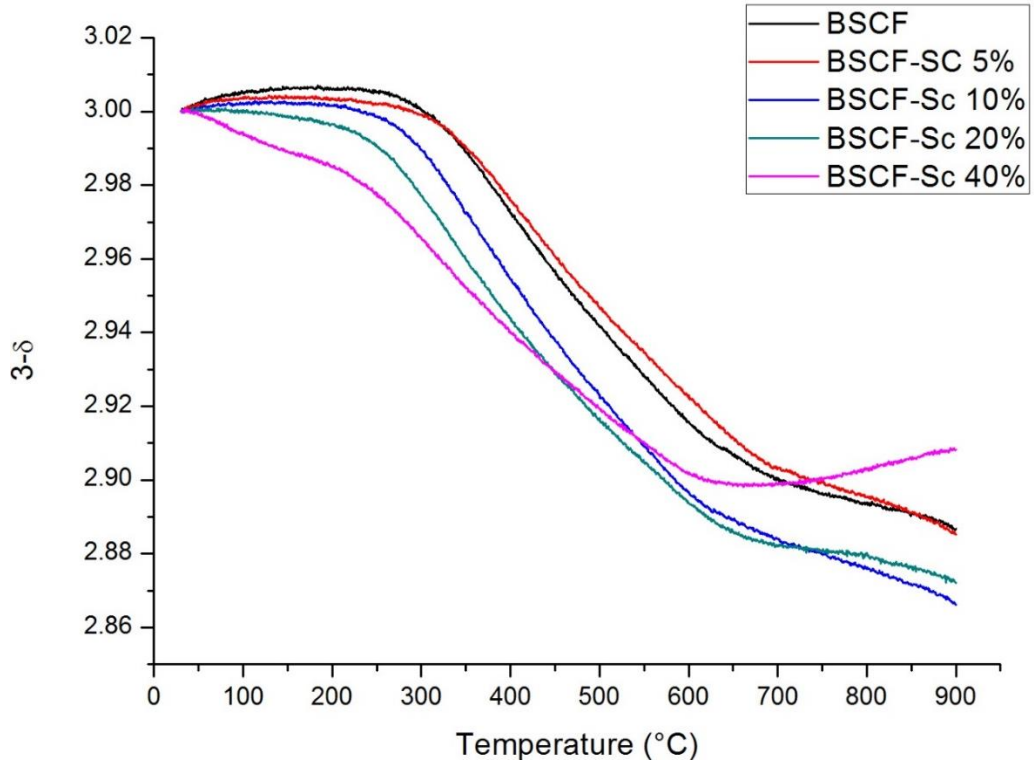

Figure 50 – Oxygen vacancy profile of the BSCF-Sc samples measured while cooling the sample

Regarding the stability of the BSCF-Sc samples under CO_2 atmosphere, the result is shown in Figure 51. One may notice that the BSCF compound could be considered stable for temperatures below 650 °C. For temperatures within the range 650-860 ° C there is an intense peak on the derivative weight curve, indicating that the reaction with the CO_2 took place in a small temperature range but with high intensity. Between 860-900 °C all

samples presented the same behavior, they lost mass probably due to degradation of the carbonates formed during the experiment, thus this range was not discussed.

The BSCF-Sc samples presented weaker peaks when compared to the BSCF. They also started reacting with CO_2 at lower temperatures, generally around 440 °C. Highest values of mass absorption rate shifted to lower temperatures when increasing the scandium substitution. For instance, the BSCF-Sc 5% had the highest value of mass increase at 735 °C, while the BSCF-Sc 40% was at 580 °C. In addition, the ranges in which they kept reacting with CO_2 were longer, and this temperature range ended at 810 °C for the BSCF-Sc 20% and at 860 °C for the BSCF-Sc 40%. These differences indicate that the BSCF-Sc samples reacted differently with CO_2 and if carbonates are formed at lower temperature, it might indicate that these samples are more unstable, since less energy is required for this reaction. Indeed, the final mass of the BSCF-Sc 40% was even higher than the BSCF sample. Therefore, it seems that these samples are less stable under CO_2 atmospheres.

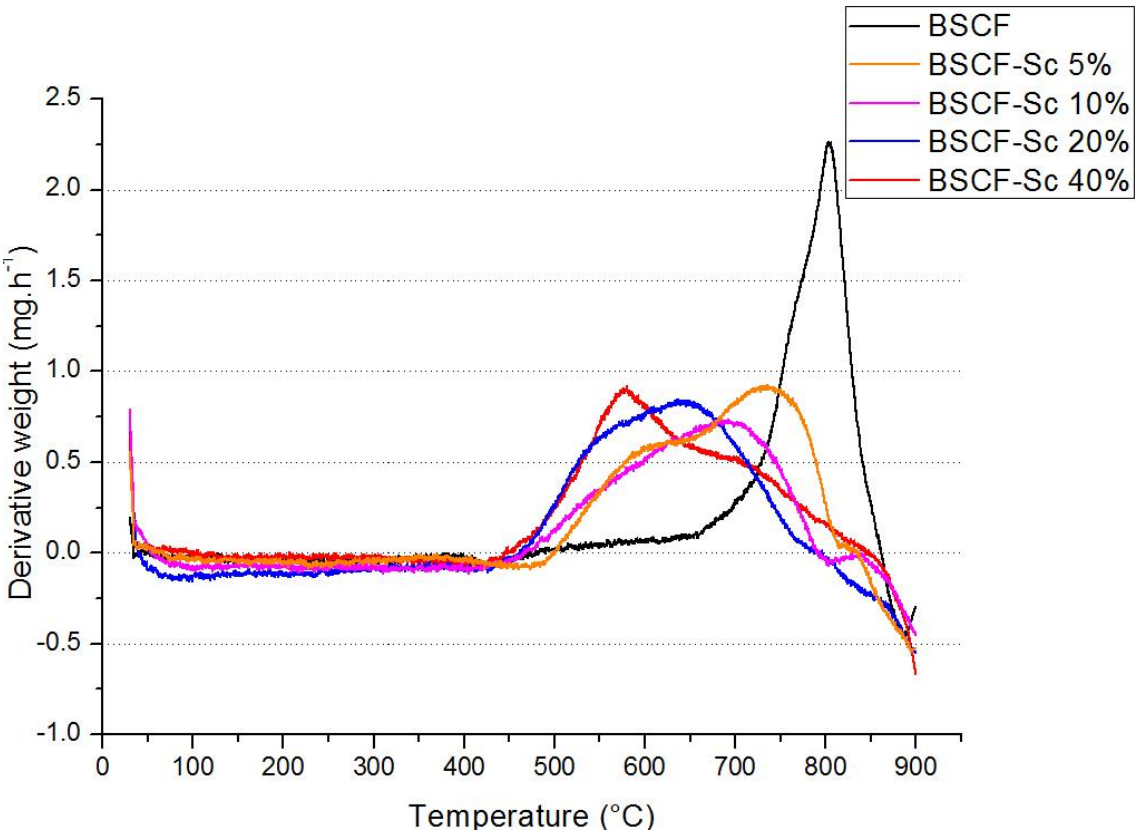

Figure 51 – Stability test of the BSCF-Sc samples under 100% CO_2 atmosphere

However, temperatures used for oxygen permeation are usually higher than 800 °C. In this range, it is obvious that the BSCF-Sc membranes were more stable than the pure BSCF. The BSCF-Sc indeed reacted with CO_2 for a longer range of temperature; nevertheless, the temperature used on industrial applications is stable and only variates around the desired temperature. In other words, the industrial operation is essentially isothermal and at temperatures higher than 800 °C. Therefore, under industrial conditions, the BSCF-Sc membranes may be considered more stable, since they absorb mass slower than the pure BSCF, indicating less intense formation of carbonates. This is an excellent outcome, since formation of carbonates on the membranes worsen the oxygen permeation and the modules efficiency decrease considerably.

When this analysis was performed considering the specific surface area, the differences became much easier to notice, as shown in Figure 52. It is clear the correlation between the scandium substitution and the intensity of mass absorption rate per area of the compound. The arrow displays the tendency that the characteristic peak of the pure BSCF tends to be weaker and shift to the left when the scandium substitution increases, leading to the lowest values of mass absorption rate per area for the BSCF-Sc 40% sample. If considered that the experiment was performed with the powder, and that the application utilizes the dense membrane, the different values of mass absorption rate per area suggest when membranes are used the BSCF would form carbonates in a higher rate than all the BSCF-Sc samples. In conclusion, this is a clear indication that the use of CO_2 as sweep gas may not interfere on the efficiency of the BSCF-Sc samples as much as already reported for the pure BSCF.

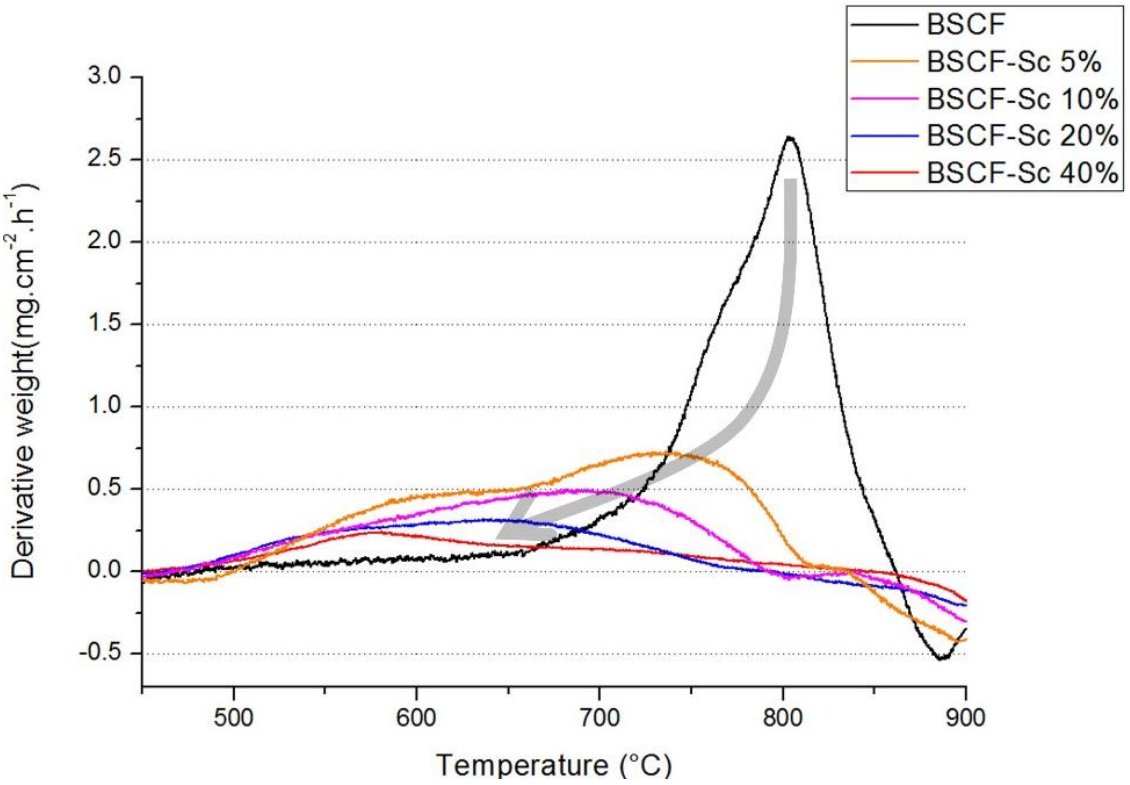

Figure 52 – Stability test of the BSCF-Sc samples under 100% CO_2 atmosphere, considering the mass absorption per area

It is important to stress that best results were achieved for temperatures higher than 800 °C. If considered the whole range that the pure BSCF reacts at high rates with CO_2, all BSCF-Sc samples exhibited improved behavior at temperatures higher than 737 °C. Below this temperature range, the BSCF-Sc samples react at higher rates when compared to the pure BSCF. Therefore, it seems that these compounds may be an alternative for oxygen applications at temperatures higher than 750 °C. For applications at temperatures lower than this, they are not recommended, since they would quickly lose efficiency.

All samples with scandium partial substitution were composed of pure perovskite phase, an exceptional result for structure stability of the cubic perovskite. The unit cell size increase was not as strong as the BSCF-Y samples, however the ability to form pure phase with all compounds was extraordinary. Also, values of oxygen vacancy suggested that the BSCF-Sc samples show a great potential for oxygen permeation applications. The fact that the BSCF-Sc with 20% and 40% scandium substitution produced membranes with high pore concentration indicates that these two still need to be studied for optimization

of the membrane sintering. In addition, it was possible to notice an instability of the BSCF-Sc 40%, which might become an issue for longer operation times.

From all the BSCF-Sc samples, the best results were for the BSCF-Sc 10% and BSCF-20%. However, the densification of the BSCF-Sc 20% was not enough and adjustment of the temperature used for the sintering have to be made. Thus, the best sample with the used experimental parameters is the BSCF-Sc 10%. The membrane from this sample was dense, the oxygen vacancy concentration was the highest and, finally, the carbonate formation rate per area under CO_2 atmosphere was considerably improved in comparison to the pure BSCF. Permeation tests under inert and CO_2 atmospheres are recommended for assessment of possible improvements on the membrane suitability for oxygen separation applications.

5.4. Final discussion

Initial trials to obtain a perovskite powder by microwave assisted synthesis did not seem productive. The system worked perfect for treatment of solutions, with excellent control of the radiation power, mixing and temperature measurements. However, when it was used for treatment of the dried gel, the system was not functional anymore. The lack of control and the low interaction between the perovskite and the microwave radiation led this experiment to be studied in a future occasion. Indeed, one compound formed perovskite phases with the presence of impurities; however, it was an exception.

Comparison between the two idealized synthesis routes confirmed that the CA-EDTA is the best option with the utilized parameters. Complete degradation of the intermediate phases at lower temperatures, higher specific surface area and absence of impurities on the membrane's surface were the main factors between the measured characteristics. In fact, the presence of cobalt oxide on the membrane's surface was the main issue, since it may lead to a material with unbalanced stoichiometry. For the CA-EDTA route, the best option was performing the calcination step at 900 °C for 4 hours. These parameters successfully produced pure perovskite material with half the time usually used on literature, an important improvement for the high-energy consumption during perovskite production. In addition, these parameters represented the best values for specific surface area, a property that plays an important role on the membrane densification.

Synthesis of the perovskites with partial substitution was performed and all samples resulted in perovskite phase. However, the incorporation of cesium at the A-site of the perovskite structure was not fruitful. The unit cell size of the material decreased, indicating that somehow the cesium was not incorporated. It was not possible to determine the presence of cesium in the sample, thus, it is suggested that this cation evaporated during the heat treatment.

Incorporation of yttrium and scandium on the B-site resulted in perovskite phase with an increase in the unit cell size, indicating that the partial substitution was successful. It is worth highlighting the high stability of the perovskite structure to accommodate substitution of percentages as high as 40 % with larger cations. The use of yttrium caused the presence of impurities when the substitution percentage was 40 %, however the other samples were composed of pure perovskite. Analysis of membrane sintering revealed that the presence of impurities strongly affect the densification stage, and it is important to have pure perovskite phase. In addition, the oxygen vacancy concentration of the BSCF-Y samples displayed similar results when compared to the pure BSCF, only the sample with partial substitution of 5 % exhibited higher values. Further improvements on the sintering step are desirable for this sample, since pores were present at the surface. There is a great potential for application of this compound, however only assessment of oxygen permeation will allow determination of the membrane performance.

The use of scandium for partial substitution resulted in remarkable results. The absence of impurities on all the BSCF-Sc is an indication that these novel compounds are extremely stable. Increase of the unit cell size was not as sharp as when using yttrium, however it was enough to result in considerable increase of the unit cell size. Measurements of the oxygen vacancy concentration only confirm that the concentration of defects is higher than in the pure BSCF at 900 °C. The best results were for the BSCF-Sc samples with 10 % and 20 % substitution, nevertheless, the sample with 20 % substitution did not produce a dense membrane. Simple adjustments on the sintering parameters may lead to complete densification, however the best sample was considered the BSCF-Sc 10 % for the parameters used in this work.

Expressive improvement was confirmed for the stability of the BSCF-Sc samples under CO_2 atmosphere. Every sample reacted slower with CO_2 when compared to the pure

BSCF. In other words, the BSCF-Sc samples exhibited more resistance for formation of carbonates. When increasing the substitution with scandium in the BSCF structure, it was confirmed that the stability increases. If the specific surface area of the compounds are considered, the improvements on stability is even more noticeable.

6. Conclusions

Perovskite materials were successfully synthesized by the two idealized Pechini methods. The material was characterized and material's properties were correlated with the synthesis route and with the parameters utilized during the calcination stage. In addition, production of perovskites with partial substitution led to outstanding results. Partial substitution with cesium was not possible; however, the use of yttrium and scandium was confirmed to be fruitful. Improvements on the oxygen vacancy concentration allied with the enhancement on the stability under CO_2 atmospheres determined that the production of partially substituted perovskites could lead to improvements yet to be explored. Therefore, the main objective of this work was performed with success.

Initial trials to obtain a perovskite powder by microwave-assisted synthesis did not result in a stable system, thus this method was discarded. Comparison between the two idealized synthesis routes confirmed that the CA-EDTA is the best option with the utilized parameters. Best parameters for the calcination step were using temperatures of 900 °C for 4 hours, a substantial improvement for the high-energy consumption, since pure perovskite was produced with half the time commonly reported on the literature.

Partial substitution of cesium at the A-site of the perovskite structure was not fruitful, and it was not possible to understand why it has happened. As for partial substitution of yttrium and scandium on the B-site, both resulted in successful incorporation on the perovskite phase. The perovskite structure displayed impressive stability, since it was possible to incorporate percentages as high as 20 % for yttrium and 40 % for scandium. The sample with 5% partial substitution for yttrium exhibited the best properties. Incorporation of scandium on the perovskite structure resulted in remarkable results. All samples produced pure perovskite phase, with absence of impurities, indicating that these novel compounds are extremely stable. Best results were found for the sample with 10 % partial substitution.

Splendid improvement was confirmed for the stability of the BSCF-Sc samples under CO_2 atmosphere, since all samples exhibited lower rates of carbonate formation. An outstanding enhancement, since formation of carbonates of the membrane's surface lowers the efficiency of the membrane for oxygen separation. Higher stability was found

for higher values of partial substitution for scandium and, if the specific surface area is considered, the results indicate impressive improvements. Therefore, there is a great potential for use of the BSCF-Sc samples for oxygen separation using CO_2 as sweep gas.

In conclusion, all objectives of this work were successfully achieved, resulting in remarkable improvements of the pure BSCF. It is important to stress that all measurements used in this work are used for estimation of the real performance of the membrane. Therefore, performance experiments must be done for further works with the studied compounds.

7. References

1. EMSLEY, J. Oxygen. In: EMSLEY, J. **Nature's building blocks:** an A-Z guide to the elements. Oxford: Oxford University Press, 2001.

2. LEO, A.; LIU, S.; DA COSTA, J. C. D. Development of mixed conducting membranes for clean coal energy delivery. **International Journal of Greenhouse Gas Control**, Brisbane, 2009. 357-367.

3. BURGGRAAF, A. J.; COT, L. **Fundamentals of Inorganic Membrane Science and Technology**. Elsevier, Amsterdam, New York, 1996.

4. HASHIM, S. M.; MOHAMED, A. R.; BHATIA, S. Current status of ceramic-based membranes for oxygen separation from air, **Advances in Colloid and Interface Science** 160, 2010. 88-100.

5. SUNARSO, J. et al. Mixed ionic-electronic conducting (MIEC) ceramic-based membranes for oxygen separation, **Journal of Membrane Science,** 320, March 2008. 13-41.

6. DOCTOR, R. D. et al. Oxygen-blown gasification combined cycle: carbon dioxide recovery, transport and disposal. **Energy Conversion and Management**, 38, 1997. 5575-5580.

7. BACHU, S. Sequestration of CO_2 in geological media: criteria and approach for site selection in response to climate change. **Energy Conversion and Management**, 9, 2000. 953-970.

8. FLETT, M.; GURTON, R.; WEIR, G. Heterogeneous saline formations for carbon dioxide disposal: Impact of carying heterogeneity on containment and trapping. **Journal of Petroleum Science and Engineering**, 1-2, 2007. 106-118.

9. SHAO, X. et al. Improvement of oxygen permemation through microchanneled ceramic membranes. **Journal of Membrane Science**, 2014. 444-450.

10. SIRCAR, S. Pressure Swing Adsorption. **Industrial Engineering Chemistry Research**, 2002. 1389-1392.

11. KAKARAS, E. et al. Economic implications of oxyfuel application in a lignite-fired power plant. **Fuel**, 2007. 2151-2158.

12. SMITH, A. R.; KLOSEK, J. A review of air separation technologies and their integration with energy conversion processes. **Fuel Processing Technology**, 70, 2001. 115-134.

13. DA COSTA, J. et al. State of Art (SOTA) report on dense ceramic membranes for oxygen separation from air. 2013.

14. HASHIM, S. S.; MOHAMMED, A. R.; BHATIA, S. Oxygen separation from air using ceramic-based membrane technology for sustainable fuel production and power generation. **Renewable and Sustainable Energy Reviews**, 15, 2011. 1284-1293.

15. RACHADEL, P. L. et al. The effect of non-ionic porous domains on supported $Ba_{0.5}Sr_{0.5}Co_{0.8}Fe_{0.2}O_{3-\delta}$ membranes for O_2 separation. **Journal of Membrane Science**, n. 454, 2014. 382-389.

16. BAUMANN, S. et al. Ultrahigh oxygen permeation flux through supported $Ba_{0.5}Sr_{0.5}Co_{0.8}Fe_{0.2}O_{3-\delta}$ membranes. **Journal of Membrane Science**, 377, 2011. 198-205.

17. BHALLA, A. S.; GUO, R.; ROY, R. The perovskite structure - a review of its role in ceramic science and technology. **Materials Research Innovation**, 2000.

18. GOLDSCHMIDT, V. M. Ionic radius of divalent copper. **Nature**, 1946. 192-193.

19. WANG, H.; CONG, Y.; YANG, W. Oxygen permeation study in a tubular $Ba_{0.5}Sr_{0.5}Co_{0.8}Fe_{0.2}O_{3-\delta}$ oxygen permeable membrane. **Journal of Membrane Science**, 2002. 259-271.

20. HAWORTH, P. et al. Yttrium doped BSCF membranes for oxygen separation. **Separation and Purification Technology**, 81, 2011. 88-93.

21. TERAOKA, Y.; NOBUNAGA, T.; YAMAZOE, N. Effect of cation substitution on the oxygen semipermeability of perovskite-type oxides. **Chemistry Letters**, 1988. 503.

22. STEELE, B. C. H. Oxygen ion conductors and their technological applications. **Materials Science and Engineering**, 1992. 79-87.

23. STEELE, B. C. H. Ceramic ion conducting membranes. **Current Opinion in Solid State and Materials Science**, 1996. 684.

24. TERAOKA, Y. et al. Oxygen permeation through pervoskite-type oxides. **Chemistry Letters**, 1985. 1743.

25. TERAOKA, Y.; ZHANG, H. M.; YAMAZOE, N. Oxygen-sorptive properties of defect perovskite-type $La_{1-X}Sr_XCo_{1-Y}Fe_YO_{3-\delta}$. **Chemistry Letters**, 1985. 1367-1370.

26. KINGERY, W. D.; BOWEN, H. K.; UHLMANN, D. R. **Introduction to ceramics**. 2nd. ed. A Wiley-Interscience Publication, 1976.

27. REICHMANN, M. et al. Effect of cation substitution in the A site on the oxygen semi-permeation flux in $La_{0.5}A_{0.5}Fe_{0.7}Ga_{0.3}O_{3-\delta}$ dense perovskite membranes with A = Ca, Sr and Ba (part I). **Journal of Power Sources**, 261, n. 175-183, 2014.

28. HUMMEL, R. E. **Electronic properties of materials**. Springer, 2011. ISBN ISBN 978-1-4419-8163-9.

29. BADWAL, S. P. S.; CIACCHI, F. T. Ceramic Membrane Technologies for Oxygen Separation. **Advanced Materials**, 2001. 993.

30. RACHADEL, P. L. et al. Current developments of mixed conducting membranes on porous substrates. **Materials Research**, 2014. 242-249.

31. VIVET, A. et al. New route for high oxygen semi-permeation through surface-modified dense $La_{1-x}Sr_xFe_{1-y}Ga_yO_{3-\delta}$ perovskite membranes. **Journal of Membrane Science**, 454, 2014. 97 - 108.

32. TEN ELSHOF, J. E.; BOUWMEESTER, H. J. M.; VERWEIJ, H. Oxygen transport through $La_{1-x}Sr_xFeO_{3-\delta}$. I. Permeation in air/He gradients. **Solid State Ionics**, 81, 1995.

33. LI, S. et al. $Ba_{0.5}Sr_{0.5}Co_{0.8}Fe_{0.2}O_{3-\delta}$ ceramic hollow-fiber membranes for oxygen permeation. **AIChE**, 52, 2006.

34. TAN, X.; LIN, K. Modeling of air separation in a LSCF hollow-fiber membrane modules with different operating modes. **AIChE**, 48, 2002.

35. XU, S. J.; THOMSON, W. J. Oxygen permeation rates through ion-conducting perovskite membranes. **Chemical Engineering Science**, 54, 1999.

36. COUSIN, P.; ROSS, R. A. Preparation of mixed oxides: a review. **Materials Science and Engineering**, Quebec, 1990. 119-125.

37. SMART, L. E.; MOORE, E. A. **Solid State Chemistry**. Boca Raton: CRC Press, 2005.

38. SEGAL, D. Chemical synthesis of ceramic materials. **Journal of Materials Chemistry**, 7, 1997. 1297-1305.

39. NAGAI, T.; ITO, W.; SAKON, T. Relationship between cation substitution and stability of perovskite structure in $SrCoO_{3-\delta}$ based mixed conductors. **Solid State Ionics**, 177, 2007. 3433 - 3444.

40. CHENG, Y. et al. Investigation of Ba fully occupied A-site $BaCo_{0.7}Fe_{0.3-x}Nb_xO_{3-\delta}$ perovskite stabilized by low concentration of Nb for oxygen permeation membrane. **Journal of Membrane Science**, 322, 2008. 484-490.

41. JUSTE, E. et al. Oxygen permeation, thermal and chemical expansion of (La, Sr)(Fe, Ga)$O_{3-\delta}$ perovskite membranes. **Journal of Membrane Science**, 319, 2008. 185-191.

42. WAINDICH, A.; MOBIUS, A.; MULLER, M. Corrosion of $Ba_{1-x}Sr_xCo_{1-y}Fe_yO_{3-\delta}$ and $La_{0.3}Ba_{0.7}Co_{0.2}Fe_{0.8}O_{3-\delta}$ materials for oxygen separating membranes under Oxycoal conditions. **Journal of Membrane Science**, 337, n. 182-187, 2009.

43. GEFFROY, P. M. et al. Oxygen semi-permeation, oxygen diffusion and surface exchange coefficient of $La_{(1-x)}Sr_xFe_{(1-y)}Ga_yO_{3-\delta}$ perovskite membranes. **Journal of Membrane Science**, 354, n. 6-13, 2010.

44. LUO, H. et al. Performance of a ceramic membrane reactor with high oxygen flux Ta-containing perovskite for the partial oxidation of methane to syngas. **Journal of Membrane Science**, 350, n. 154-160, 2010.

45. FANG, S. M.; YOO, C. Y.; BOUWMEESTER, H. J. M. Performance and stability of niobium-substituted $Ba_{0.5}Sr_{0.5}Co_{0.8}Fe_{0.2}O_{3-\delta}$ membranes. **Solid State Ionics**, 195, n. 1-6, 2011.

46. VIVET, A. et al. $La_{(1-x)}Sr_xFe_{(1-y)}Ga_yO_{3-\delta}$ perovskite membrane: oxygen semi-permeation, thermal expansion coefficient and chemical stability under reducing conditions. **Journal of Membrane Science**, 372, n. 373-379, 2011.

47. IWAHARA, H.; ESAKA, T.; MANGAHARA, T. Mixed conduction and oxygen permeation in the substituted oxydes for $CaTiO_3$. **Journal of Applied Electrochemistry**, 18, n. 173, 1988.

48. QIU, L. et al. Oxygen permeation studies of $SrCo_{0.8}Fe_{0.2}O_{3-\delta}$. **Solid State Ionics**, 76, n. 321, 1995.

49. ULLMANN, H. et al. Ionic/electronic mixed conduction relations in perovskite-type oxides by defect structure. **Journal of the European Ceramic Society**, n. 791-796, 1998.

50. YAREMCHENKO, A. A. et al. Oxygen ionic and electronic transport in $LaGa_{1-x}Ni_xO_{3-\delta}$ perovskites. **Journal of Solid State Chemistry**, 142, n. 325, 1999.

51. ISHIHARA, T. et al. Mixed electronic-oxyde ionic conductivity and oxygen permeating property of Fe-, Co- or Ni doped $LaGaO_3$ perovskite oxide. **Solid State Ionics**, 135, n. 631, 2000.

52. ULLMAN, H. et al. Correlation between thermal expansion and oxide ion transport in mixed conducting perovskite-type for SOFC cathodes. **Solid State Ionics**, n. 138, 2000. 79-90.

53. JIN, W. et al. Preparation of an asymmetric perovskite-type membrane and its oxygen permeability. **Journal of Membrane Science**, 185, 2001. 237 - 243.

54. KHARTON, V. V. et al. Oxygen permeability and Faradaic efficiency of $Ce_{0.8}Gd_{0.2}O_{2-\delta}$ - $La_{0.7}Sr_{0.3}MnO_{3-\delta}$ composites. **Journal of the European Ceramic Society**, 21, 2001. 1763 - 1767.

55. LEE, K. S. et al. Enhancement of oxygen permeation by $La_{0.6}Sr_{0.4}CoO_{3-\delta}$ coating in $La_{0.7}Sr_{0.3}Ga_{0.6}Fe_{0.4}O_{3-\delta}$ membrane. **Desalination**, 147, 2002. 439 - 444.

56. KHARTON, V. V. et al. Oxygen transport in $Ce_{0.8}Gd_{0.2}O_{3-\delta}$ - based composite membrane. **Solid State Ionics**, 160, 2003. 247 - 258.

57. DENG, Z. Q. et al. Relationship between transpor properties and phase transformations in mixed-conducting oxides. **Journal of Solid State Chemistry**, 179, 2006. 362 - 369.

58. ETCHEGOYEN, G.; CHARTIER, T.; DEL-GALLO, P. An architectural approach to the oxygen permeability of $La_{0.6}Sr_{0.4}Fe_{0.9}Ga_{0.1}O_{3-\delta}$ perovskite membrane. **Journal of the European Ceramic Society**, 26, 2006. 2807 - 2815.

59. ITO, W.; NAGAI, T.; SAKON, T. Oxygen separation from compressed air using mixed conductiong perovskite-type oxide membrane. **Solid State Ionics**, 178, 2007. 809 - 816.

60. ZHANG, K. et al. Systematic investigation on new $SrCo_{1-y}Nb_yO_{3-\delta}$ ceramic membranes with high oxygen semi-permeability. **Journal of Membran Science**, 323, 2008. 436 - 443.

61. LI, W.; LIU, J.; CHEN, C. Hollow fiber membrane of yttrium-stabilized zirconia and strontioum-doped lanthanum manganite dual-phase composite for oxygen separation. **Journal of Membrane Science**, 340, 2009. 266 - 271.

62. HSU, K. et al. Effects of zirconium oxide on the sintering of $SrCe_{1-x}Zr_xO_{3-\delta}$ ($0.0 \leq x \geq 0.5$). **Journal of Alloys and Compounds**, 615, 2014. 5491-5495.

63. OHARA, S. et al. Rapid mechanochemical synthesis of fine barium titanate nanoparticles. **Materials Letters**, 62, 2008. 2957-2959.

64. CUSHING, B. L.; KOLESNICHENKO, V. L.; O'CONNOR, C. J. Recent advances in the liquid-phase syntheses of inorganic nanoparticles. **Chemical Reviews**, 104, 2004. 3893 - 3946.

65. ZENG, Y.; LIN, Y. S.; SWARTZ, S. L. Perovskite-type ceramic membrane: synthesis, oxygen permeation and membrane reactor performance for oxidative coupling of methane. **Journal of Membrane Science**, 150, 1998. 87 - 98.

66. QI, X.; LIN, Y. S.; SWARTZ, S. L. Electric transport and oxygen permeation properties of lanthanum cobaltite membranes synthesized by different methods. **Industrial & Engineering Chemistry Research**, 39, 2000. 646 - 653.

67. KHORASANI-MOTLAGH, M. et al. Chemical synthesis and characterization of perovskite NdFeO3 nanocrystals via a co-precipitation mehtod. **International Journal of Nanoscience and Nanotechnology**, 9, 2013. 7-14.

68. HARON, W.; WISITORAAT, A.; WONGNAWA, S. Comparison of nanocrystalline $LaMO_3$ (M=Co, Al) perovskite oxide prepared by co-precipitation method. **International Journal of Chemical Engineering and Applications**, 5, 2014.

69. HENCH, L. L.; VASCONCELOS, W. Gel-Silica Science. **Annual Review of Materials Science**, 20, 1990. 269-298.

70. INOUE, O.; KASHIMA, S. **Process for the preparation of complex perovskite type compounds**. Eur. Patent 87103686.9, 16 September 1987.

71. PECHINI, M. P. **Method of preparing lead and alkaline earth titanates and niobates and coating method using the same to form a capacitor**. Patent 3330697, 11 July 1967.

72. SHAO, J. et al. Investigation of precursors in the preparation of nanostructured $La_{0.6}Sr_{0.4}Co_{0.2}Fe_{0.8}O_{3-\delta}$ via a modified combined complexing method. **Journal of Power Sources**, 484, 2009. 263-267.

73. ABDULLAH, N. A.; HASAN, S.; OSMAN, N. Role of CA-EDTA on the synthesizing process of cerate-zirconate ceramics electrolyte. **Journal of Chemistry**, 2013, 2012.

74. BONTURIM, E. et al. Effect pH variation of powder materials of the composite oxide $Ba_xSr_{1-x}Co_yFe_{1-y}O_{3-\delta}$ obtained by Citrate-EDTA Method. **Materials Science Forum**, 727-728, 2012. 764-768.

75. KAKIHANA, M. et al. Synthesis of high surface area $LaMnO_{3+\delta}$ by a polymerizable compex method. **Journal of Alloys and Compounds**, 1999. 102-105.

76. SMITH, R. M.; MARTELL, A. E. **Critical Stability constants**. New York: Plenum Press, v. Vol. 6, 1989.

77. MARTELL, A. E.; SMITH, R. M. **Critical Stability Constants**. New York: Plenum Press, v. Vol. 5, 1982.

78. FELDHOFF, A. et al. The sol-gel synthesis of perovskites by an EDTA/citrate complexing method involves nanoscale solid state reactions. **Solid State Sciences**, 2008, 2008. 689 - 701.

79. LIU, S. et al. Preparation and characterisation of $SrCe_{0.95}Yb_{0.05}O_{2.975}$ hollow fiber membranes. **Journal of Membrane Science**, 193, 2001. 249-260.

80. LIU, S. et al. Synthesis of strontium cerates-based perovskite ceramics via water-soluble complex precursor routes. **Ceramics International**, 28, 2002. 327-335.

81. PATRA, H. et al. Effect of process parameters on combined EDTA-citrate synthesis of $Ba_{0.5}Sr_{0.5}Co_{0.8}Fe_{0.2}O_{3-\delta}$ perovskite. **Powder Technology**, 209, 2011. 98-104.

82. WU, Z. et al. Effect of pH on synthesis and properties of perovskite oxide via a citrate process. **American Institute of Chemical Engineers Journal**, 52, 2006.

83. JAMES, M. et al. Oxygen vacancy ordering and magnetism in the rare earth stabilised perovskite form of "$SrCoO_{3-\delta}$". **Solid State Sciences**, 6, 2004. 655-662.

84. DING, X. et al. Synthesis and characterization of doped $LaCrO_3$ perovskite prepared by EDTA-citrate complexing method. **Journal of Alloys and Compounds**, 458, 2008. 346-350.

85. ZENG, P. et al. Efficient stabilization of cubic perovskite $SrCoO_{3-\delta}$ by B-site low concentration scandium doping combined with sol-gel synthesis. **Journal of Alloys and Compounds**, 455, 2008. 465-470.

86. ZHANG, S. et al. Synthesis of single-cristalline perovskite barium titanate nanorods by a combined route based on sol-gel and surfactant-templated methods. **Materials Letters**, 62, 2008. 2225-2228.

87. ALAEE, M. A.; MOHAMMADI, T. Preparation and characterisation of $Ba_xSr_{1-x}Co_{0.8}Fe_{0.2}O_{3-\delta}$ perovskite-type membranes: Part I. **Membrane Technology**, 2009.

88. ALAEE, M. A.; MOHAMMADI, T. Preparation and characterisation of $Ba_xSr_{1-x}Co_{0.8}Fe_{0.2}O_{3-\delta}$ perovskite-type membranes: Part II. **Membrane Technology**, 2009.

89. SILVA, G. R. O. et al. Synthesis and Characterization of $LaNi_xCo_{1-x}O_3$ perovskites via complex precursor methods. **Materials Sciences and Applications**, 1, 2010. 39-45.

90. HUÍZAR-FÉLIX, A. M. et al. Sol-gel based Pechini method synthesis and characterization of $Sm_{1-x}Ca_xFeO_3$ perovskite $0.1 \leq x \geq 0.5$. **Powder Technology**, 229, 2012. 290-293.

91. GWON, O. et al. Optimization of $La_{1-x}Sr_xCoO_{3-\delta}$ perovskite cathodes for intermediate temperature solid oxide fuel cells through the analysis of crystal structure and electrical properties. **International Journal of Hydrogen Energy**, 39, 2014. 20806-20811.

92. CHEN, Y. et al. The influence of impurity ions on the permeation and oxygen reduction properties of $Ba_{0.5}Sr_{0.5}Co_{0.8}Fe_{0.2}O_{3-\delta}$ perovskite. **Journal of Membrane Science**, 449, 2014. 86-96.

93. KUTTY, T. R. N.; VIVEKANANDAN, R. Preparation of $CaTiO_3$ fine powders by the hydrothermal method. **Materials letters**, 5, 1987.

94. SUCHANEK, W. L.; RIMAN, R. E. Hydrothermal synthesis of advanced ceramic powders. **Advances in Science and Technology**, 45, 2006. 184-193.

95. GOH, G. K. L. et al. Hydrothermal synthesis of perovskite and pyrochlore powders of potassium tantalate. **Journal of Materials Research**, 17, 2002.

96. CHEN, C. et al. Hydrothermal synthesis of perovskite bismuth ferrite crystallites. **Journal of Crystal Growth**, 291, 2006. 135-139.

97. SARDAR, K. et al. Direct hydrothermal synthesis and physical properties of rare-earth and yttrium orthochromite perovskites. **Chemistry of Materials**, 23, 2011. 48-56.

98. THAMPI, K. R. et al. Preparation of $SrTiO_3$ by sol-gel techniques for the photoinduced production of H2 and surface peroxides from water. **Journal of the Chemical Society**, 84, 1988. 1703-1712.

99. KIRCHNEROVA, J. et al. Evaluation of some cobalt and nickel based perovskites prepared by freeze-drying as combustion catalysts. **Catalysis Letters**, 21, 1993. 77-87.

100. BUCHLER, O. et al. Preparation and properties of thin $La_{1-x}Sr_xCo_{1-y}Fe_yO_{3-\delta}$ perovskitic membranes supported on tailored ceramic substrates. **Solid State Ionics**, 178, 2007. 91-99.

101. MARTIN, L. O. S. et al. Factors determining the effect of Co(II) in the ordered double perovskite structure: Sr_2CoTeO_6. **Journal of Materials Chemistry**, 15, 2004. 183-193.

102. TRAINA, K. et al. Synthesis of $La_{0.9}Sr_{0.1}Ga_{0.8}Mg_{0.2}O_{2.85}$ by successive freeze-drying and self-ignition of a hydroxypropylmethyl cellulose solution. **Journal of the European Ceramic Society**, 27, 2007. 2469-3474.

103. GIACOMUZZI, R. A. M. et al. A new method for preparing nanometer-size perovskite catalysts for CH_4 flameless combustion. **Studies in Surface Science and Catalysis**, 130, 2000.

104. PURWANTO, A. et al. Formation of $BaTiO_3$ nanoparticles from an aqueous precursor by flame-assisted spray pyrolysis. **Journal of the European Ceramic Society**, 27, 2007. 4489-4497.

105. JUNG, D. S. et al. Nano-sized barium titanate powders with tetragonal crystal structure prepared by flame spray pyrolysis. **Journal of the European Ceramic Society**, 28, 2008. 109-115.

106. JUNG, D. S. et al. Morphologies and crystal structures of nano-sized $Ba_{1-x}Sr_xTiO_3$ primary partciles prepared by flame spray pyrolysis. **Materials Research Bulletin**, 43, 2008. 1789-1799.

107. ROSSETI, I.; FORNI, L. Catalytic flameless combustion of methane over perovskites prepared by flame-hydrolysis. **Applied Catalysis B: Environmental**, 33, 2001. 345-352.

108. CHIARELLO, G. L.; ROSSETI, I.; FORNI, L. Flame-spray pyrolysis preparation of perovskites for methane catalytic combustion. **Journal of Catalysis**, 236, 2005. 251-261.

109. CHIARELLO, G. L. et al. Preparation by flame spray pyrolysis of $ABO_{3-\delta}$ catalysts for the flameless combustion of methane. **Catalysis Today**, 117, 2006. 549-553.

110. CHIARELLO, G. L. et al. Solvent nature effect in preparation of perovskites by flame-pyrolysis 1. Carboxylic acids. **Applied Catalysis B: Environmental**, 72, 2007. 218-226.

111. CHIARELLO, G. L. et al. Solvent nature effect in preparation of perovskites by flame pyrolysis 2 alcohols and alcohols + propionic acid mixtures. **Applied Catalysis B: Environmental**, 72, 2007. 227-232.

112. YAN, H. et al. Microwave synthesis of $LiCoO_2$ cathode materials. **Journal of Power Sources**, 68, 1997. 530-532.

113. KINGSTON, H. M.; JASSIE, L. B. **Introduction to microwave sample preparation - Theory and Practice**. [S.l.]: American Chemical Society, 1988.

114. ATHAWALE, A. A.; CHANDWADKAR, A. J.; SAHU, P. K. **A process for the synthesis of perovskite ceramics**. WO 2006/103548 A2, 5 October 2006.

115. BALBAA, I. S.; ODA, S. J. **Apparatus for processing ceramics using microwave oven with resistance heating unit**. US 5191183 A, 2 March 1993.

116. VASCONCELOS, J. S. et al. **Método e aparato para obtenção de nanopartículas de alumina gama na cor preta usando forno microondas**. PI 0600360-5 A, 30 October 2007.

117. FANG, C. Y. et al. Microwave synthesis of nano-sized barium titanate. **Materials Letters**, 62, 2008. 2551-2553.

118. MOREIRA, M. L. et al. Structural and optical properties of $CaTiO_3$ perovskite-based materials obtained by microwave-assisted hydrothermal synthesis: An experimental and theoretical insight. **Acta Materialia**, 57, 2009. 5174-5185.

119. SHARMA, S. et al. Structural, dielectric and ferroelectric study of microwave sintered lanthanum substituted $BaTiO_3$ ceramics. **Materials Chemistry and Physics**, 130, 2011. 191-195.

120. RU, J. et al. Microwave-assisted preparation of sumicron-sized $FeTiO_3$ powders. **Ceramics International**, 40, 2014. 6799-6805.

121. LIU, S.; QIAN, X.; XIAO, J. Synthesis and characterization of $La_{0.8}Sr_{0.2}Co_{0.5}Fe_{0.5}O_{3-\delta}$ nanopowders by microwave assisted sol-gel route. **Journal of Sol-Gel Science and Technology**, 44, 2007. 187-193.

122. ZHAI, Y. et al. A microwave-induced solution-polymerization synthesis of doped $LaGaO_3$ powders. **Journal of Power Sources**, 163, 2006. 316-322.

123. ZHAI, Y. et al. Preparation of $La_{0.8}Sr_{0.2}Ga_{0.83}Mg_{0.17}O_{2.815}$ powders by microwave-induced poly(vinyl alcohol) solution polymerization. **Journal of Power Sources**, 162, 2006. 146-150.

124. GUO, L. et al. Microwave hydrothermal synthesis of barium titanate powders. **Materials Letters**, 60, 2006. 3011-3014.

125. MUKASYAN, A. S. et al. Perovskite membranes by aqueous combustion synthesis. **Separation and Purification Technology**, 25, 2001. 117-126.

126. ZHANG, J. et al. Combustion synthesis and characterization of nanocrystalline proton conducting $Sr(Ce_{0.6}Zr_{0.4})_{0.95}Yb_{0.05}O_{3-\delta}$. **Journal of Alloys and Compounds**, 473, 2009. 308-313.

127. DOROFTEI, C. et al. The influence of Zn^{2+} ions on the microstructure, electrical and gas sensing properties of $La_{0.8}Pb_{0.2}FeO_3$ perovskite. **Sensors and Actuators B: Chemical**, 191, 2014. 239-245.

128. TAN, L. et al. Influence of powder synthesis methods on microstructures and oxygen permeation performance of $Ba_{0.5}Sr_{0.5}Co_{0.8}Fe_{0.2}O_{3-\delta}$ perovskite-type membranes. **Journal of Membrane Science**, 212, 2003. 157-165.

129. BAUMANN, S. et al. Influence of sintering conditions on microstructure and oxygen permeation of $Ba0.5Sr_{0.5}Co_{0.8}Fe_{0.2}O_{3-\delta}$ (BSCF) oxygen transport membranes. **Journal of Membrane Science**, 359, 2010. 102-109.

130. BRINKER, C.; SCHERER, G. **Sol-Gel Science:** The Physics and Chemistry of Sol-Gel Processing. Boston: Academic Press, 1990.

131. DE JONGHE, L. C.; RAHAMAN, M. N. Sintering of Ceramics. In: SOMIYA, S. **Handbook of Advanced Ceramics**. Amsterdan: Elsevier/Academic Press., 2003.

132. KHARTON, V. V.; MARQUES, F. M. B. Mixed ionic-electronic conductors: effects of ceramic microstructure on transport properties. **Current Opinion in Solid State and Materials Science**, 6, 2002. 261-269.

133. WANG, H. et al. Investigation of phase structure, sintering, and permeability of perovskite-type $Ba_{0.5}Sr_{0.5}Co_{0.8}Fe_{0.2}O_{3-\delta}$ membranes. **Journal of Membrane Science**, 262, 2005. 20-26.

134. MOSADEGHKHAH, A.; ALAEE, M. A.; MOHAMMADI, T. Effect of sintering temperature and dwell time and pressing pressure on $Ba_{0.5}Sr_{0.5}Co_{0.8}Fe_{0.2}O_{3-\delta}$ perovskite-type membranes. **Materials and Design**, 28, 2007. 1699-1706.

135. ARNOLD, M. et al. Grain boundaries as barrier for oxygen transport in perovskite-type membranes. **Journal of Membrane Science**, 316, 2008. 137-144.

136. SALEHI, M. et al. A case study of the effect of grain size on the oxygen permeation flux of BSCF disk-shaped membrane fabricated by thermoplastic processing. **Journal of Membrane Science**, 382, 2011. 186-193.

137. KLANDE, T.; RAVKINA, O.; FELDHOFF, A. Effect of microstructure on oxygen permeationf of $Ba_{0.5}Sr_{0.5}Co_{0.8}Fe_{0.2}O_{3-\delta}$ and $SrCo_{0.8}Fe_{0.2}O_{3-\delta}$ membranes. **Journal fo the European Ceramic Society**, 33, 2013. 1129-1136.

138. ZENG, P. et al. Significant effects of sintering temperature on the performance of $La_{0.6}Sr_{0.4}Co_{0.2}Fe_{0.8}O_{3-\delta}$ oxygen selective membranes. **Journal of Membrane Science**, 302, 2007. 171-179.

139. WEIL, K. S. et al. Brazing as a means of sealing ceramic membranes for use in advanced coal gasification processes. **Fuel**, 85, 2006. 156-162.

140. MIURA, N. et al. Oxygen semipermeability of mixed-conductive oxide thick-film prepared by slip casting. **Solid State Ionics**, 79, 1995. 195-200.

141. LEO, A. et al. Oxygen permeation through perovskite membranes and the improvement of oxygen flux by surface modification. **Science and Technology of Advanced Materials**, 7, 2006. 819-825.

142. CARO, J. et al. Evaluation of perovskites in hollow fibre and disk geometry in catalytic membrane reactors and in oxygen separators. **Catalysis Today**, 118, 2006. 128-135.

143. SUNARSO, J. et al. High performance BaBiScCo hollow fibre membranes for oxygen transport. **Energy & Environmental Science**, 4, 2011.

144. ZHAN, M. et al. Effects of hydrogen treatment on the surface microstructure and oxygen permeability of $La_{0.7}Sr_{0.3}Ga_{0.3}Fe_{0.7}O_{3-\delta}$ membrane. **Solid State Ionics**, 179, 2008. 1382-1386.

145. DEVILLE, S. Freeze-casting of porous ceramics: a review of curent achievements and issues. **Advanced Engineering Materials**, 10, 2008.

146. GAUDILLERE, C.; GARCIA-FAYOS, J.; SERRA, J. M. Enhancing oxygen permeation through hierarchically-structured perovskite membranes elaborated by freeze-casting. **Journal of Materials Chemistry A**, 2, 2014. 3828-3833.

147. SOUZA, D. F. et al. Synthesis and structural evaluation of freeze-cast porous alumina. **Materials Characterization**, 96, 2014. 183-195.

148. VAN DER HAAR, M. **Mixed-conducting perovskite membranes for oxygen separation**. [S.l.]. 2001. (ISBN 90-365-1615-3).

149. NUERNBERG, R. B.; MORELLI, M. R. Microwave assisted synthesis and sintering of $Ba_{0.5}Sr_{0.5}Co_{0.8}Fe_{0.2}O_{3-\delta}$ perovskite. **Materials Research**, 18, 2015. 85-91.

150. RAVKINA, O.; RATHEL, J.; FELDHOFF, A. Influence of different sintering techniques on microsctructure and phase composition of oxygen-transporting ceramic. **Journal of the European Ceramic Society**, 35, 2015. 2833-2843.

151. WATANABE, K. et al. Preparation of oxygen evolution layer/$La_{0.6}Ca_{0.4}CoO_3$ dense membrane/porous support asymmetric structure for high performance oxygen permeation. **Solid State Ionics**, 179, 2008. 1377-1381.

152. SCHULZE-KÜPPERS, F. et al. Manufacturing and performance of advanced supported $Ba_{0.5}Sr_{0.5}Co_{0.8}Fe_{0.2}O_{3-\delta}$ (BSCF) oxygen transport membranes. **Journal of Membrane Science**, 433, 2013. 121-125.

153. CHANG, X. et al. A comparative study of the performance of symmetric and asymmetric mixed-conducting membranes. **Separation Science and Engineering**, 17, 2009. 562-570.

154. SHAO, X. et al. A microchanneled ceramic membrane for highly efficient oxygen separation. **Journal of Materials Chemistry**, 1, 2013. 9641-9644.

155. LIU, S.; GAVALAS, G. R. Oxygen selective ceramic hollow fiber membranes. **Journal of Membrane Science**, 246, 2005. 103-108.

156. LEO, A. et al. High performance perovskite hollow fibres for oxygen separation. **Journal of Membrane Science**, 368, 2011. 64-68.

157. HE, B. et al. A surface modified $La_{0.6}Sr_{0.4}Co_{0.2}Fe_{0.8}O_{3-\delta}$ ultrathin membrane for highly efficient oxygen separation. **Journal of Membrane Science**, 464, 2014. 55-60.

158. HE, B. et al. Efficient modification for enhancing surface activity of $Ba_{0.5}Sr_{0.5}Co_{0.8}Fe_{0.2}O_{3-\delta}$ oxygen permeation membrane. **Journal of Membrane Science**, 477, 2015. 7-13.

159. YAKOVLEV, S. et al. Phase transformation and oxygen equilibration kinects of pure and Zr-doped $Ba_{0.5}Sr_{0.5}Co_{0.8}Fe_{0.2}O_{3-\delta}$ perovskite oxide probed by electrical conductivity relaxation. **Applied Physics Letters**, 96, 2010. 254101-254103.

160. ZHU, X.; WANG, H.; YANG, W. Structural stability and oxygen permeability of cerium lightly doped $BaFeO_{3-\delta}$ ceramic membranes. **Solid State Ionics**, 177, 2006. 2917-2921.

161. KLANDE, T.; RAVKINA, O.; FELDHOFF, A. Effect of A-site lanthanum doping on the CO2 tolerance of $SrCo_{0.8}Fe_{0.2}O_{3-\delta}$ oxygen-transporting membranes. **Journal of Membrane Science**, 437, 2013. 122-130.

162. XUE, J. et al. A CO2-tolerance oxygen permeable $60Ce_{0.9}Gd_{0.1}O_{2-\delta}$ - $40Ba_{0.5}Sr_{0.5}Co_{0.8}Fe_{0.2}O_{3-\delta}$ dual phase membrane. **Journal of Membrane Science**, 443, 2013. 124-130.

163. ZHANG, Z. et al. Faciel fabrication and improved carbon dioxide tolerance of a novel bilayer-structured ceramic oxygen permeating membrane. **Journal of Membrane Science**, 472, 2014. 10-18.

164. YI, J.; WEIRICH, T. E.; SCHROEDER, M. CO2 corrosion and recovery of perovskite-type $BaCo_{1-x-y}Fe_xNb_yO_{3-\delta}$ membranes. **Journal of Membrane Science**, 437, 2013. 49-56.

165. GUI, L. et al. A comparison of oxygen permeation and CO_2 tolerance of $La_{0.6}Sr_{0.4}Co_{0.2}Fe_{0.6}Nb_{0.2}O_{3-\delta}$ and $La_{0.6}Sr_{0.4}Fe_{0.8}Nb_{0.2}O_{3-\delta}$ ceramic membranes. **Journal of Alloys and Compounds**, 644, 2015. 788-792.

166. ZHENG, Q. et al. CO_2-tolerant alkaline-earth metal-free single phase membrane for oxygen separation. **Chemical Engineering Science**, 101, 2013. 240-247.

167. WU, C. et al. Microstructure evolution and oxidation states of CO in perosvkite-type oxide $Ba_{1.0}Co_{0.7}Fe_{0.2}Nb_{0.1}O_{3-\delta}$ annealed in CO_2 atmosphere. **Journal of Energy Chemistry**, 23, 2014. 575-581.

168. RAVKINA, O.; KLANDE, T.; FELDHOFF, A. Investigation of carbonates in oxygen-transporting membrane ceramics. **Journal of Membrane Science**, 480, 2015. 31-38.

169. TAN, X. et al. Pilot-scale production of oxygen from air using perovskite hollow fibre membranes. **Journal of Membrane Science**, 352, 2010. 189-196.

170. AIR PRODUCTS AND CHEMICALS, INC. **ITM oxygen technology: scale-up toward clean energy applications**. Pittsburgh. 2012.

171. AIR PRODUCTS AND CHEMICASL, INC. **Ceramic and Coal: ITM oxygen for power generation with reduced CO_2-emissions, detailed engineering study results**. San Antonio. 2013.

172. AIR PRODUCTS AND CHEMICALS, INC. **ITM oxygen technology for gasification applications**. 2014.

173. AIR PRODUCTS AND CHEMICASL, INC. **Advances in ITM Technology for oxygen and syngas production**. 2015.

174. ANDERSON, L. L. et al. Advances in ion transport membrane technology for oxygen and syngas production. **Solid State Ionics**, 2015.

175. CULLITY, B. Elements of X-ray diffraction. Addison-Wesley Pub. Co., 1956.

176. PARK, J. H.; KIM, K. Y.; PARK, S. D. Oxygen permeation and stability of $La_{0.6}Sr_{0.4}Ti_xFe_{1-x}O_{3-\delta}$. **Desalination**, 245, 2009. 559-569.

177. HWANG, S. W. et al. Low-temperature growth of well-crystalline Co_3O_4 hexagonal nanodisks as anode material for lithium-ion batteries. **Electrochimica Acta**, 56, 2011. 8534-8538.

178. VASCONCELOS, D. C. L. et al. Structural investigation of cobalt-doped silica derived from sol-gel synthesis. **Journal of Non-Crystalline Solids**, 378, 2013. 1-6.

179. HE, G.; CAI, J. H.; NI, G. ZnO thin films prepared by a modified water-based Pechini method. **Materials Chemistry and Phsysics**, 110, 2008. 110-114.

180. HIDAKA, A. et al. Experimental and analytical study on the behavior of cesium iodide aerosol/vapor deposition onto inner surface of pipe wall under severe accident conditions. **Journal of Nuclear Science and Technology**, 32, 1995. 1047-1053.

181. HAWORTH, P. et al. Yttrium doped BSCF membranes for oxygen separation. **Separation and Purification Technology**, 81, 2011. 88-93.

182. VOYTOVYCH, R. et al. The effect of yttrium on densification and grain growth in α-alumina. **Acta Materialia**, 50, 2002. 3453-3463.

183. ZENG, P. et al. Influence of M cations on structural, thermal and electrical properties of new oxygen selective membranes based on $SrCo_{0.95}M_{0.05}O_{3-\delta}$ perovskite. **Separation and Purification Technology**, 67, 2009. 304-311.